TITLE PAGE

Report Title: LOW-ENGINE-FRICTION TECHNOLOGY FOR ADVANCED NATURAL-GAS RECIPROCATING ENGINES

Annual Technical Progress Report

Reporting Period: June 1, 2003 – June 30, 2004

for

DoE Cooperative Agreement No. DE-FC26-02NT41339

Submitted by

Victor W. Wong, Tian Tian, Grant Smedley, Jeffrey Jocsak

Massachusetts Institute of Technology
Room 31-155, 77 Massachusetts Avenue
Cambridge, MA 02139

September 30, 2004

Sub-Contractor
Colorado State University
Fort Collins, CO 80523

Submitted to:

NETL AAD Document Control Building 921
Department of Energy
National Energy Technology Laboratory
P.O. Box 10940
Pittsburgh, PA 15236-0940

DISCLAIMER

ABSTRACT

This program aims at improving the efficiency of advanced natural-gas reciprocating engines (ANGRE) by reducing piston/ring assembly friction without major adverse effects on engine performance, such as increased oil consumption and emissions. An iterative process of simulation, experimentation and analysis, are being followed towards achieving the goal of demonstrating a complete optimized low-friction engine system. To date, a detailed set of piston/ring dynamic and friction models have been developed and applied that illustrated the fundamental relationships between design parameters and friction losses. Various low-friction strategies and ring-design concepts have been explored, and engine experiments have been done on a full-scale Waukesha VGF F18 in-line 6 cylinder power generation engine rated at 370 kW at 1800 rpm.

Current accomplishments include designing and testing ring-packs using a subtle top-compression-ring profile (skewed barrel design), lowering the tension of the oil-control ring, employing a negative twist to the scraper ring to control oil consumption. Initial test data indicate that piston ring-pack friction was reduced by 35% by lowering the oil-control ring tension alone, which corresponds to a 1.5% improvement in fuel efficiency. Although small in magnitude, this improvement represents a first step towards anticipated aggregate improvements from other strategies. Other ring-pack design strategies to lower friction have been identified, including reduced axial distance between the top two rings, tilted top-ring groove. Some of these configurations have been tested and some await further evaluation. Colorado State University performed the tests and Waukesha Engine Dresser, Inc. provided technical support.

Key elements of the continuing work include optimizing the engine piston design, application of surface and material developments in conjunction with improved lubricant properties, system modeling and analysis, and continued technology demonstration in an actual full-sized reciprocating natural-gas engine.

TABLE OF CONTENTS

LIST OF FIGURES

LIST OF TABLES

LOW-ENGINE-FRICTION TECHNOLOGY FOR ADVANCED NATURAL-GAS RECIPROCATING ENGINES

Annual Technical Progress Report
Reporting Period: June 1, 2003 – June 30, 2004

Submitted by:
Victor W. Wong, Tian Tian, Grant Smedley, Jeffrey Jocsak
Massachusetts Institute of Technology
DoE Cooperative Agreement No. DE-FC26-02NT41339

EXECUTIVE SUMMARY

This program aims to improve the efficiency of advanced natural-gas reciprocating engines (ANGRE) by reducing piston/ring assembly friction without major adverse effects on engine performance, such as increased oil consumption and emissions. The approach is to apply or adapt existing computer models to evaluate the friction reduction potential of various power-cylinder component design concepts. The promising low-friction candidate design concepts are validated experimentally on an actual full-size large-bore natural-gas engine at Colorado State University (CSU). Waukesha Engine Dresser, Inc. provides an engine, parts, and engineering support for the program.

The program has five major tasks: (1) Organize the work plan and project team and define the overall strategy and approaches; (2) Assess opportunities for friction reduction by performing preliminary analyses and evaluating existing empirical data; (3) Modify or adapt existing engine friction and lubrication models to ANGRE engines and to develop friction reduction concepts and recommendations; (4) Test and demonstrate these concepts in an actual engine experimentally; (5) Analyze the test results and iterate the designs for an optimal low-friction system. Task (1) and (2) have been completed during the first year. The major tasks for this reporting period (Year 2) focused primarily on (a) identifying the major sources and opportunities for friction reduction in the piston ring-pack, and (b) designing, procuring and testing of the recommended designs on a Waukesha VGF F18 engine rated at 13.6 bars brake mean effective pressure (bmep) at 1800 rpm (370 kW).

Except for the experimental data awaiting further analyses that were obtained near or after the end of the reporting period, most of the intended tasks have been accomplished. Current accomplishments focused on improvements obtained from the piston ring-pack only, however. Specific recommendations include using a subtle top-compression-ring profile (skewed barrel design), lowering the tension of the oil-control ring, employing a negative twist to the scraper ring to control oil consumption. Initial test data indicate that piston ring-pack friction was reduced by 35% by lowering the oil-control ring tension alone, which corresponds to a 1.5% improvement in fuel efficiency. Although small in magnitude, this improvement represents a first step towards anticipated aggregate improvements from other strategies. Other ring-pack design strategies to lower friction have been identified, including reduced axial distance between the top two rings, tilted top-ring groove. Some of these configurations have been tested and some still await further evaluation. Colorado State University performed the tests and Waukesha Engine Dresser, Inc. provided technical support.

The modeling and analysis effort (Task 3) was on schedule. Existing friction, ring dynamics, and lubrication models have been adapted to the large-engine configurations. We applied our analyses to a Waukesha F18 VGF engine, in-line 6-cylinder [152 mm bore, 165 mm stroke], 18-liter natural gas SI engine. We then performed detailed studies that illustrated the fundamental relationships between design parameters and friction losses. Results indicate that the most significant contributors to friction are the oil control ring throughout the engine cycle and the top ring around top dead center of compression/expansion. As planned, we have developed strategies and guidelines for an initial set of low-friction piston-ring-pack designs.

The experimental validation effort required a longer elapsed time than anticipated, primarily due to long lead times required to procure specially-designed components. A cumulative six-month no-cost extension was requested and granted.

During the course of the program, we identified opportunities to further reduce friction. Specifically, additional gains can be realized by optimizing the piston itself, as well as incorporating the latest developments in material, lubricant, and surface improvements. Combining mechanical design of the piston, lubricant and material selection in a systems approach will produce multiplicative benefits and further improve engine efficiency. These opportunities will be addressed in the next phase of the program.

The project team participated in an ARES-AUREP (Advanced University Reciprocating Engine Program) Workshop held in conjunction with ASME in October 2003 in Washington DC, as well as a Roundtable Workshop on friction at Argonne National Laboratory earlier that summer at Argonne. In addition to the above presentations, four technical papers have been prepared and submitted for publication: one at a large-bore engine conference (CIMAC 2004), two for the ARES-ARICE Symposium on Gas-Fired Engines in conjunction with the Fall 2004 ASME Engine Division Conference, and one for the Oct 2004 SAE Powertrain Meeting. A technical project briefing was made individually at both Caterpillar and Cummins Inc, in additional to periodic meetings with Waukesha. We aim at enhancing our interactions with industry and others in the ARES community, including universities and national laboratories in the coming year.

This current Annual Report covers progress through June 2004 and focuses on ring-pack analyses and design recommendations, and initial experimental data on the baseline and low-tension oil-control ring configurations on the Waukesha VGF F18 engine.

For the next reporting period, through June 2005, the test data for the remaining recommended ring-pack configurations will be thoroughly evaluated. Team discussions will be held to ensure that the potential for ring-pack improvements will have been fully and practically explored. Key elements of the continuing work include optimizing the design of the engine piston itself, application of surface and material developments in conjunction with improved lubricant properties, system modeling and analysis, and continued technology demonstration in an actual full-sized reciprocating natural-gas engine. Specifically tasks will include (1) Expanded analysis of piston friction, including the effects of piston skirt material rigidity (material compliance or stiffness matrix), piston mechanical design parameters, (2) Incorporation of material and surface characteristics in the power cylinder friction analysis to develop specific recommendation for actual engine parts to be tested, (3) System analysis of lubricants, mechanical design, and materials as an integrated system for overall friction reduction, and (4) Experimental validation and demonstration of the next phase of a low-friction system.

LOW-ENGINE-FRICTION TECHNOLOGY FOR ADVANCED NATURAL-GAS RECIPROCATING ENGINES
Annual Technical Progress Report
(June 1, 2003 – June 30, 2004)

DoE Cooperative Agreement No. DE-FC26-02NT41339

I. INTRODUCTION

A. Objectives

By reducing piston/ring assembly friction, parasitic losses of advanced natural gas reciprocation engines (ANGRE) will be lowered. Computer models will be evolved to assess the opportunities of piston/ring-pack design strategies aimed at friction loss minimization. Fundamental design parameters and performance relationships will be investigated to reduce friction, without causing adverse effects such as increased wear and oil consumption or emissions. The analysis will be accompanied by experimental validation. This will be accomplished through systematic analysis of experimental data sets, providing recommendations of promising low-friction piston/ring-pack options, and actual testing and demonstration in an ANGRE engine.

B. Scope of Work

A combined analytical and experimental program is to be undertaken. The scope of work includes evaluating the performance and design of current large-bore natural gas engine and power cylinder components, modifying or adapting existing analytical tools for ANGRE applications. Computer modeling and analysis will be used to understand and to optimize friction reduction concepts. Concept validation will be conducted experimentally on a Waukesha VGF engine; concurrent computer parametric studies on design parameters will be performed and validated by engine tests. Testing will be done at Colorado State University. There will be a system demonstration of an actual engine (Waukesha VGF).

C. Tasks to Be Performed

The program has five major tasks, as shown in the following Milestones chart, updated midway through the reporting period: (1) Organize the work plan and project team and define the overall strategy and approaches; (2) Assess opportunities for friction reduction by performing preliminary analyses and evaluating existing empirical data; (3) Modify or adapt existing engine friction and lubrication models to ANGRE engines and to develop friction reduction concepts and recommendations; (4) Test and demonstrate these concepts in an actual engine experimentally; (5) Analyze the test results and iterate the designs for an optimal low-friction system. Task (1) and (2) have been completed during the first year. The major tasks for this reporting period (Year 2) focused primarily on (a) identifying the major sources and opportunities for friction reduction in the piston ring-pack, and (b) designing, procuring and testing of the recommended designs on a Waukesha VGF F18 engine rated at 13.6 bars brake mean effective pressure (bmep) at 1800 rpm (370 kW).

D. Major Accomplishments

In brief, the major accomplishments to date include the following:

- Developed/adapted computer simulations for piston and ring-pack friction applicable to ANGRE engines.
- Reduced-friction ring-pack designs developed, with overall ring-pack friction reduction potential of 35%.
- Top ring and oil control ring identified as major friction sources. Scraper ring strategy improves oil consumption
- A parallel study on piston friction shows skirt waviness and stiffness as offering up to 50% friction reduction.
- Improved liner roughness model to better assess friction reduction potential through changes in liner design.
- Tests on full-scale Waukesha engine at CSU measured friction reduction of 30% with low-friction OCR design

E. Current Status

The first round of piston ring-pack analysis and design studies has been completed. Validation and demonstration of optimized combination of ring-pack designs are continuing on full-scale engine tests. The early test data (spring 2004) have been analyzed and included in this report. Additional data were obtained close to the end of June and in the summer of 2004 which will require further analyses. The need for design iterations to fully explore piston ring-pack strategies will be evaluated.

During the course of the program, we identified opportunities to further reduce friction. Specifically, additional gains can be realized by optimizing the piston itself, as well as incorporating the latest developments in material, lubricant, and surface improvements. Combining mechanical design of the piston, lubricant and material selection in a systems approach will produce multiplicative benefits and further improve engine efficiency. These opportunities will be addressed in the next phase of the program.

F. Report Outline

This report presents a comprehensive investigation of sources of friction in the power cylinder of a reciprocating engine, which will be useful to researchers involved in similar studies in the future. Next, RESULTS AND DISCUSSION contains 5 sections, beginning with introduction of the basic concepts and the fundamentals of friction and lubrication in the piston ring pack in Sections 1 and 2. Section 3 identifies and illustrates in detail the various sources of friction in the ring pack. Section 5 describes the various friction reduction strategies possible, and Section 5 enumerates the specific design recommendation to a Waukesha natural-gas power generation engine. The EXPERIMENTAL section, Section 6, describes the experimental validation work carried out on an actual engine. CONCLUSIONS, and the appendices containing details of the fundamental equations and metrics follow. The parallel study on piston dynamics and friction reduction, as well as surface effects on friction have not been included in the report but are subjects of two technical papers, incorporated here by reference: (1) “The Effects of Cylinder Liner Finish on Piston Ring-Pack Friction,” ASME Paper ICEF2004-952, ASME-ICED Fall Technical Conference, Long Beach, CA, October 2004 and (2) “Effects of Piston Design Parameters on Piston Secondary Motion and Skirt-Liner Friction,” SAE Paper 2004-01-2911 SAE Powertrain & Fluid Systems Conference, Tampa Florida, October 2004.

DOE Form 4600.3

PROJECT MILESTONE PLAN

Updated: December 10, 2003

1. Program/Project Identification No. **DE-FC26-02NT41339** 2. Program/Project Title: **Low Engine Friction Technology for Advanced Natural Gas Reciprocating Engines**

3. Performer (Name, Address) **Massachusetts Institute of Technology, 77 Massachusetts Ave., Cambridge, MA 02139**
Technical: Dr. Victor W. Wong, Room 31-155, MIT Business: Mr. Jeffrey Friedland, Room E19-750, MIT. Tel: 617-253-4734
Tel: 617-253-5231 Fax: 617-253-9453 vwong@mit.edu

4. Program/Project Start Date **4/1/02**

8. Program/Project Duration **(4/1/02 – 6/30/04)**

5. Program/Project Completion Date **6/30/04**

Calendar Year 2002: A M J J A S O N D | Calendar Year 2003: J F M A M J J A S O N D | CY 2004: J F M A M J

6. Task New #	7. Planning Category (Task/Subtask Description)	9. Comments (Notes, Name of Performer)
1	**Develop Program Plan**	**Completed**
1.1	Develop Project Milestone Plan	**Completed**
1.2	Deliver Program Fact Sheet	**Completed**
1.3	Prepare Powerpoint Project Presentation	**Completed**
2	**Engine Comparison: Assess Opportunities**	**Completed**
	Preliminary analyses & empirical observations	
3	**Model Concepts: Design & Perf. Analyses**	**Completed**
3.1	(a) Modify and adapt lubrication models	**Completed Early**
3.2	(b) Apply models to study fundamental friction behavior. Develop and explore low friction concepts. Perform parametric studies.	**Completed**
3.3	(c) Recommend low friction design options. Request prototype components for tests	**Completed**
4	**Demonstrate Optimal Design Concepts**	Colorado State U.
4.1	Establish baseline test engine measurements	**Completed**
4.1.1	- install engine and make standard measurements	**Completed**
4.1.2	- instrument and test engine with special diagnostics	**Completed**
4.2	Test components in controlled engine experiments to validate design concepts	To be performed next
4.3	Demonstrate complete low-friction engine system	To be performed
5	**Analyze Test Results and Iterate Designs**	Currently in process
5.1	- Analyze more in-depth various design options	Currently in process
5.2	- Refine models and iterate tests as necessary	Currently in process
6	**Project Management, Reporting & Education**	**Continuous**
6.1	Conduct/prepare periodic reviews and reports	Three team reviews
6.1.1	- Monthly team conferences (involving students)	Monthly teleConfs
6.1.2	- Deliver semi-annual/annual reports	Semi-annual & annual report
6.1.3	- Deliver Final Report	

Charting Information:
Major Milestones △ Milestone Reached ▲
Task/subtask planned completion point ▽
Task/subtask actual completion point ▼
Schedule Deviation (early or slippage) ◇

10. Remarks: This updated project milestone plan is hereby submitted for review and approval. A consensus for the project plan was reached at a team review meeting on 9/30/03.

11. Signature of Recipient and Date: [redacted] Victor W. Wong, 12/10/03, MIT

12. Signature of U.S. Department of Energy (DoE) Reviewing Representative and Date

II. RESULTS AND DISCUSSION

(A) MODEL CONCEPTS: DESIGN AND PERFORMANCE ANALYSIS

1. Introduction to the Model Concepts

1.1 Overview

MIT's computer models [1-5] have been applied to target the most important contributors to friction in the piston-cylinder assembly of the engine. Specifically, three models were applied to analyze the behavior of the piston rings and these are described in some detail in the section that follows. Preliminary results from the models indicate that the most significant contributors to friction in the piston-cylinder assembly are from the oil control ring throughout the engine cycle and from the top ring around TDC (top dead center) of compression/expansion. Strategies for design changes to reduce these contributions are suggested in the sections that follow. A detailed parametric study was conducted to explore the effect of these proposed design changes on friction using the computer models. In the months ahead, the limits of these design changes will need to be established in order to translate the results of the parametric study into low-friction design guidelines.

Section 2 presents an overview of the fundamentals of friction and lubrication in the piston ring pack, and introduces the modeling tools that were used in this study. Section 3 details the application of the modeling tools to identify the primary sources of friction in the piston ring pack. Section 4 presents several general design strategies to reduce piston ring friction. In Section 5, these general strategies are applied to redesign the piston rings in a Waukesha natural gas power generation engine. Part (B) contains the EXPERIMENTAL Section, Section 6, in which model predictions and experimental results are compared in evaluating the performance of these new ring designs.

1.2 Methodology

The following are our accomplishments in brief versus our plans:

1. We modified and applied existing computer models to evaluate selected baseline ANGRE engine performance. This sub-task has been completed.
2. We used the models to investigate the fundamental behavior of piston rings, piston, lubricant behavior, lubricant and solid-solid contact conditions. We have made substantial progress in analyzing the piston rings for both hydrodynamic and boundary lubrication, as well as illustrating the fundamental effects of piston-ring design and dynamics on friction.
3. We developed initial recommendations of proposed piston-ring designs for low friction. The design guidelines focus on top piston ring profile and oil-control ring tension.
4. We worked with component or engine manufacturers to fabricate or furnish the prototype designs. These components were being procured and some testing was in progress.

1.3. Sources of Friction in Modern Internal Combustion Engines

Mechanical losses due to friction account for between 4 and 15% of the total energy consumed in modern internal combustion engines [1]. 40-55% of those total mechanical losses occur in the power cylinder [2], and half of the power cylinder friction losses come from friction generated by the piston rings [1,3,4]. As a result, a reduction in piston ring friction has the potential to improve engine efficiency, lower fuel consumption and reduce emissions. These are important objectives for today's engine manufacturers, who are striving to improve engine performance while trying to meet increasingly stringent emission standards.

1.4. Overview of the Piston Ring-Liner System

1.4.1. Description of the Piston Ring-Liner System

The piston ring pack in an internal combustion engine typically consists of three circular rings located in grooves in the piston, as shown in Figure 1-1. The rings move with the piston along the cylinder liner during engine operation. The primary function of the rings is to prevent high-pressure gases from leaking through the piston-liner interface, which would result in power losses. Effective sealing is thus needed between the rings and the liner. However, without lubrication, this close contact between the ring and the liner would result in large friction power losses. As a result, the other main objective of the piston rings is to effectively distribute lubricant along the ring-liner interface, without allowing excessive oil to pass the interface and leak into the combustion chamber where it could be consumed. A third function of the piston rings that is particularly important for the top ring is the dissipation of heat from the piston to the cylinder liner.

In order for the system to effectively achieve these overall objectives, each piston ring has a unique role. The top ring seals the ring-liner interface in order to prevent high-pressure gas from escaping from the cylinder into the lower parts of the ring pack. The oil control ring regulates the amount of oil that passes the ring-liner interface to lubricate the upper rings. A second ring is also present in most engines. This ring scrapes down excessive oil that passes the oil control ring-liner interface. The second ring-groove interface thus provides a barrier against oil flow into the top ring groove from the lower parts of the piston, which reduces oil consumption. Since the second ring only serves to control excess oil that passes the oil control ring-liner interface, its presence is not critical and it may not be used in certain types of engines depending on their purpose. In racing engines where minimizing weight is a critical objective and life expectancy is low, no second ring is used because this reduces the required piston height, decreasing the overall engine weight. In larger diesel engines where long life is desired and high pressures are generally reached in order to provide high torque, reducing oil consumption is a critical objective, and thus two second rings are sometimes used to control oil flow more effectively.

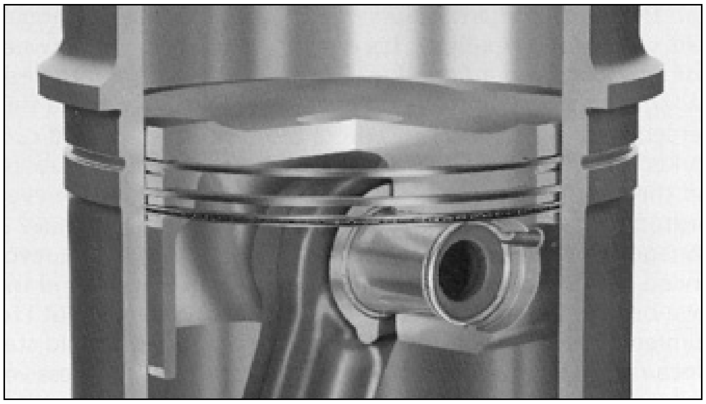

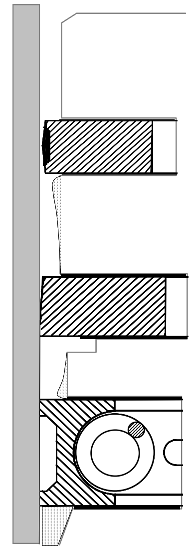

Figure 1-1: The Piston Ring Pack

1.4.2. Typical Piston Ring Designs

As can be seen in Figure 1-1 , the cross-section of each of the rings is different. The different designs reflect the unique purpose of each of the rings.

The top two rings are designed with a diameter that is larger than the size of the cylinder bore in which they are to be installed. They are made with a gap in their circumference so that they can be compressed to fit into the cylinder bore during installation. Once they are installed, their own tension allows them to maintain an effective seal against the liner.

The top ring has a barrel-shaped face profile, which has been shown to be most effective for lubrication [5]. Sufficient lubrication is critical for the top ring as it is subjected to the high cylinder pressures, which can result in large radial forces acting on the back of the ring. If there is no lubrication between the top ring and the liner, large contact pressures can be generated, and this can result in significant wear and an increase in the top ring gap over time. This will result in higher power losses due to the larger amount of high-pressure gases in the cylinder that can escape through the larger gap.

The second ring, also called the scraper ring, has a tapered face so that it cannot accumulate oil on its upper edge to scrape it in the upward direction towards the combustion chamber. However, it can very effectively accumulate oil on its lower edge to scrape it down toward the crankcase to prevent excessive oil from reaching the top ring. This idea is illustrated below in Figure 1-2.

The design of the oil control ring is quite different from that of the compression rings. There are several design variations that exist for different types of engines. The focus of this study was on the twin-land oil control ring, which is typically used in large diesel engines. This ring consists of a spring mounted inside two rails to ensure adequate conformability to the liner. The circumferential length of the spring determines the tension of the oil control ring once installed in the cylinder bore. The high tension force from the ring on the liner created by the spring is necessary to achieve adequate conformability when thermal and mechanical deformation of the cylinder bore occurs during engine operation. The design takes advantage of the high unit pressure exerted on the oil film by the large tension force acting on the small lands, which results in a reduction in oil film thickness, controlling oil more effectively. Two lands are used because it is believed that at least one of the lands will control oil at any given time in the engine cycle, depending on the relative angle between the ring and the liner.

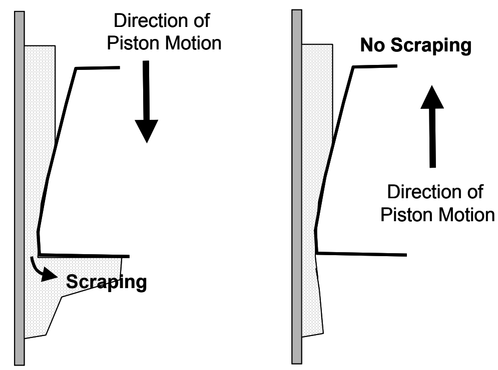

Figure 1-2: Effect of Taper Face Profile on Oil Transport

The rings are manufactured with different materials depending on the type of engine in which they are to be installed. In larger diesel engines, the rings are typically made of ductile cast iron due to the high thermal stability of the material, which makes it suitable to the high operating temperatures in these engines. Steel is the more popular material for rings to be used in smaller gasoline engines because it is stronger that cast iron, and therefore, the size of the rings can be reduced and conformability improved without a reduction in ring life. Cast iron ring faces are typically coated with a chrome layer for wear reduction, although considerable research is currently being devoted to the identification and development of materials and face coatings for reduced friction and wear [2,4]. Some studies have been conducted in which steel rings were investigated for larger diesel engines [6]. These rings showed promise for use in this type of engine, except for temperature limitations and some significant wear observed with certain steel materials used in articulated pistons.

The function and performance of the piston rings is significantly affected by the dynamics of the piston ring-liner system. These dynamic phenomena are introduced in the section that follows.

1.4.3. Dynamic Phenomena in the Piston Ring-Liner System

There is a small clearance between the rings and their respective piston grooves, which is present as a result of manufacturing tolerances in the ring and groove axial heights. Although this clearance is only on the order of 100 microns, it can cause strong gas flows and create significant pressure differences. The gas dynamics and pressure variations throughout the engine cycle cause the rings to undergo significant axial lift and twist relative to their grooves. These ring dynamics play an important role in the determination of the amount of oil between the rings and the liner as well as the amount of friction generated between them.

Several other factors also affect ring-liner lubrication as well as the ability of the rings to seal the ring-liner interface. Bore distortion occurs because of mechanical stresses and thermal expansion due to the temperature gradient along the liner in the direction of piston motion. This overall bore distortion is comprised of radial expansion and circumferential out-of-roundness, and it is therefore a complex 3-D phenomenon that can significantly affect the conformability of the piston rings to the liner. Ring-liner lubrication is also significantly affected by the asymmetric geometry of the crank and connecting rod. As a result of this asymmetry and the various forces encountered during the engine cycle, the piston will tend to tilt about the axis of the piston pin throughout the engine cycle, which will affect angle between the ring and the liner.

The dynamics that arise due to the clearances between the ring and the grooves, combined with bore distortion and piston tilt, ultimately determine the ring-liner relative angle. This angle significantly affects the lubrication between the ring and the liner, and the friction generated by their interaction. The link between these dynamic phenomena and piston ring friction and lubrication is discussed in more detail in Section 2.

1.5. Objectives and Approach used in the Present Study

The goal of the present study was to develop designs to reduce piston ring friction, without increasing oil consumption, blowby, and wear. Achieving this objective was facilitated to a great extent by the use of the extensive modeling tools developed at MIT over the past decade. An experimental evaluation of the designs was also conducted to validate the model predictions and to evaluate certain effects that could not be predicted quantitatively by the model. The use of this combined approach with the goal of developing an optimized piston ring pack in which friction is reduced without adverse effects on oil consumption, blowby and wear, is what distinguishes this work from many of the previous studies that have been conducted in this area.

It should also be emphasized that efforts were focused on developing designs that would not increase cost or introduce any need for major modification of current engine components. As a result, changes in ring materials, the introduction of face coatings, and changes in the type of lubricant used in the engine were considered to be outside the scope of the present study and were not considered as a result.

The following approach was used this study. The modeling tools developed at MIT were first used to identify the primary sources of friction in the piston ring packs of modern internal combustion engines. Reduced friction design strategies were then developed and model predictions were obtained for the friction reduction potential of each of the designs. The design strategies were then applied to redesign the piston rings of a large-bore natural gas power generation engine. The reduced friction rings were manufactured and tested on the full-scale natural gas engine in the Engine and Energy Conversion Lab at Colorado State University to validate the model predictions.

2. Fundamentals of Friction and Lubrication in the Piston Ring Pack

2.1. Modes of Lubrication in the Piston Ring-Liner System

Due to the variation in oil supply to the different piston rings throughout the engine cycle, each ring encounters different modes of lubrication while traveling along the liner. If a sufficient amount of oil exists on the liner to support a load, hydrodynamic lubrication conditions are present. Otherwise, the load from the ring on the liner is supported by contact between the asperities on the two surfaces and boundary lubrication conditions are said to be present. As will be seen in later sections, these modes of lubrication have a profound effect on the magnitude of the friction force generated by the motion of the rings along the liner.

A schematic of a typical lubrication condition between the ring and the liner is shown below in Figure 2-1. As can be seen in the figure, due to the roughness of the surfaces in contact, it is possible for certain portions of the two surfaces to have asperity contact and for other parts to be sufficiently lubricated such that the ring is supported by the load from the oil film. To simplify this situation, the modes of lubrication are typically characterized by the spacing between nominal lines that define smooth surfaces representing the average of the asperities.

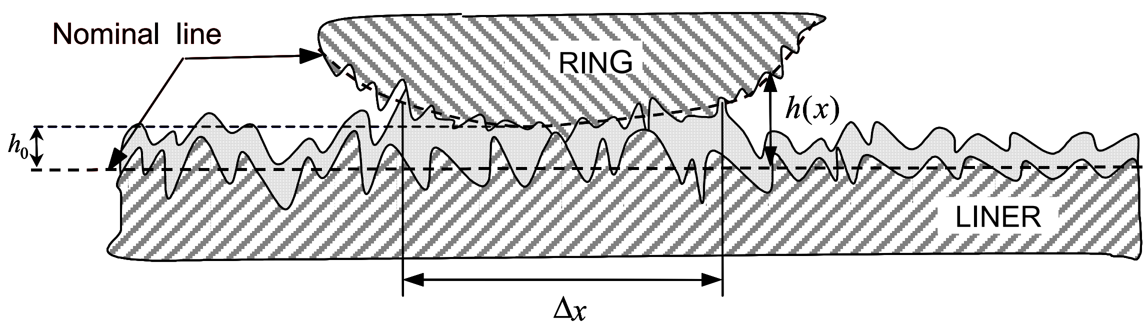

Figure 2-1: Typical Lubrication Conditions Encountered by Piston Rings

Depending on the distance between the nominal lines, h(x), three different modes of lubrication are possible:

a) Pure Hydrodynamic Lubrication
b) Mixed Lubrication
c) Pure Boundary Lubrication

In pure hydrodynamic lubrication, a sufficient amount of oil separates the two surfaces such that there is no asperity contact between them. The transition from pure hydrodynamic lubrication to mixed lubrication occurs when the following criterion is met:

$$\frac{h}{\sigma} < 4 \tag{2.1}$$

where $\sigma = \sqrt{\sigma_{ring}^{\ 2} + \sigma_{liner}^{\ 2}}$ is the combined roughness between the ring surface and the liner [11]. In mixed lubrication, there is oil between the two surfaces in contact, but there is also portion of the ring and liner surfaces between which the spacing is sufficiently small that Equation (2.1) is satisfied, and therefore these parts of the surfaces are also considered to be in boundary contact. The transition between mixed lubrication and pure boundary lubrication occurs when the wetting between the ring and the liner completely disappears, and there is therefore no more oil between the ring and the liner.

The method for the determination of the friction force in each of these lubrication conditions is outlined in the sections that follow.

2.1.1. Pure Hydrodynamic Friction

In this mode of lubrication, the oil supports the load from the ring on the liner, and therefore the amount of friction generated by the ring-liner interaction depends on the properties of the lubricant as well as the film height and width under the ring surface. Determining the friction force thus requires solving coupled equations governing the fluid mechanics of the lubricant and the forces acting on the ring.

The system under consideration is shown in Figure 2-2. In the most general case, the unknowns are the minimum oil film thickness h_o, the inlet wetting coordinate x_1 and the outlet wetting coordinate x_2 (the profile of the ring surface is assumed to be known, in which case once h_o is known, h(x) is also known). It should be noted that although there appears to be a transitional region in which oil attaches to the ring and detaches from the ring at x_1 and x_2, respectively, it was shown in [11] that if viscous diffusion is the method of attachment, this region is of negligible axial width compared to the axial width of the ring, B, and can thus be neglected.

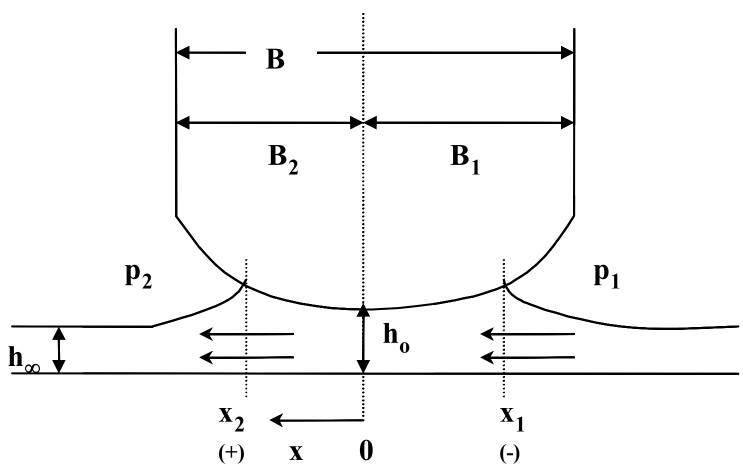

Figure 2-2: Hydrodynamic Lubrication Between the Ring and the Liner

In the most general case, three equations are needed to solve for the unknowns. One equation comes from consideration of conservation of mass and conservation of momentum applied to the oil film under the ring surface. This equation relates the pressure gradient in the oil film to its height and width. A second comes from a radial force balance on the system. A third equation comes from either application of mass conservation on the oil film assuming that the oil supply h_∞ is known, or from an empirical condition for the pressure gradient at the outlet. These governing equations are derived in detail in Section 2.2.

The number of unknowns may be reduced depending on the wetting condition at the leading edge or trailing edge of the ring running surface. The wetting condition describes the point on the ring running surface at which the oil attaches and detaches. The following possible wetting conditions exist:

a) Fully-flooded inlet and outlet
b) Fully-flooded inlet and partially-flooded outlet
c) Partially-flooded inlet and fully-flooded outlet
d) Partially-flooded inlet and outlet

Fully-flooded conditions occur when there is an excess of oil available to fit under the ring, as illustrated below in Figure 2-3 (for fully-flooded inlet).

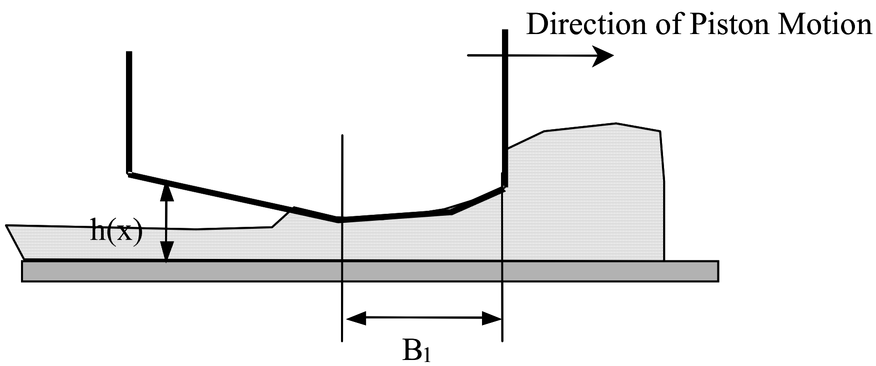

Figure 2-3: Illustration of the Fully-Flooded Inlet Condition

For this condition, $x_1 = -B_1$ and there are thus only two unknowns in the problem (x_2 and h_o). The fully-flooded outlet condition is defined analogously, and also involves only two unknowns as well (x_1 and h_o). In partially-flooded conditions, there is an insufficient amount of oil supply to the ring to completely fill the space between the ring and the liner, and therefore the point of attachment (or detachment) of the oil film is somewhere underneath the ring running surface rather than at its edge.

In the general case where partially-flooded conditions are present at both the leading edge and the trailing edge, the friction between the ring and the liner is determined as follows:

$$F_f = \int_{x_1}^{x_2} \tau dx$$

The shear stress, τ, appearing in the above equation is defined by Eq. (A.5) and is derived in detail in Appendix A. Using Eq. (A.5), the friction force can be expressed as a function of the oil film height and width:

$$F_f = \int_{x_1}^{x_2} \left(\frac{\mu U}{h} - \frac{h}{2} \frac{dp}{dx} \right) dx \tag{2.2}$$

Therefore, once the oil film height and width are determined from the solution of the governing equations, the friction force from hydrodynamic lubrication can be determined.

2.1.2. Pure Boundary Friction

Pure boundary friction occurs when no oil exists between the ring and the liner, and therefore the load from the ring on the liner is completely supported by asperity contact. Since there is no oil between the ring and the liner, $x_1=x_2=0$, and therefore the only unknown in the problem is h_o, which can be determined using a radial force balance. This will be shown in detail in Section 2.2.

In this case, the friction force is given by the following expression:

$$F_f = \int_{xc1}^{xc2} a_{asp} p_c dx \tag{2.3}$$

where a_{asp} is the friction coefficient governed by the surface properties, x_{c1} and x_{c2} define the boundaries of the portion of the ring-liner surfaces that are in asperity contact according to Eq. (2.1), and p_c is the contact pressure between the two surfaces. The contact pressure is given by the following empirical fit used by Hu [12] based on Greenwood-Tripp's theory [13]:

$$p_c = K_c \left(4 - \frac{h}{\sigma}\right)^z \tag{2.4}$$

where K_c depends on asperity and material properties and z is a correlation constant described in [12].

2.1.3. Mixed Friction

As would be expected, the friction between the ring and the liner in mixed lubrication is the sum of the contributions from pure hydrodynamic and pure boundary friction. Mixed friction is thus calculated as follows:

$$F_f = \int_{x1}^{x2} \tau dx + \int_{xc1}^{xc2} a_{asp} p_c dx \tag{2.5}$$

2.2. Governing Equations for Piston Ring Friction and Lubrication

In this section, the governing equations describing piston ring friction and lubrication that were introduced briefly in the previous section will be developed in detail. The method of solution of these equations will then be outlined for the different wetting conditions that can be present throughout the engine cycle. The solution of the governing equations yields the unknowns that are required to determine the friction force between the ring and the liner according to the equations derived in the previous section.

2.2.1. The Reynolds Equation

The Reynolds Equation relates the height, width and shape of the oil film between the ring and the liner with the pressure gradient that is generated therein. A detailed derivation of the 2-D Reynolds Equation for incompressible lubricants can be found in Appendix A. In the present study, a quasi 2-D approach is used in which the parameters defining ring-liner lubrication are determined at specific circumferential locations on the piston, and the Reynolds Equation thus reduces to a 1-D form at each of these locations. Eq. (A.9) thus becomes:

$$\frac{\partial}{\partial x}\left(\frac{h^3}{\mu}\frac{dp}{dx}\right) = 6U\frac{\partial h}{\partial x} + 12\frac{\partial h}{\partial t} \tag{2.6}$$

To further simplify this equation, the terms in Eq. (2.6) can be scaled as follows:

$$U\frac{\partial h}{\partial x} \sim LN\left(\frac{h}{B}\right)$$

$$\frac{\partial h}{\partial t} \sim hN$$

where N is the engine speed in rev/s, L is the stroke length, h is the oil film thickness under the ring, U is the piston velocity, and B is the axial height of the ring. Comparison of the above terms yields:

$$\frac{\frac{\partial h}{\partial t}}{U\frac{\partial h}{\partial x}} \sim \frac{B}{L} << 1$$

Therefore, the unsteady term in the Reynolds Equation can be neglected everywhere in the cycle except near dead centers where the piston velocity U becomes very small. With this simplification, valid in all parts of the cycle other than at end-strokes, Eq. (2.6) reduces to:

$$\frac{\partial}{\partial x}\left(\frac{h^3}{\mu}\frac{dp}{dx}\right) = 6U\frac{\partial h}{\partial x} \tag{2.7}$$

2.2.2. Radial Force Balance

A radial force balance on the ring shown in Figure 2-2 yields:

$$\sum F_r = p_1(B_1 + x_1) + \int_{x_1}^{x_2} p(x)dx + p_2(B_2 - x_2) - p_1(B_1 + B_2) - W = 0 \tag{2.8}$$

Setting Eq. (2.8) to zero assumes that the system is quasi-static in the radial direction, which has been shown to be a reasonable assumption in previous work in this area [11].

It should be noted that within the integral term, the asperity contact pressure p_c given in Eq. (2.4) should be added to p(x) wherever the condition given by Eq. (2.1) is met and boundary lubrication conditions are present.

2.2.3. Conservation of Mass

In partially-flooded conditions, conservation of mass can be applied to the oil at the inlet of the ring surface as depicted in Figure 2-2. The following expression is obtained:

$$Q(x_1) = Uh_\infty \tag{2.9}$$

$Q(x_1)$ is derived in Appendix A and is given by Eq. (A.6). This equation is not valid for the fully-flooded cases because the oil entering or exiting the ring in those cases may be in excess and therefore does not have a uniform velocity at a height of h_∞ as implied in Eq. (2.9).

2.2.4. Boundary Conditions

Values for the pressures at the inlet and outlet of the oil film are assumed to be known:

$$\begin{aligned} p(x_1) &= p_1 \\ p(x_2) &= p_2 \end{aligned} \tag{2.10}$$

If the outlet is partially-flooded, the Reynolds exit condition has been shown to be valid [11]:

$$\frac{dp}{dx}(x_2) = 0 \tag{2.11}$$

This equation does not apply at the end strokes because of the small piston velocity. In these regions of the cycle, another exit condition is needed, which accounts for the unsteadiness of the inlet or exit point of oil attachment. This condition is only applicable a few crank degrees from the end-stroke regions, and is discussed in detail in [11].

2.3. Effect of Dynamic Phenomena in the Piston Ring Pack

As discussed in Section 1.4.3, the dynamics of the piston ring-liner system have a considerable effect on the lubrication conditions between the ring and the liner, and the friction generated by their interaction. Several dynamic phenomena have a significant impact on the relative angle between the ring and the liner, which alters the position of the point on the ring running surface that is closest to the liner (hereafter referred to as the minimum point). If the position of the minimum point changes, the amount of space available for oil to fit between the ring and the liner will change, and therefore the friction and lubrication conditions will also change.

In general, the ring-liner relative angle is the sum of the contributions due to ring static twist, ring dynamic twist, piston tilt, groove tilt, and bore distortion. These effects vary around the circumference of the ring due to the asymmetry introduced by the presence of the ring gap. All of these effects must be taken into account in order to determine the lubrication and friction between the ring and the liner.

2.4. Model Formulation

2.4.1. Overview of Modeling Tools

The determination of the friction and lubrication conditions between the ring and the liner, taking into account the dynamic effects discussed in the previous section, requires the simultaneous solution of the system of nonlinear equations that were derived in Section 2.2. This calculation cannot be performed analytically. It is further complicated by the roughness of the surfaces of the ring and the liner that must be taken into account through the introduction of flow factors in the governing equations [14]. In addition, the oil supply to a given piston ring depends on the oil film thickness left on the liner by the passage of the previous ring during the engine cycle, and therefore mass conservation must be preserved between the three rings in the piston ring pack to accurately model the system. These requirements necessitated the development of modeling tools in order to predict the performance of the piston ring pack for a given set of design parameters. These models have been developed at MIT over the past decade. Since their initial development, the models have been tested and applied extensively to a wide range of engine types and sizes, from large-bore heavy-duty diesel engines to Formula one racing engines. This section contains a brief description of the aspects of the models that are most relevant to the present study. A more complete description of these models and their capabilities can be found in [11,15,16].

2.4.2. Solution of Governing Equations

The model solves the governing equations derived in the previous section at each crank angle of the engine cycle, for each of the rings. The link between the equations and unknowns for each combination of inlet and outlet conditions is briefly summarized in this section.

It should be noted that the governing equations derived in Section 2.2 and the equations used to solve for the unknowns in the model are slightly different. In the model, the volumetric flow rate of the oil at the trailing edge of the ring is introduced as an additional unknown. This allows the use of Eq. (A-6) instead of the Reynolds Equation. The two methods are entirely equivalent, and the introduction of the flow rate as an additional unknown replaces the additional integration constant that would need to be determined if the Reynolds Equation were used. This can be seen by the appearance of the derivative of the pressure distribution in the Reynolds Equation, which requires that this equation be integrated once before being combined with any of the other equations to solve for the unknowns. In Eq. (A-6), the pressure distribution does not appear as a derivative, and this equation can therefore be directly combined with the other equations to solve for the unknowns. It should also be noted that the averaged forms of Eq. (A-4) and Eq. (A-6) were used in the model. These averaged forms take into account the roughness of the surfaces using the approach mentioned in Section 2.1 and by the inclusion of flow factors as mentioned in the previous section. Derivations of the averaged forms of these governing equations can be found in [14].

Table 2-1 below contains a description of the method of solution of the governing equations for the different inlet and outlet conditions that are encountered. It should be noted that there is an additional case that is not considered here for simplicity. In the model, the exit condition near the end of the strokes takes into account the unsteadiness of the wetting location, and the unsteady terms cannot be eliminated from the Reynolds Equation as they were in Eq. (2.7). In addition, it should be noted that the model actually uses equations that include flow factors to account for the roughness of the surfaces of the ring and the liner. Finally, the model accounts for the dynamic twist of the piston rings, which alters the ring-groove relative angle and therefore the position of the minimum point on the ring running surface. A more complete description of all of these specific aspects of the model can be found in [11,15,16].

Inlet/Outlet Conditions	**Unknown(s)**	**Method of Solution**
Fully-flooded inlet Fully-flooded outlet	h_o	• Integrate Eq. (2.7) once, yielding an unknown constant • Express p(x) in Eq. (2.8) as dp/dx by integrating by parts, then substitute in the result of the integration of Eq. (2.7) • Integrate Eq. (2.7) once more, using boundary conditions given by Eq. (2.10), and combine the result with the above equation to solve for the unknown constant and h_o simultaneously
Partially-flooded inlet Fully-flooded outlet	x_1, h_o	• Apply the approach for the fully-flooded inlet and outlet case • The additional equation which is needed to solve for the additional unknown comes from Eq. (2.9) and Eq. (A.6)
Fully-flooded inlet Partially-flooded outlet	x_2, h_o	• Follow the approach for the fully-flooded inlet and outlet case, but use Eq. (2.11) after the first integration of Eq. (2.7) to solve for the unknown constant
Partially-flooded inlet Partially-flooded outlet	x_1, x_2, h_o	• Follow the approach for the fully-flooded inlet, partially-flooded outlet case • The additional equation which is needed to solve for the additional unknown comes from Eq. (2.9) and Eq. (A.6)

Table 2-1: Summary of Method of Solution of Governing Equations

In two of the cases considered, solving the governing equations requires that the oil film thickness on the liner, h_∞, be known. Mass conservation is thus preserved between the three rings so that the oil left on the liner by the passage of the previous ring is the oil supply to the ring that follows. The calculations must therefore be performed in a specific order in the model. The oil control ring is first considered for an entire engine cycle, assuming that it is fully-flooded on both the upstroke and the downstroke. This is used to establish an initial estimate for the oil film thickness on the liner. There is a region on the liner in which the piston travels, but where the oil control ring cannot reach (between top dead center of the top ring and top dead center of the oil control ring as illustrated in Figure 3-7 in Section 3.2.1). In this region, no oil is initially assumed to be present. Following the initial determination of the liner oil film thickness based on the fully-flooded oil control ring, the calculation subsequently considers each ring in succession, with the order depending on whether or not the piston is traveling in an upstroke or downstroke. On downstrokes, the oil supply to the second ring is what is left on the liner by the oil control ring, and similarly for the top ring. On upstrokes, the oil supply to the top ring is what the top ring leaves behind on the previous downstroke.

2.4.3. Additional Modeling Considerations

There is an uncertainty in the model that significantly affects the calculated friction and lubrication conditions between the ring and the liner. In actual engine operating conditions, the oil supply to the second ring during downstrokes comes from both the oil control ring-liner interface and any oil that might be accumulated on the third land of the piston. Oil transport on the third land on the piston is the subject of considerable research at this time, and as a result, the amount of oil accumulated on the third land at any moment in the engine cycle is not known exactly [17,18]. As a result, the approach taken in this study was to consider two oil supply conditions as upper and lower bounds for the actual oil supply to the second ring during downstrokes, as was done by Tian in [19]. The upper bound case for oil supply, hereafter referred to as OS1, considers the second ring to be fully-flooded during downstrokes, which is the maximum possible oil supply that could be provided to the second ring. The lower bound case, hereafter referred to as OS2, considers the second ring to be supplied by the oil control ring-liner interface only, and assumes no oil accumulated on the third land of the piston. These two conditions were used in this study when exploring different potential piston ring designs in order to bracket the true oil supply and therefore the true magnitude of the friction force generated between the ring and the liner. The two oil supply sources are illustrated below in Figure 2-4.

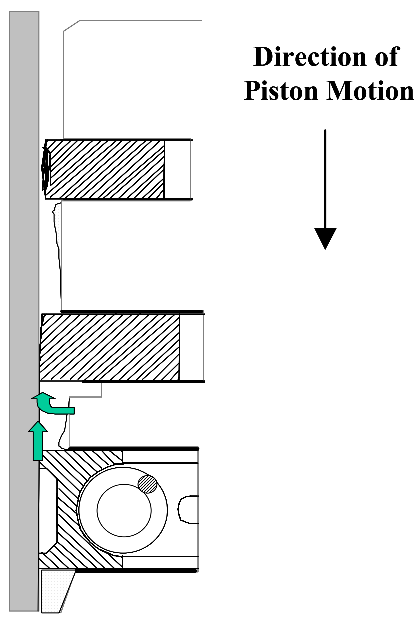

Figure 2-4: Illustration of the Two Sources of Oil Supply to the Second Ring During Downstrokes

The model was used extensively in this study to predict the performance of the piston ring pack in terms of friction and lubrication for different ring designs. This model facilitated the identification of the primary sources of friction in the piston ring pack of modern internal combustion engines, which is the subject of the Section 3, as well as the development of reduced friction designs, which is discussed in detail in subsequent sections.

3. Primary Sources of Friction in the Piston Ring Pack

In this Section, the primary sources of friction in the piston ring pack are identified. Since the results depend on the operating conditions of the engine under consideration, this Section begins with an investigation of the effect of engine operating conditions on friction in the piston ring pack. The primary sources of friction are then identified for the different operating conditions, and physical insight is provided to explain why these are the largest sources of friction.

3.1. Effect of Engine Operating Conditions on Sources of Friction

3.1.1. Modern Internal Combustion Engine Operating Conditions

Modern internal combustion engines operate in a variety of speed and load conditions depending on their application. In passenger cars and larger transport trucks, loads and speeds vary considerably due to the variety of driving conditions encountered. Racing engines typically operate at high speeds and high loads. Stationary power generation engines operate in high load, low speed conditions because the high load generates more power and the low speed is needed to interface with the electric generator and the power grid.

Both engine speed and load affect the friction generated between the piston rings and the liner. In addition, oil supply plays a very important role in ring-liner lubrication. In the sections that follow, these effects are analyzed separately and general trends are then developed for the dominant contributors to piston ring friction in the different engine operating conditions.

3.1.2. Effect of Engine Speed

The effect of engine speed on the friction generated between the piston rings and the liner can be seen from the relations developed in Section 2 and Appendix A. In Eq. (A.5), the second term involving the pressure gradient integrated over the wetted width typically ends up resulting in a much smaller contribution than the first term. Therefore, friction scales roughly as follows:

$$F_f \sim \frac{\mu U}{h} B \tag{3.1}$$

where h is the oil film thickness and B is the ring axial width. The minimum oil film thickness can be related to the piston velocity through the following scaling relationship derived from Eq. (2.7):

$$h \sim \sqrt{\frac{\mu U B}{p}} \tag{3.2}$$

where p is the pressure in the oil film, which is assumed to be a sole function of x as shown in [11]. Combining Eq. (3.1) and Eq. (3.2), it can be seen that the friction power loss scales with piston speed as follows:

$$P_f \sim \mu^{1/2} U^{3/2} \tag{3.3}$$

The viscosity term is included in this relationship because it depends on the piston speed. The extent of this dependence varies according to the type of oil under consideration. In the case of multigrade oils, which are considered to be shear-thinning fluids, the viscosity is controlled by the shear rate, which depends directly on the piston speed, as explained in Appendix A. As piston speed increases, the viscosity will decrease, and therefore the net effect of these changes on friction power loss is the result of a compromise between them.

For a single grade oil, the viscosity of the oil depends only on its temperature, which is controlled primarily by the temperature distribution along the liner. As piston speed increases, the liner temperature may increase, causing a reduction in lubricant viscosity. Therefore, for the case of single grade oils, friction power losses only increase with higher engine speeds if the reduction in lubricant viscosity does not offset the increase in piston speed.

It should be noted that Eq. (3.3) is only valid for hydrodynamic or mixed lubrication. The dependence of friction power loss on piston velocity would be linear for pure boundary lubrication conditions.

It should also be noted that for a given set of engine geometric parameters (crank radius, connecting rod length, etc.), the piston speed is directly related to the rotational speed of the crankshaft [20]. Therefore, the piston speed can also be replaced by the rotational speed of the engine crankshaft in Eq. (3.3). This modified form of Eq. (3.3) will be used later in this Section.

3.1.3. Effect of Engine Load

The effect of engine load on friction is less straightforward. In order to maintain constant engine speed when the load on the engine increases, the amount of air and fuel brought into the cylinder to be compressed and burned during combustion must be increased. As a result, higher peak pressures are reached in the cylinder.

The friction generated by the piston rings is significantly affected by the pressures attained in the cylinder throughout the engine cycle. The cylinder pressure controls the land pressures, which affect the ring dynamics and therefore the lubrication conditions encountered by the rings throughout the engine cycle. Although in general, the contribution of friction as a percentage of the engine's indicated power output reduces as load increases, major changes in load may result in a change in the type of piston ring-liner friction that dominates in different parts of the cycle. This is best illustrated through the use of an example, which is described in the following section.

3.1.4. Illustration of Effect of Speed and Load on Piston Ring Friction

To illustrate the effect of speed and load on friction, the friction model introduced in Section 2 was used to analyze the piston ring friction generated throughout the cycle in a Waukesha natural gas power generation engine for different operating conditions. More detailed specifications for the engine are provided in Section 5. Since it used in power generation applications, it is designed for low speed, high load operation (1800 rpm and 200 psi BMEP). The results in this section were all obtained assuming the maximum oil supply condition (OS1).

Figure 3-1 shows the friction power losses of each of the piston rings throughout the engine cycle at the standard low speed, high load operating condition. It can be seen from the figure that the highest contributors to friction in the engine cycle are the top ring around top dead center (TDC) of compression/expansion and the oil control ring throughout the engine cycle.

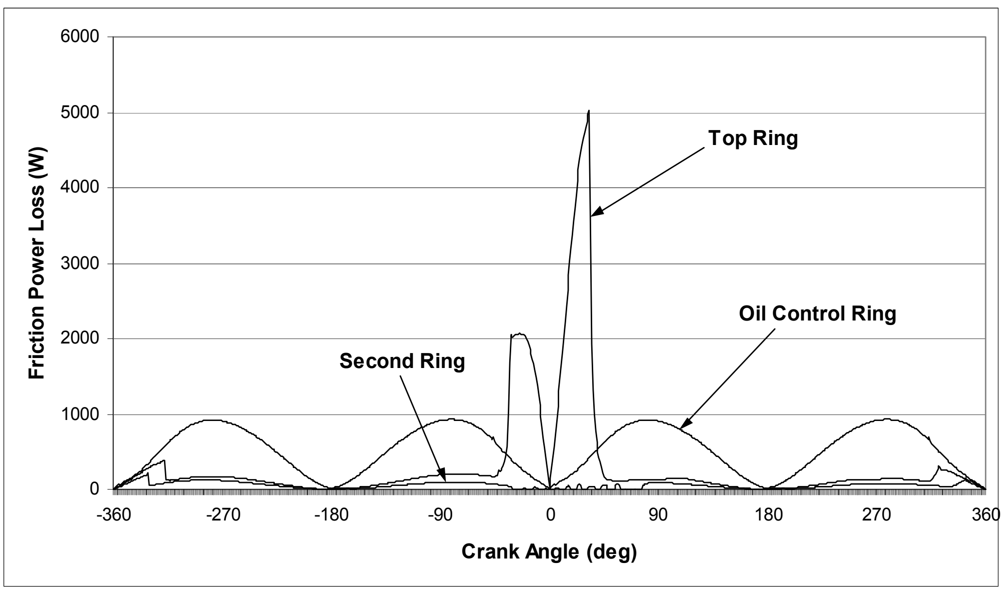

Figure 3-1: Friction Power Loss Contributions in the Piston Ring Pack

This is confirmed in Figure 3-2, which shows the FMEP contributions of each of the piston rings. The determination of FMEP from friction power losses is derived in Appendix B. This figure also shows the FMEP contributions from each of the rings from boundary lubrication. It is clear that most of the top ring friction comes from boundary lubrication in the part of the cycle around TDC of the compression/expansion strokes.

To demonstrate the effect of varying engine load, a different set of cylinder pressure data was used as an input into the friction model. This pressure data was taken from another engine, but nevertheless it can still be used to illustrate the effect of decreasing engine load on friction. The peak pressure is approximately 20 bars for this case compared to a value of 80 bars at the standard operating condition. Figure 3-3 shows the friction power losses of each of the piston rings throughout the engine cycle, and Figure 3-4 shows the FMEP contributions of each of the rings. By comparing these figures with the earlier results for the higher load conditions, the effect of reducing engine load on friction can immediately be seen. In this case, the contribution of the top ring friction generated near TDC of compression/expansion is reduced and the portion of top ring friction coming from boundary lubrication conditions is lower as well, indicating a higher overall contribution from top ring friction generated at midstroke. The main contributor to friction in the low load case is clearly the oil control ring.

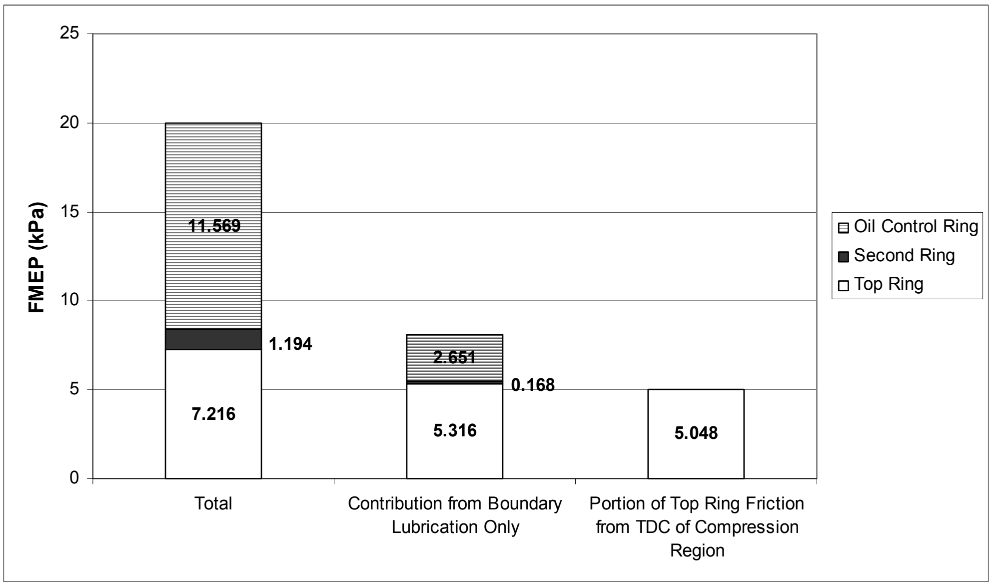

Figure 3-2: FMEP Contributions in the Piston Ring Pack

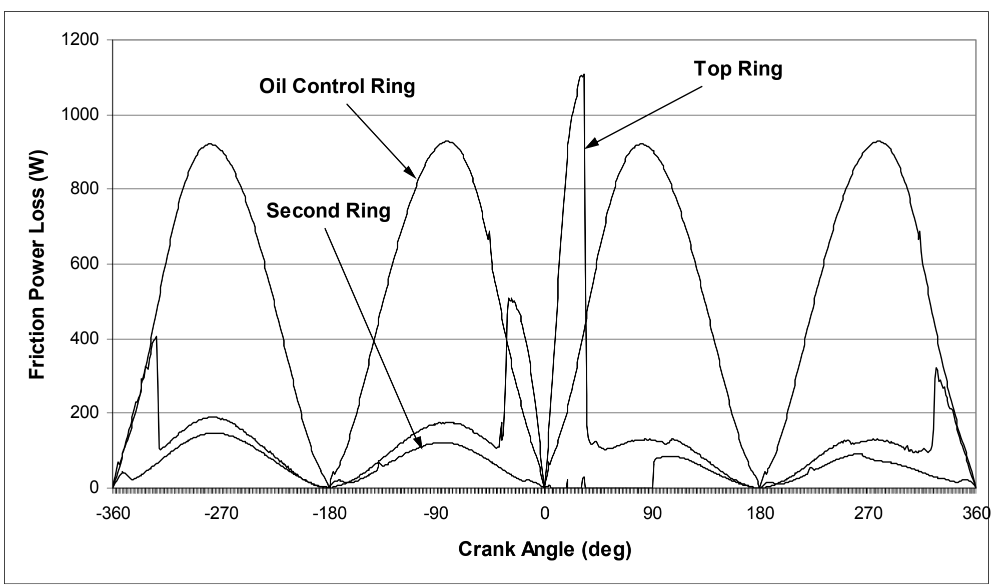

Figure 3-3: Friction Power Loss Contributions of the Ring Pack at Lower Load Condition

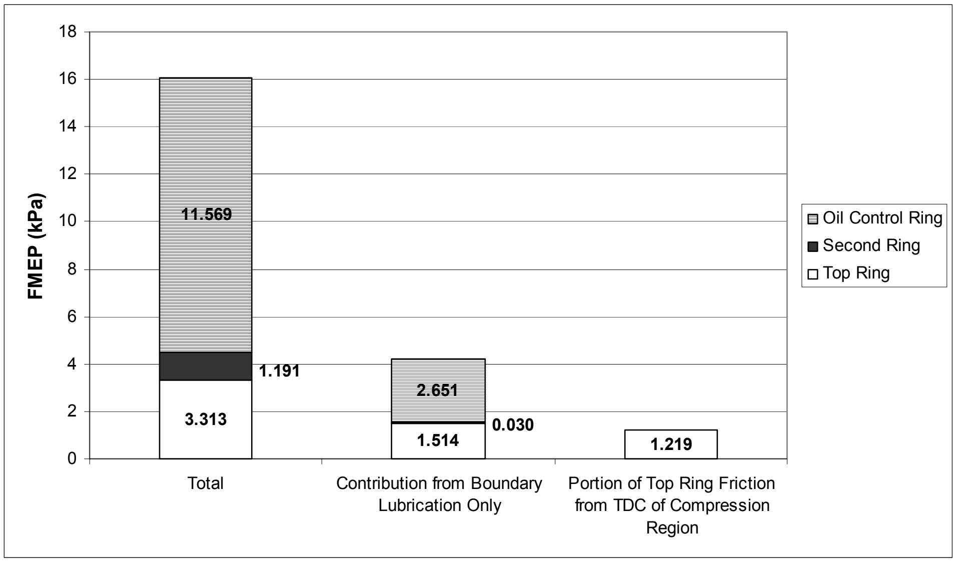

Figure 3-4: FMEP Contributions of the Ring Pack at Lower Load Condition

To illustrate the effect of engine speed, results were obtained for an engine speed of 3000 rpm for the same cylinder pressure data used to generate the low load, low speed case. It should be noted that the increased engine speed may have an effect on the liner temperature distribution and therefore on the lubricant viscosity, as pointed out in Section 3.1.2. Justification for neglecting this effect can be provided using the Waukesha engine data for this specific case. According to Eq. (3.3), for an increase in engine speed from 1800 to 3000 rpm to be offset by a change in oil viscosity, the viscosity would need to be reduced by a factor of approximately 4.5. According to the Vogel Equation, which is used by the model to determine the viscosity of the oil at a specific temperature along the liner, the change in temperature that would be required to achieve a reduction in viscosity by a factor of 4.5 would be between 50 and 100°C, depending on the point in the engine cycle under consideration [11]. Such a change in liner temperature could not feasibly result from this change in engine speed. Therefore, the effect of the change in viscosity can be neglected in this case. This analysis also shows that in general, for the purpose of comparing the main contributors to friction between a low speed and a high speed case, the effect of the change in viscosity can safely be neglected.

With this in mind, the friction power losses of the piston ring pack and the FMEP contributions are plotted again in Figure 3-5 and Figure 3-6, respectively, for the high speed case.

In this case, the contribution of the top ring friction from boundary lubrication around TDC of compression/expansion is reduced even more compared to the low load, low speed case, although this difference would be less significant if the higher cylinder pressure data corresponding to the higher speed were used. Still, for this case, the portion of the total top ring friction from hydrodynamic lubrication conditions during the midstroke region of the engine cycle is larger. This result is expected because of the stronger dependence of friction power losses on engine speed in hydrodynamic lubrication conditions compared to boundary lubrication conditions. It can also be seen from these results that friction from the oil control ring is the most significant contributor to piston ring pack friction in the low load case.

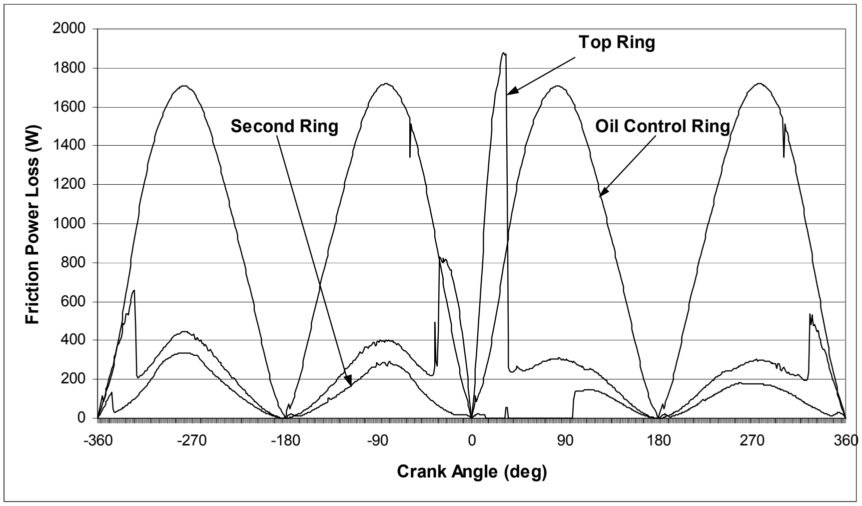

Figure 3-5: Friction Power Losses in the Piston Ring Pack at Low Load, High Speed

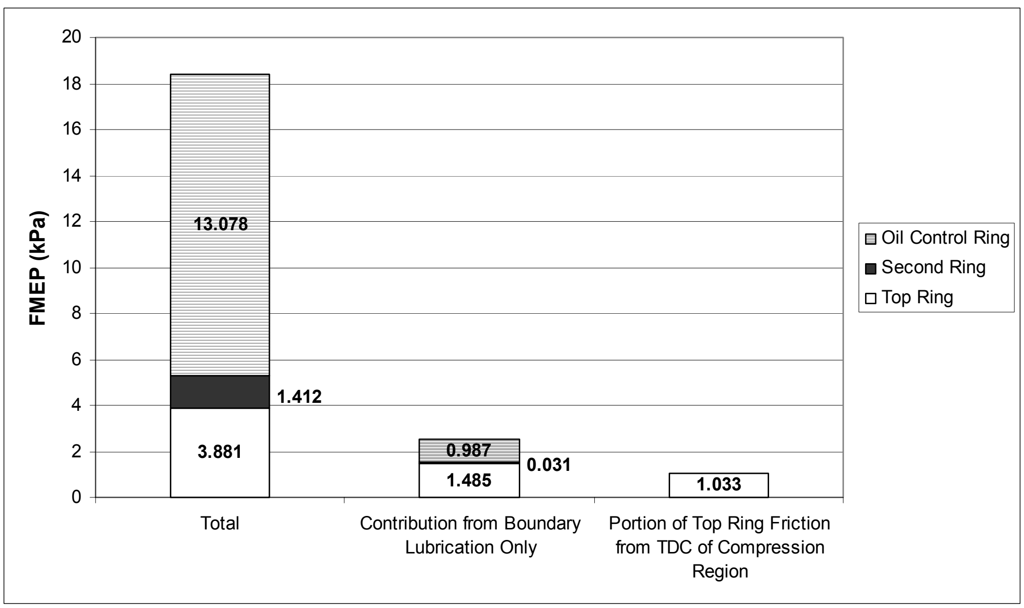

Figure 3-6: FMEP Contributions in the Ring Pack at Low Load, High Speed

The scaling relationship between friction power loss and speed can also be seen from these results. Comparing Figure 3-5 and Figure 3-6, around TDC of compression/expansion, the ratio of top ring friction power loss for the high speed case to the low speed case is about 1900/1100=1.7, which is roughly the same as the ratio of the engine speed, 3000/1800=1.7. This was expected for pure boundary lubrication conditions. In the midstroke region, the ratio of peak top ring friction power losses during the intake stroke is roughly 443/200=2.2, which is approximately equal to the engine speed ratio as defined in Eq. (3.3), namely $(3000/1800)^{3/2}=2.2$.

3.1.5. Effect of Oil Supply on Piston Ring Friction

The amount of oil supplied to the different piston rings throughout the engine cycle has a significant effect on the friction and lubrication conditions between the rings and the liner. In Section 2, the approach used to model oil supply in this study was described. This involved evaluating each of the reduced friction designs at both a maximum (OS1) and minimum (OS2) oil supply condition, since the exact oil supply rate is unknown. In the previous section, all of the results were obtained assuming the maximum oil supply condition (OS1). It turns out that for all of the speed and load conditions that were investigated in the previous section, the results are quite similar for the OS2 case. The main difference is that the top ring contributes more significantly to friction in all speed and load conditions because of the reduced oil supply. Previous studies conducted using the friction model have shown that the top ring typically encounters boundary lubrication conditions throughout a considerable portion of the engine cycle for the minimum oil supply condition [19].

It was also briefly noted in Section 2 that the amount of oil on the liner in the region above TDC of the oil control ring was set to zero in the first cycle of the calculation. This is because the oil control ring can never travel above its own TDC position, and there is thus no direct oil supply to the upper rings between TDC of the oil control ring and TDC of the top ring. As a result, the only source of oil to this part of the liner is what is brought into this region by the top ring or the second ring in subsequent cycles. There is therefore much less oil supply to this section of the liner, and it is thus hereafter as the 'dry region.' The dry region is illustrated in Figure 3-7 below.

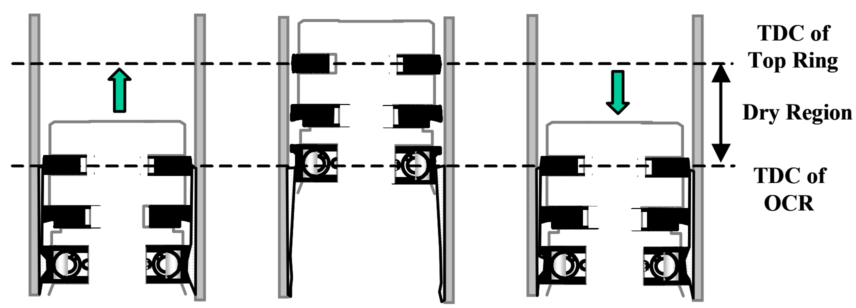

Figure 3-7: Illustration of the Dry Region

It may be possible to bring oil into this region in certain circumstances. The effect of the presence of oil in the dry region during the first engine cycle should be investigated in order to understand the implications of the assumption of zero initial oil film thickness along the liner in this region, since it was used throughout this study. In the remainder of this section, the impact of the initial oil film thickness on the evolution of the lubrication conditions in the dry region will be discussed, and the effect of the oil film thickness in this region on friction will be identified.

Figure 3-8 shows the evolution of the lubrication conditions in the dry region for the case where no oil is initially assumed to be present. Figure 3-8 a), b), and c) show the oil film thickness on the liner before (light black line) and after (dark black line) passage of the top ring during the first, second, and third cycles, respectively. As can be seen from these plots, there is no oil in the dry region, which extends from roughly 40 degrees before to 40 degrees after top dead center (TDC is located at 0 degrees in these plots). However, there is a slight difference between the exact amounts of oil brought into this region by the top ring in the compression stroke and brought out during the expansion stroke. This can be seen by comparing Figure 3-8 a) and Figure 3-8 b). In Figure 3-8 a), the liner oil film thickness before passage of the top ring is slightly smaller than the film thickness left behind by the top ring as the top ring enters the dry region during the compression stroke. Then, on the expansion stroke, the liner oil film thickness is unchanged after the passage of the top ring, and therefore, the additional oil that was brought into the region during the compression stroke remains on the liner for the next cycle. In Figure 3-8 b), during the second cycle, the location of the nonzero oil film thickness is advanced from 33 to 31 degrees before TDC. Similarly, the nonzero oil film thickness location is advanced from 31 to 30 degrees before

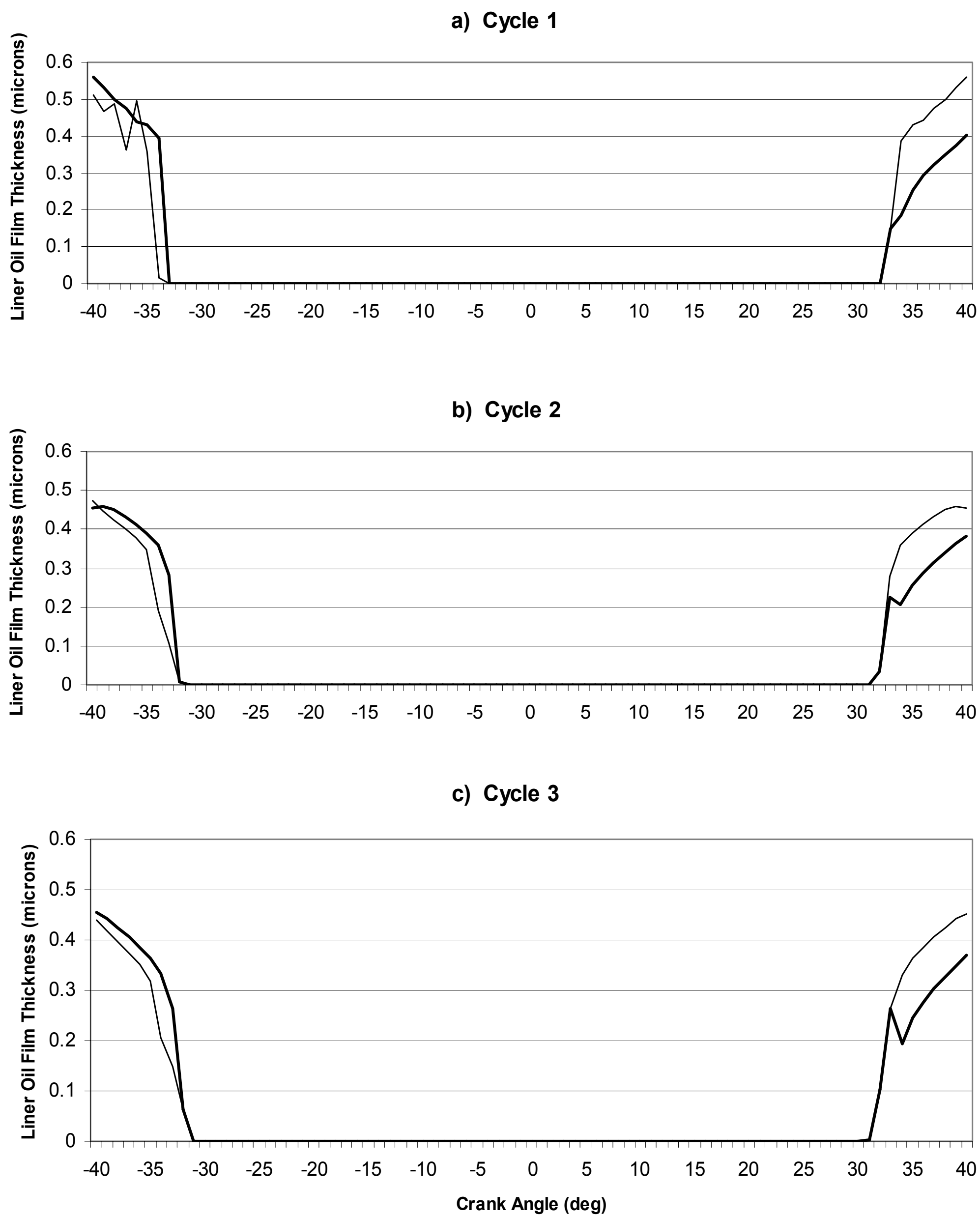

Figure 3-8: Evolution of the Dry Region

TDC between the second and the third cycle. After 4 cycles, there is no further advancement of the nonzero oil film thickness, and the dry region is therefore fully evolved. It can be concluded from this analysis that if zero oil film thickness is initially assumed to be present in the dry region, it is unlikely that this region will become wetted during any subsequent engine cycle.

For comparison, model predictions were also obtained assuming that the oil film thickness in the dry region was initially 1 micron. Figure 3-9 a), b), and c) show the liner oil film thickness before (light black line) and after (dark black line) passage of the top ring for the third, fourth and fifth cycles, respectively. Figure 3-9 a) shows that in the third cycle, oil is available in the dry region until about 5 degrees before TDC, at which point oil starts to accumulate under the top ring and no oil is left behind on the liner. Just before this occurs, between 10 and 5 degrees before TDC, a larger oil film thickness is left on the liner after passage of the top ring than before, and the top ring is clearly releasing some of the oil that was accumulated in the earlier part of the stroke. Then, after passing TDC, on the expansion stroke, the liner oil film thickness before and after passage of the top ring is the same, which indicates that the top ring does not carry out the oil that was brought into this region. As a result, in the fourth cycle, as shown in Figure 3-9 b), a much larger oil film thickness is available to the top ring before it reaches TDC compared to the third cycle. The top ring releases some of its accumulated oil just before TDC, but this time, it carries out all of the oil from in this region to the other parts of the cycle, as indicated by the zero oil film thickness after passage of the top ring during the expansion stroke. In the fifth cycle, as shown in Figure 3-9 c), the top ring is able to bring some oil into the dry region, much like the case in the third cycle. In fact, the fifth and third cycles are almost identical. This is also true for all of the subsequent even cycles. It can thus be concluded from this analysis that if nonzero oil film thickness is initially assumed to be present in the dry region, a balance is eventually reached in which the amount of oil brought into the dry region in odd cycles is balanced by the amount of oil brought out during even cycles.

The effect of the oil film thickness in the dry region on friction is the most relevant issue in this study. For the cases in which zero initial oil film thickness was assumed in the dry region, the model predictions indicated that the top ring was in pure boundary lubrication near TDC of the compression/expansion strokes, and that this contributed to high friction power losses. If oil could be brought into the dry region, then the top ring would no longer be in pure boundary lubrication, and the friction generated due to boundary contact would be reduced. Figure 3-10 and Figure 3-11 below show the friction power loss and FMEP contributions, respectively, for the case where initial oil film thickness in the dry region is assumed to be 1 micron. As can be seen from the figures, the main contributors to friction are still the top ring and the oil control ring, but the relative contribution of the oil control ring is larger. The lower FMEP contribution from the top ring around TDC of compression/expansion is a result of the larger portion of the overall radial load acting on the back of the ring being supported by hydrodynamic pressure. Since hydrodynamic friction is typically much smaller than boundary friction, if a greater portion of the load is sustained by hydrodynamic lubrication, the overall friction losses are reduced.

More detailed studies with the friction model in the past have indicated that it is difficult to bring oil into the dry region on the pin side of the piston [19]. It was also shown in these studies that if piston tilt is sufficiently large, the top ring can bring oil into the dry region on the minor thrust side of the piston, due to the large oil film thickness that is untouched by the rings on the intake stroke which becomes available just before the top ring enters the dry region on the compression stroke. Significant bore distortion, leading to poor conformability of the oil control ring and the second ring, was also identified as a possible method by which oil could become available to be brought into the dry region [19].

It is therefore unlikely that any significant amount of oil exists in the dry region on the pin side of the piston. Therefore, for the remainder of this study, model predictions were obtained assuming that the oil film thickness in the dry region is initially zero. The implications of this assumption will be mentioned where appropriate.

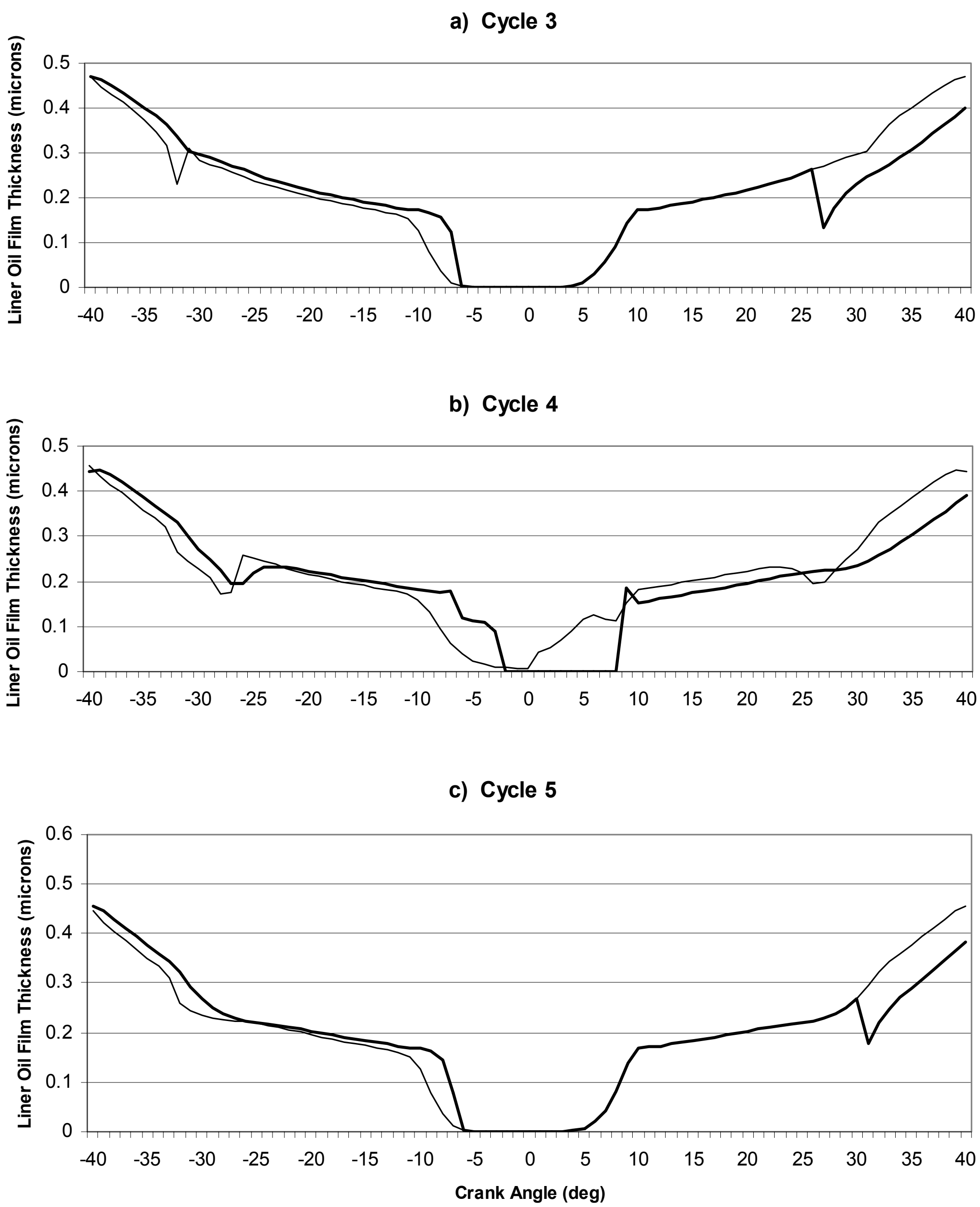

Figure 3-9: Evolution of the Dry Region with Nonzero Initial Oil Film Thickness

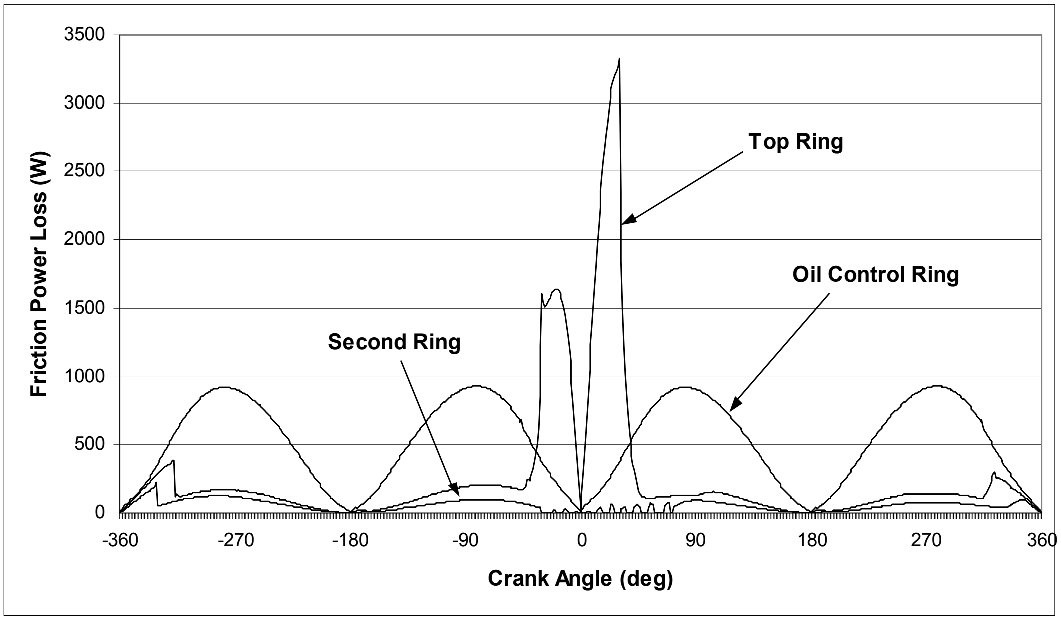

Figure 3-10: Friction Power Losses in Dry Region with Nonzero Initial Oil Film Thickness

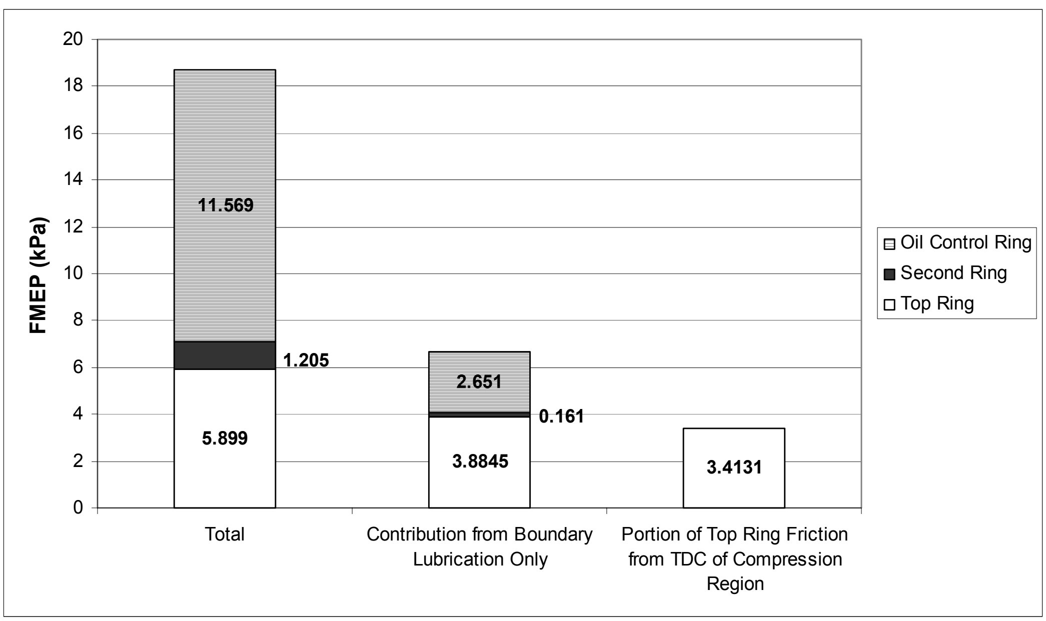

Figure 3-11: FMEP Contributions in Dry Region with Nonzero Initial Oil Film Thickness

3.1.6. Summary of the Effect of Engine Operating Conditions on Piston Ring Friction

Table 3-1 below identifies the main contributors to friction in different engine operating conditions.

It should be noted that this table is only valid for engines using single grade oil. As was pointed out in Section 3.1.2, for multigrade oil, the engine speed has a strong dependence on the viscosity of the lubricant, and therefore it is difficult to draw conclusions about the main contributors to friction in this case.

		Increasing contribution from top ring boundary friction around TDC of compression	
		Low load	High load
Boundary friction power loss increasing as U	Low speed	-Oil control ring throughout engine cycle	-Oil control ring throughout engine cycle -Top ring around TDC of compression/expansion
Hydrodynamic friction power loss increasing as $\mu^{1/2}U^{3/2}$	High speed	-Oil control ring throughout engine cycle	-Oil control ring throughout engine cycle -Top ring around TDC of compression/expansion

Table 3-1: Summary of Main Contributors to Friction for Different Engine Operating Conditions

The remainder of this study is focused on developing friction reduction strategies for high load, low speed engines using single grade oil because in this case, high pressures are generated and severe lubrication conditions are present due to the effect of engine speed on oil film thickness. It was therefore the most interesting case to consider in order to study friction and oil transport. In addition, since both the top ring near TDC of compression and the oil control ring throughout the engine cycle contribute most significantly to friction power losses at this speed and load, the same strategies developed to reduce friction in this case could be applied to reduce oil control ring friction in the lower load condition.

For high load, low speed operating conditions, the largest contributors to friction were identified as the top ring around TDC of compression and the oil control ring throughout the engine cycle. In the sections that follow, physical explanations for each of these high contributions are provided.

3.2. Physical Insight into Primary Sources of Friction in High Load, Low Speed Engines

3.2.1. Top Ring around TDC of Compression

The high friction generated by the top ring in the region around TDC of compression is a result of the combination of poor oil supply to the top ring in the dry region, and high pressure generated in the cylinder by compression and combustion. In high load operating conditions, high peak pressures are generated in the cylinder by compression and combustion. As the pressure in the cylinder rises during the compression stroke, the top ring gradually conforms to the lower groove flank, as shown in Figure 3-12 below. No oil is depicted between the top ring and the liner in this figure in order to reflect the poor oil supply to this region, which was discussed in Section 3.1.5.

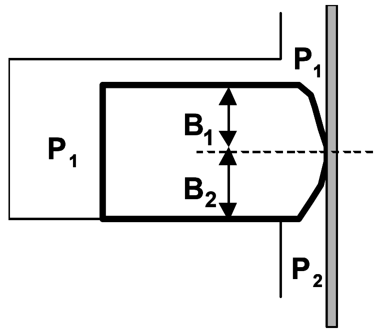

Figure 3-12: Illustration of the Top Ring near TDC of Compression

If no oil is assumed to exist between the ring and the liner in this region around TDC of compression/expansion, and the top ring is assumed to conform well to the lower groove flank, the friction force acting on the top ring is from pure boundary lubrication conditions and can thus be estimated as the product of the radial load acting on the back of the ring and the coefficient of friction:

$$F_f = a_{asp}\left[(p_1 - p_2)B_2 + W\right] \tag{3.4}$$

where a_{asp} is the coefficient of friction between the ring and the liner, and W is the ring load due to tension.

The power loss due to friction is the product of the friction force in Eq. (3.4) and the piston speed at that instant. Although the piston speed is small near TDC, the friction force is very high and therefore the product of friction and piston speed is large, as was shown in Figure 3-1 for the Waukesha natural gas engine. Significant top ring friction power losses occur in this region of the engine cycle as a result. This effect would be even more significant in larger diesel engines, where the peak cylinder pressure can reach 200 bars.

3.2.2. Oil Control Ring Throughout Engine Cycle

The high friction generated by the oil control ring throughout the engine cycle is a result of its high tension. Here, the tension is generated by the ring's own elasticity, and is thus equivalent to the amount of force required to close the ring gap in order to fit the ring inside the cylinder bore. As explained in Section 1, the principal function of the oil control ring is to regulate the amount of oil that reaches the upper rings. As a result, the high tension is necessary in order to promote conformability of the oil control ring to the bore. Good conformability is difficult to achieve in practice because of the non-uniform distortion of the cylinder bore due to mechanical deformation and thermal gradients. As a result, the best way in which to ensure adequate conformability of the oil control ring to the bore is by designing the oil control ring with a high tension.

The high tension force acting on the small lands of the oil control ring results in a high unit pressure exerted on the oil film under the lands. This idea is illustrated in below in Figure 3-13.

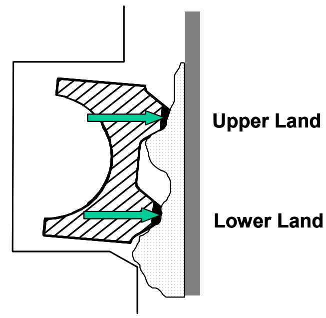

Figure 3-13: Illustration of Effect of Oil Control Ring Tension on Oil Film Thickness

As a result, the oil film thickness that passes under the oil control ring is reduced and adequate oil control is achieved in this way. This can be seen by consideration of the radial force balance in Eq. (2.8). Assuming that the land pressures around the oil control ring are equal and close to atmospheric pressure, they can be neglected in this analysis. Therefore, the force due to ring tension is balanced by the pressure generated in the oil film:

$$W = \int_0^B p dx$$

Here, for simplicity, the oil control ring is assumed to be fully-flooded with oil, and therefore the pressure developed in the oil film is related to the load due to tension through the following scaling relationship:

$$p \sim \frac{W}{B} \tag{3.5}$$

Now, scaling the Reynolds' Equation (Eq. (2.7)) yields the relationship between the pressure developed in the oil film and the film height:

$$h \sim \sqrt{\frac{\mu UB}{p}} \tag{3.6}$$

Eq. (3.5) shows that a high ring load due to tension results in higher pressure developing in the oil film, which reduces the film thickness according to Eq. (3.6). The reduced film thickness leads to higher friction between the ring and the liner according to Eq. (3.1).

If no oil were to exist between the oil control ring and the liner, the high tension force would result in more severe asperity contact pressure according to Eq. (2.4), which would result in higher friction according to Eq. (2.3).

Therefore, regardless of the amount of lubrication under the oil control ring, the high tension generates high friction between this ring and the liner. In the Section that follows, several design strategies will be developed to reduce the friction generated by both the oil control ring and the top ring along the liner.

4. Friction Reduction Strategies

The following Section contains a description of recommended strategies to reduce the friction generated by the main contributors identified in Section 3. The relative friction reduction potential of each design strategy is investigated using the modeling tools described in Section 2. Adverse effects that may result from implementation of the designs are discussed, and additional designs to minimize these adverse effects are developed and recommended.

4.1. Top Ring

An equation describing the friction generated by the top ring along the liner in the region near TDC of compression was given in the previous Section (Eq. (3.4)). Due to the high pressures generated near TDC of compression, the pressure term typically exceeds the ring load due to tension by at least an order of magnitude. Therefore, designs to reduce friction should be focused on reducing the contribution from the pressure difference acting on the lower part of the top ring. Since the pressure difference is controlled by the compression and combustion process, which will not be changed in this study, the most effective way to reduce top ring friction in this region is by reducing the area exposed to the high pressure difference (B_2 in Figure 3-12).

At this point, it should be noted that this design strategy was developed assuming that there is no oil in the dry region. Pure boundary lubrication conditions were indeed predicted to be present in the dry region by the model, as was discussed in Section 3.1.5. However, it was also pointed out in this section that in certain circumstances, oil can be brought into the dry region and mixed lubrication may be achieved. If this were the case, the suggested design strategy of reducing B_2 would still reduce friction, but it would be slightly less effective because in mixed lubrication conditions, the portion of the net radial load supported by the oil film is much greater than the portion supported by asperity contact. The reduction in B_2 would still reduce boundary friction by reducing the net radial load, but since the part of the load supported by hydrodynamic pressure is generally larger than that supported by asperity contact, the strategy would be less effective at reducing friction overall if oil were present in the dry region.

There are several practical ways in which the reduction of B_2 can be accomplished, and they are described in the sections that follow.

4.1.1. Skewed Barrel Profile

The top ring can be manufactured such that the physical length of the region below the minimum point is reduced. This is generally referred to as a skewed barrel profile design. Such a design clearly reduces the area over which the high pressure difference acts, which reduces the friction generated between the top ring and the liner in this region. This design was investigated in some of the previous studies described in Section 1, and a reduction in friction was observed by its implementation [1,6]. The design is illustrated below in Figure 4-1, where it is compared to a symmetric barrel profile.

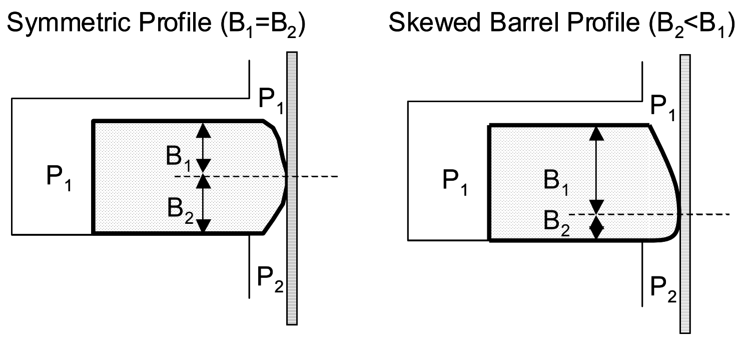

Figure 4-1: Illustration of Skewed Barrel Profile Design

4.1.2. Top Ring Groove Upward Tilt

The high pressures generated in the cylinder due to compression and combustion force the top ring to conform well to the lower groove flank around TDC of compression. As a result, if an upward groove tilt angle were introduced in the top ring groove, the point on the ring that is closest to the liner (the minimum point) would move down along the profile if the top ring were to conform to the upward tilted groove around TDC of compression. This idea is illustrated below in Figure 4-2. As would be the case for the skewed barrel profile design, this design would result in a reduction of area over which the high radial pressure difference acts, and would therefore reduce friction.

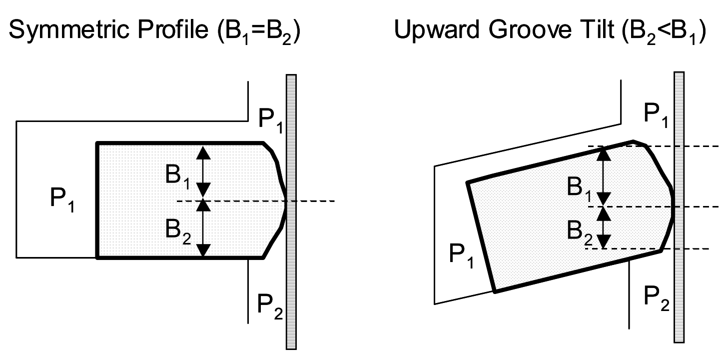

Figure 4-2: Illustration of Top Ring Upward Groove Tilt Design

4.1.3. Reduced Top Ring Axial Height

One other method by which to reduce the area over which the high radial pressure difference acts around TDC of compression would be to reduce the overall axial height of the top ring. This would reduce both B_1 and B_2, and since the high pressure difference acts over B_2, friction could be reduced using this design. This idea is illustrated below in Figure 4-3.

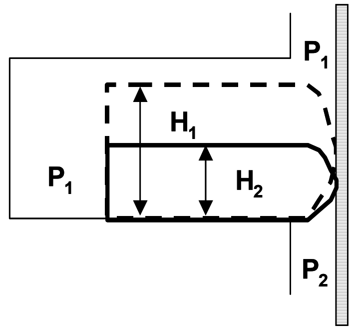

Figure 4-3: Illustration of Reduced Axial Height Design

4.2. Oil Control Ring

4.2.1. Reduced Tension Oil Control Ring

Since the friction generated by the oil control ring is a result of its high tension, the best way in which to reduce oil control ring friction would be to reduce the ring tension. This would almost certainly be accompanied by an increase in oil consumption due to poorer conformability. This will be discussed in more detail in the following section, and designs will be recommended to compensate for this adverse effect.

4.3. Adverse Effects of Reduced Friction Designs

4.3.1. Reduced Ring Life

Reduced ring life was reported in previous studies that were conducted on reduced axial height rings. In particular, Hill and Newman identified reduced axial height as causing reductions in axial stiffness [4]. Based on their experimental results, they concluded that compression rings should be at least 1.5 mm in axial height. Failures were observed and the tests had to be terminated after 50 hours when rings whose axial heights were below this value were used in their study.

4.3.2. Increased Top Ring Groove Wear

One of the adverse effects of the upward top ring groove tilt design discussed in Section 4.2.2 is that it can result in increased top ring groove wear. When the cylinder pressure rises sufficiently to push the top ring downward to conform to the groove, concentrated contact is first made at the outer diameter (OD) corner of the lower groove flank because of the upward tilt angle. This effect is illustrated in Figure 4-4 below, in which the contact pressure distribution between the ring and the lower groove flank is compared between the baseline design with no upward groove tilt and the upward groove tilt design. The graph shows the contact pressure distribution between 100 degrees before TDC and 100 degrees after TDC since this is the region of interest in the engine cycle. As can be seen in the graph, fairly uniform contact pressure distribution is achieved from ID to OD in the baseline design, although there is a slight increase in the contact pressure at the OD corner for this design. This is because the high pressure above the top ring in the area between the groove edge and the liner can cause the ring to rotate around the OD corner by a small amount close to TDC of compression. The upward groove tilt design therefore results in a large concentrated contact pressure at the OD corner of the groove.

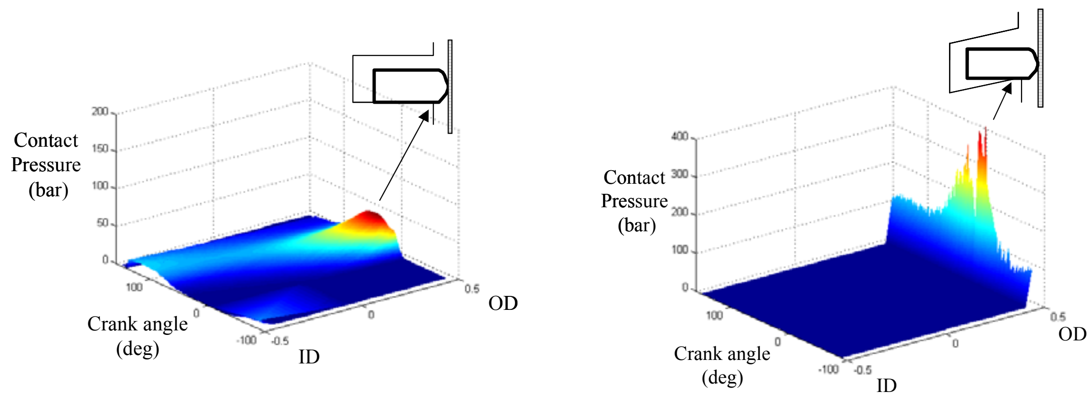

Figure 4-4: Effect of Upward Top Ring Groove Tilt

Because of the highly concentrated contact pressure at the OD corner of the upward tilted top ring groove, this corner will be subjected to significant wear and will likely flatten out over time. As a result, the upward groove tilt angle will gradually decrease until the design is effectively undone and the groove is no longer tilted. Clearly, a design to compensate for this effect is needed if this upward groove tilt design is to be useful for practical purposes. Such a design will be recommended in Section 4.4.1.

4.3.3. Increased Oil Consumption

In Section 4.2.1, it was noted that reducing oil control ring tension will compromise the ring's conformability to the liner, which will likely result in increased engine oil consumption. In reality, this depends on whether or not the oil that passes the oil control ring-liner interface is able to reach the combustion chamber. It also depends on the extent of the bore distortion in the engine, which is not known exactly. Nevertheless, it is likely that if a significant amount of excess oil passes the oil control ring-liner interface, at least part of this oil will reach the crown land and will be consumed. Therefore, the reduced tension oil control ring design should be implemented with another design to compensate for the likely increase in oil consumption. Two designs that could potentially achieve this purpose will be described in Sections 4.4.2 and 4.4.3

4.4. Designs to Compensate for Adverse Effects

4.4.1. Effect of Top Ring Static Twist on Top Ring Groove Wear

As discussed in Section 4.3.2, the upward top ring groove tilt design results in a large concentrated contact pressure at the OD corner of the groove, which can quickly wear the OD corner and render the design ineffective. One way in which to compensate for this effect is by introducing a positive static twist in the top ring. This can be accomplished by adding a small groove in the in the upper ID corner of the top ring.

If there is no groove in the upper ID corner of the ring, the cross-section is approximately symmetric. As a result, when the ring is installed in the cylinder bore and the radial load due to tension is applied, pure bending occurs about the axis that is normal to the plane of the ring as the ring gap is closed. If a small section of material is removed from the upper ID corner of the ring, the cross-section becomes asymmetric, and the location of the centroid and the angle of the principal axes of the cross-section will change. As a result, when the ring is installed in the cylinder bore and the uniform radial load due to tension force is applied, the cross-section will be subjected to a twisting moment as well as a bending moment.

If a certain amount of material is removed from the upper ID corner of the ring such that the positive twist introduced by this change is larger than the upward groove tilt angle, the ring will settle down on the lower groove flank much more gradually as the cylinder pressure rises during the compression stroke. As a result, a more uniform contact pressure distribution between the ring and the lower groove flank will be achieved with such a design, as illustrated in Figure 4-5 below. This will prevent the upward groove tilt design from becoming worn. The contact pressure distribution in the case of the upward groove tilt combined with the positive top ring static twist yields roughly the same uniformity in the contact pressure distribution as the baseline design with no upward groove tilt. It is therefore reasonable to expect that this design would wear no less than the baseline design. The combination of the upward groove tilt with the positive top ring static twist thus reduces friction without introducing any adverse effects.

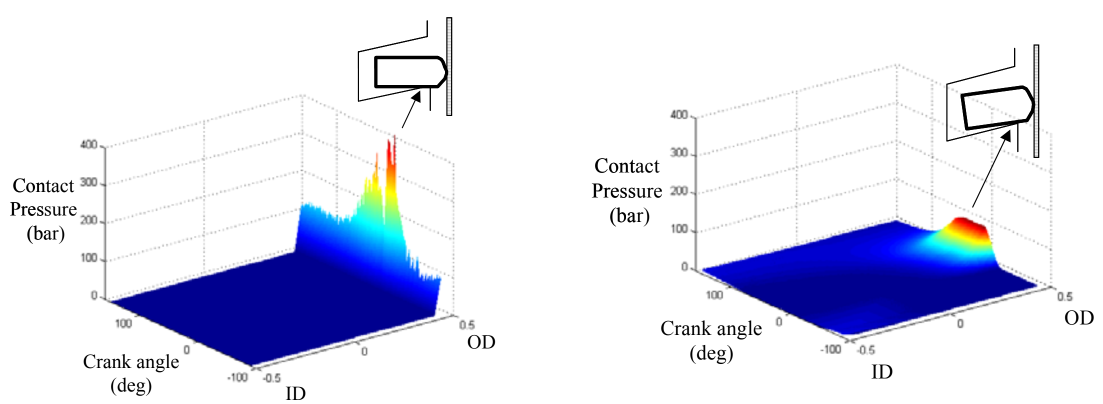

Figure 4-5: Effect of Top Ring Static Twist

4.4.2. Effect of Second Ring Design on Oil Consumption

The second ring is typically designed with either a positive static twist or a negative static twist. With a positive static twist, the ring is more stable and therefore no ring flutter occurs near TDC of compression. A complete description of the flutter phenomenon as well as a more thorough discussion of the link between static twist and ring stability can be found in [21]. It is commonly believed that second ring flutter near TDC of compression results in oil transport to the crown land and eventually to oil consumption. As a result, the second ring is often designed with a positive static twist so that no flutter occurs around TDC of compression.

One of the consequences that can occur as a result of the use of such a design is that the second ring can remain fixed on the lower groove flank for most of the cycle. This is because a second ring with positive static twist can seal the path where gas would normally flow to the lower lands, as shown below in Figure 4-6. As a result, there is a significant pressure rise in the second land and this pressure cannot be relieved to the lower lands through the blocked path. Because of the inability of the gas to flow from the second land to the lower lands, pressure in the second land builds, and can exceed the cylinder pressure near the end of the expansion stroke. At the beginning of the exhaust stroke, this pressure difference tends to force the top ring to lift, whereas the downward pointing inertia force pushes the top ring down, resulting in a phenomenon called top ring reverse flutter. Previous studies have shown that top ring reverse flutter may be an important source of oil consumption [18,21,22].

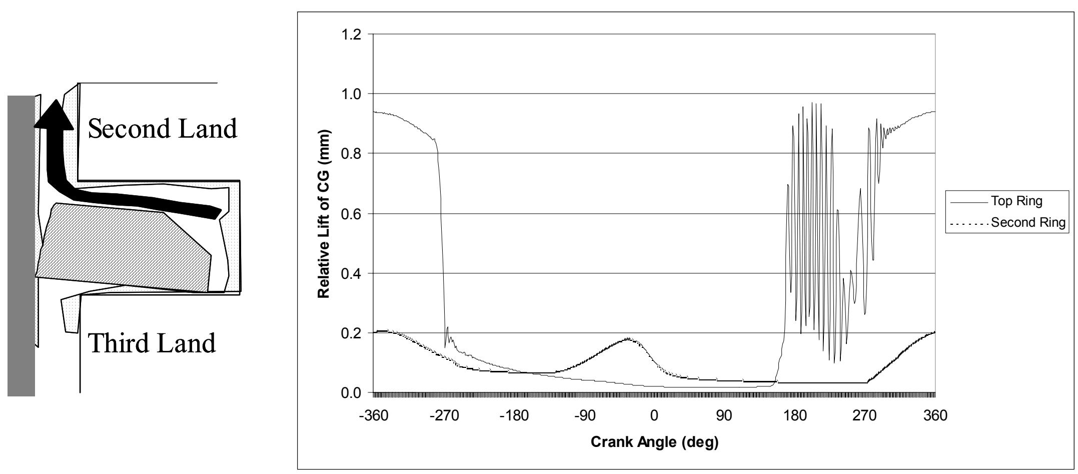

Figure 4-6: Top Ring Reverse Flutter

There is another potential adverse consequence that can result from the use of a second ring with positive static twist. With a larger second ring static twist, a more significant portion of the taper face becomes exposed to the higher second land gas pressure. Due to the sealing created between the second ring and the top OD corner of the second ring groove, the high gas pressure can push the ring inward to allow the gas flow to pass through the ring-liner interface. This is a phenomenon called second ring collapse, and it is illustrated in Figure 4-7 below. Operating conditions and designs to avoid second ring collapse are discussed in [21]. Second ring collapse is undesirable for oil consumption because it allows a significant amount of gas to flow past the ring-liner interface and to reach the third land, where pressure builds up and gas flow can subsequently carry oil into the second ring groove and upwards towards the combustion chamber.

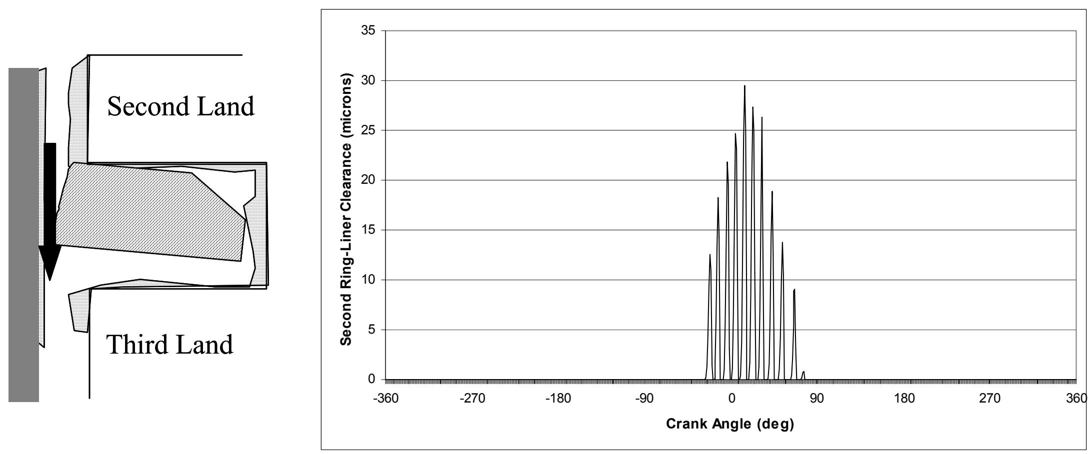

Figure 4-7: Second Ring Collapse

A second ring with a negative static twist allows the gas flow to penetrate to the lower lands from the second land, and therefore eliminates top ring reverse flutter, and the potential second ring collapse. This result is illustrated in Figure 4-8.

The elimination of top ring reverse flutter through the use of the negative static twist second ring design has the potential to reduce oil consumption in the engine. It is therefore recommended that this design be used with the reduced tension oil control ring so that the reduction in tension does not significantly increase oil consumption overall.

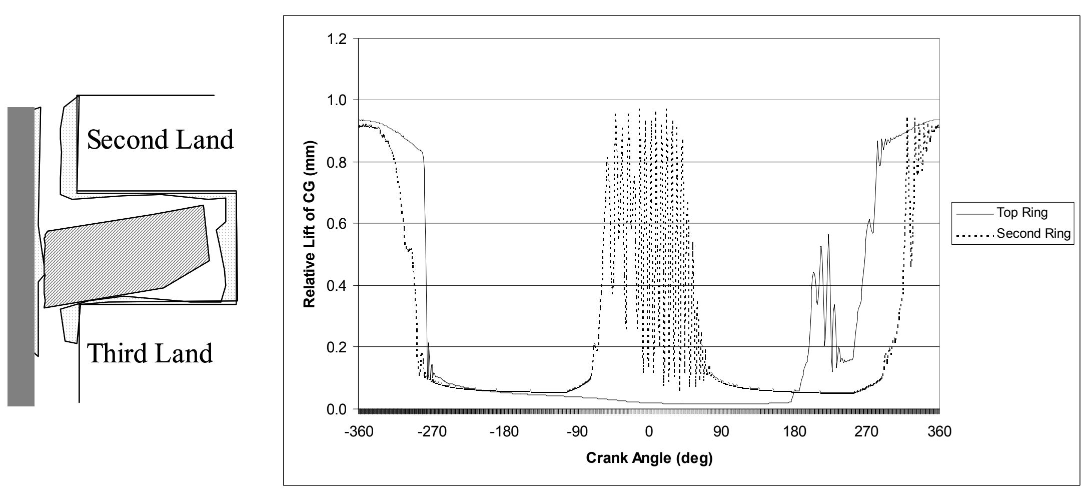

Figure 4-8: Second Ring with Negative Static Twist

4.4.3. Effect of Oil Control Ring Conformability on Oil Consumption

Another design strategy that could be used in combination with the reduced tension oil control ring to compensate for the increased oil consumption is the reduction of the radial thickness of the cross-section of the oil control ring. If the cross-sectional area is reduced, the moment of inertia is also reduced. This is because the moment of inertia is determined by the sum of the squares of the radial distances between the centroid of the cross-section and the origin at each element of area of the ring. Therefore, if the overall area is reduced, there are fewer contributions to the overall area, and the moment of inertia is thus reduced. If this is the case, bending is promoted about the axis perpendicular to the plane of the ring, leading to improved conformability.

However, designing the oil control ring with a smaller area results in a reduction in the structural strength of the ring, which may compromise ring life. A stiffer material could be used to compensate for this effect, but this would result in a decrease in conformability overall, since the stiffness of the material has a more significant effect on conformability than the cross-sectional area of the ring. Therefore, the improvement in conformability that can be achieved by a reduction in the cross-sectional area of the ring is limited by structural considerations, and may not be the most effective design strategy.

4.5. Additional Design Limitations

4.5.1. Manufacturing Limitations

Typical axial heights of piston rings range from 1 mm to 4 mm. As a result, machining the rings to precisely match the design specifications is difficult, and tolerances are often on the order of the design values themselves. Care thus needs to be taken when developing designs to ensure that allowances are made for such tolerances.

Certain designs are limited by these tolerances. In particular, the top ring profile can only be machined within certain tolerances, and as a result, there are limitations on the design values that can be specified.

In this study, the effect of producing designs at the limits of the various tolerances was evaluated using the modeling tools. In other words, the friction reduction potential of each of the designs was assessed for each case with an upper and a lower limit representing the extreme cases for machining the rings at the edge of the tolerance ranges. This facilitated the optimization of the final designs to ensure that a reduction in friction was predicted by the modeling tools.

4.5.2. Transition to Boundary Lubrication at Midstroke

In several of the designs presented in the previous sections, the physical length between the top ring's minimum point and its lower edge in the untwisted state (B_2 in Figure

3-12) was reduced. If this length is reduced significantly, it can result in the onset of boundary lubrication conditions throughout the entire engine cycle.

For most of the engine cycle, the top ring is typically designed to be in hydrodynamic lubrication, except near dead centers when piston speed is reduced significantly and hydrodynamic lubrication cannot be sustained. If B_2 is reduced beyond a certain extent, the top ring will become fully-flooded at the leading edge on downstrokes. This is because the oil supply is fixed, but the amount of space available under the ring is decreasing as B_2 is reduced. Once the top ring becomes fully-flooded on downstrokes, because of the fixed oil supply, less oil can fit under the ring as B_2 is reduced further. Therefore, further reduction in B_2 results in a reduction in oil film thickness, h_o, and eventually, the condition defined in Eq. (2.1) is met and boundary lubrication conditions are present even in the midstroke regions of the engine cycle. As was pointed out throughout this study, boundary friction losses are much higher than friction losses from hydrodynamic lubrication, and therefore the onset of this condition throughout the cycle causes a significant increase in the friction generated by the top ring along the liner. This condition thus sets an upper limit on the potential reduction of B_2 through a reduction in axial height or through the use of a skewed barrel profile.

In general, as long as boundary lubrication conditions are not present in the midstroke regions of the engine cycle, the top ring friction generated in the midstroke region is a negligible part of the total friction generated by the top ring for high load, low speed operating conditions. However, as pointed out in Section 3, for low load, high speed conditions, midstroke friction generated by the top ring becomes significant. Although the present study focuses on high load, low speed engines, an approach to identify strategies for the reduction of top ring midstroke friction was also suggested. This was included because once the contribution of the top ring friction generated around TDC of compression/expansion is reduced through various design changes, the top ring friction at midstroke is the next area which can be targeted for further friction reduction.

5. Application of Reduced Friction Design Strategies to a Natural Gas Power Generation Engine

In the following Section, the reduced friction strategies developed in Section 4 are applied to re-design the piston rings of a natural gas power generation engine with the goal of reducing friction to improve the engine's efficiency. Model predictions are first obtained to compare the effectiveness of each of the low-friction design strategies in the Waukesha engine. Based on the results of this comparison, several low-friction designs were selected for experimental investigation. The logic behind this selection process is briefly described. The experimental procedure used to evaluate the designs is then described in detail in a later section, and the results are presented and compared with the corresponding model results for those specific changes.

5.1. Description of Engine and Relevant Specifications

The engine selected for this study was a Waukesha spark-ignited natural gas power generation engine. Relevant specifications for this engine are shown in below in Table 5-1. The operating condition selected for this study was based on a typical operating condition that is ideal for interfacing with power generation equipment. It should be noted that all of the model predictions that will be presented in the sections that follow are based on normalized design values so that the current design values remain confidential.

Engine Configuration	6 Cylinders, Inline
Displacement	18 liters
Bore, Stroke	152 mm, 165 mm
Speed	1800 rpm
Load Condition	1360 kPa BMEP

Table 5-1: Waukesha Engine Specifications

5.2. Reduced Friction Designs and Model Predictions

In the section that follows, model predictions are presented to illustrate the effect of implementing the different design strategies investigated in this study on friction in the Waukesha engine. The results are presented in terms of FMEP, which is the integrated effect of the friction power losses over the engine cycle, normalized by the engine's displaced volume. Details on the determination of FMEP from friction power losses throughout the engine cycle are given in Appendix B. In this study, model predictions were obtained for both oil supply conditions, OS1 and OS2, to bracket the actual FMEP between the upper and lower limits.

5.2.1. Reduced Tension Oil Control Ring

Model predictions for the effect of reducing oil control ring tension on friction in the Waukesha engine are presented in the figures below. Figure 5-1 and Figure 5-2 show the effect of reducing oil control ring tension on oil control ring FMEP and total ring pack FMEP, respectively.

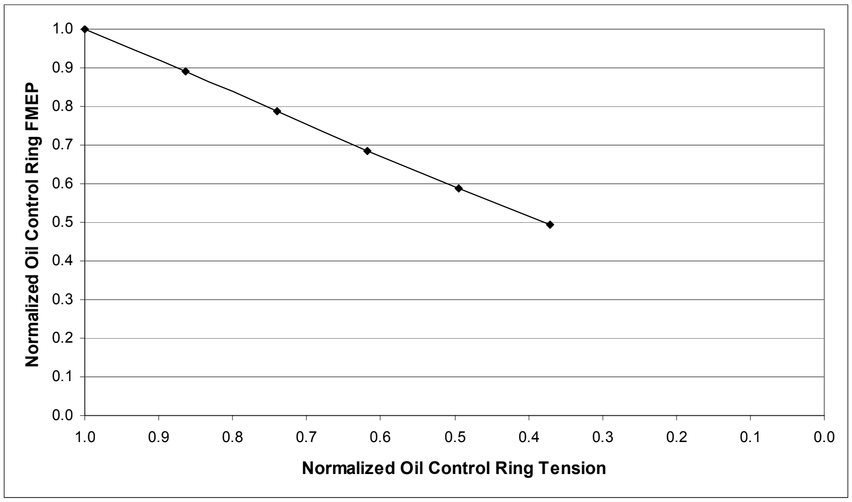

Figure 5-1: Effect of Oil Control Ring Tension on Oil Control Ring FMEP

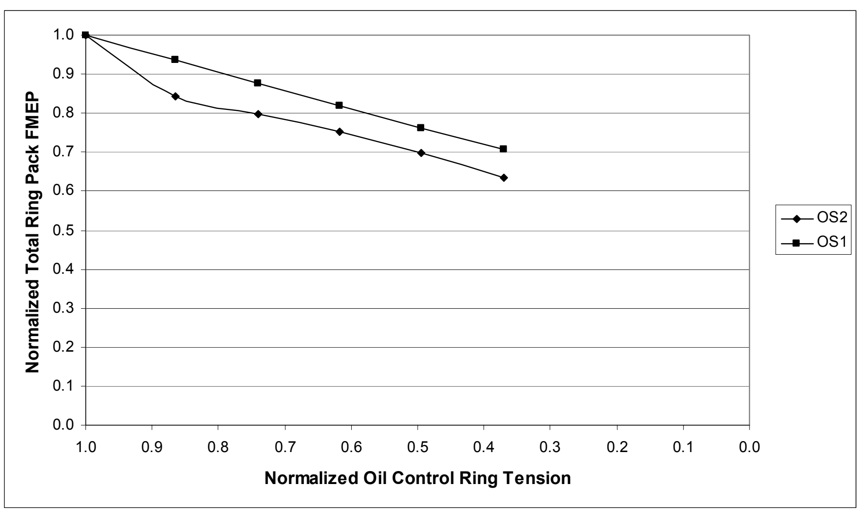

Figure 5-2: Effect of Oil Control Ring Tension on Total Ring Pack FMEP

It should be noted that in Figure 5-2, there is no distinction between OS1 and OS2 as the oil supply conditions do not affect the oil control ring, which is assumed to be fully-flooded on both upstrokes and downstrokes in the model as discussed in Section 2. It can be seen in the above figures that if oil control ring tension were reduced by half of its total value, oil control ring FMEP would be reduced by 40% and total ring pack FMEP would be reduced by 30-35%.

The sharp decrease in total ring pack FMEP in the case of OS2 for a reduction in oil control ring tension from a normalized value of 1.000 to 0.864 can be attributed to the top ring gaining hydrodynamic lubrication on the expansion stroke for the cases where the tension is below the normalized value of 0.864. If the tension is larger than this value, the oil control ring leaves an insufficient amount of oil on the liner and the top ring is in pure boundary lubrication conditions throughout the engine cycle.

5.2.2. Skewed Barrel Top Ring

Model predictions for the effect of a skewed barrel top ring profile on top ring friction in the Waukesha engine are presented in the figures below. In Section 4.1.1, the effect of decreasing B_2 on friction was discussed. Figure 5-3 and Figure 5-4 show the effect of the reduction of B_2 on top ring FMEP and total ring pack FMEP, respectively.

As can be seen from the figures, the introduction of a skewed barrel profile can reduce top ring FMEP by up to 45% irrespective of the oil supply condition, and total ring pack FMEP by 15-25%. The reduction in total ring pack FMEP is larger for the case of OS2 because the top ring contributes much more significantly to the total ring pack FMEP due to the poorer oil supply assumed in this case.

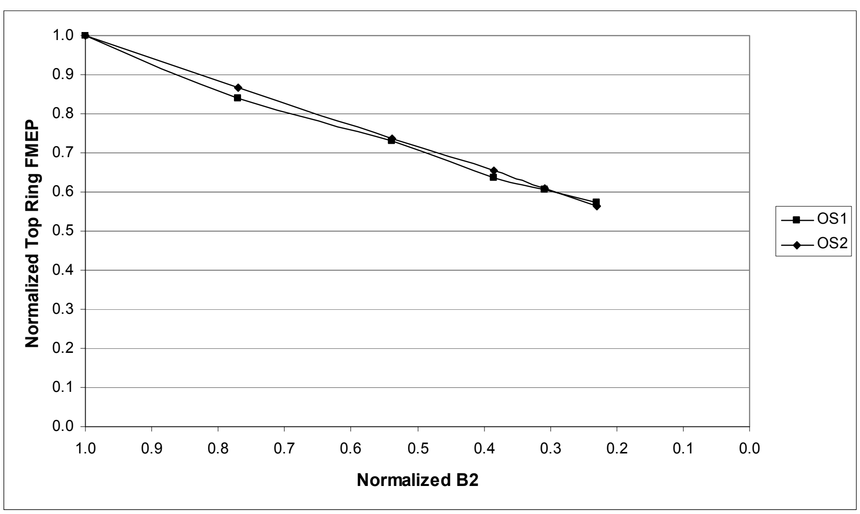

Figure 5-3: Effect of Skewed Barrel Profile on Top Ring FMEP

5.2.3. Reduced Axial Height Top Ring

Model predictions for the effect of reducing the axial height of the top ring on friction in the Waukesha engine are presented in the figures below. Figure 5-5 and Figure 5-6 show the effect of the reduction of axial height on top ring FMEP and total ring pack FMEP, respectively.

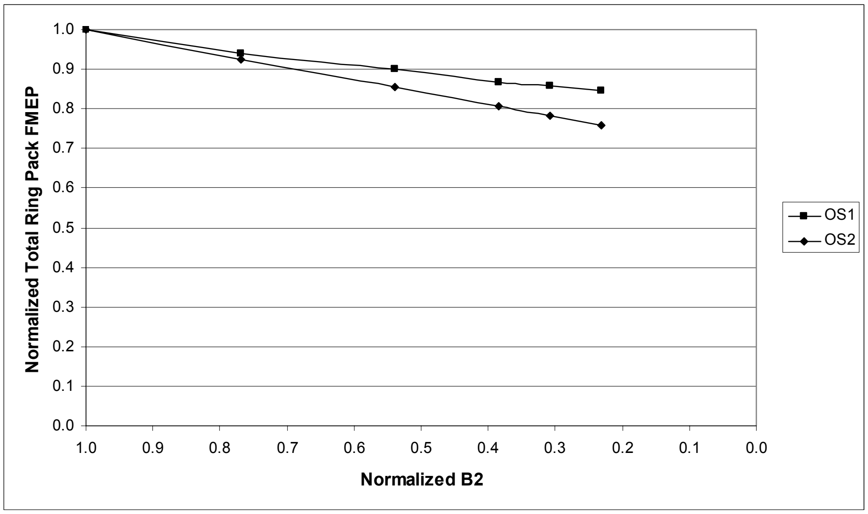

Figure 5-4: Effect of Skewed Barrel Profile on Total Ring Pack FMEP

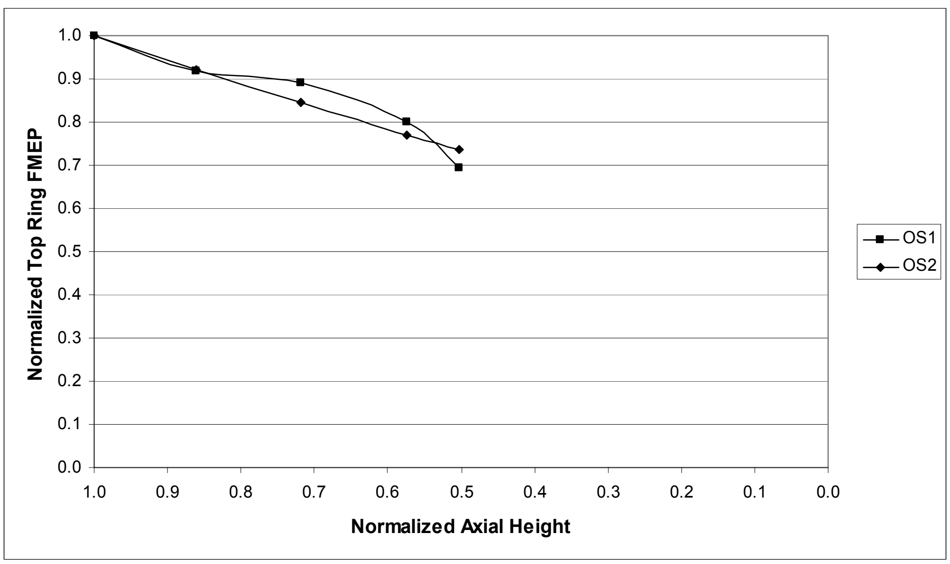

Figure 5-5: Effect of Top Ring Axial Height on Top Ring FMEP

As can be seen in the figures, a reduction in the axial height of the top ring can result in a reduction in top ring FMEP of up to 25%, regardless of the oil supply condition. For the case of the total ring pack, FMEP can be reduced by 10-15% by a reduction in top ring axial height. Again, as in the case of the skewed barrel profile, the reduction of total ring pack FMEP is higher for the case of OS2 because of the larger contribution of the top ring to total ring pack friction in that case.

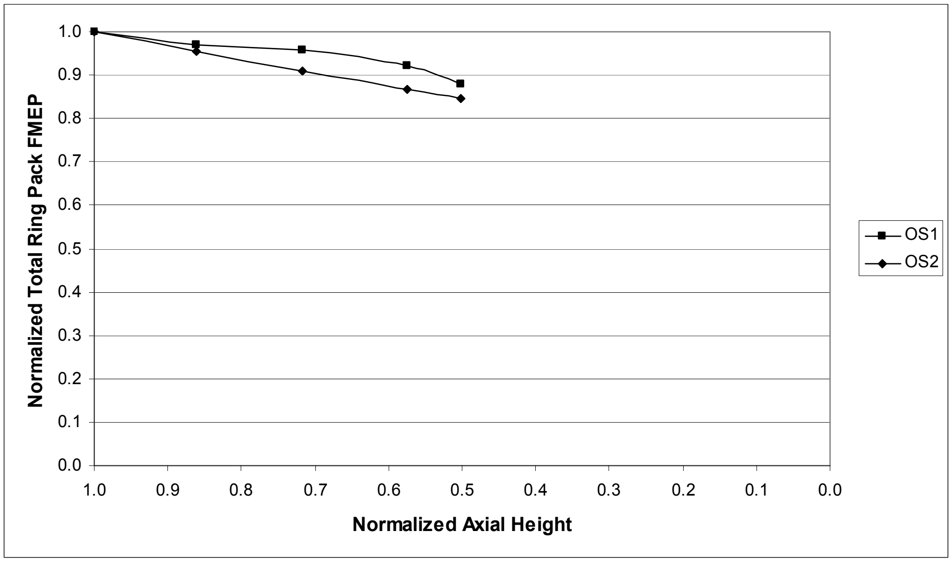

Figure 5-6: Effect of Top Ring Axial Height on Total Ring Pack FMEP

It should be noted that since the focus of this study is on the reduction of top ring boundary friction around TDC of compression, the objective is to reduce B_2 and therefore either the skewed barrel profile or the axial height reduction should yield similar results. However, the reduced axial height rings have been shown to have lower structural strength, leading to earlier failure, as discussed in Section 4.3.1. Therefore, the skewed barrel profile design is more advantageous from the standpoint of ring life and reduced friction.

5.2.4. Upward Top Ring Groove Tilt

Model predictions for the effect of increasing the top ring groove tilt on friction in the Waukesha engine are presented in the figures below. Figure 5-7 and Figure 5-8 show the effect a top ring groove with an upward tilt on top ring FMEP and total ring pack FMEP, respectively.

As can be seen in the figures, the upward top ring groove tilt can result in a reduction in top ring FMEP of up to 25%, regardless of the oil supply condition. For the case of the total ring pack, FMEP can be reduced by 10%.

There are several trends that can be observed from these figures that require more detailed explanation. Firstly, for the case of both OS1 and OS2, for an increase in groove tilt beyond a normalized value of 0.571, the FMEP remains fairly constant. This can be explained by considering the dynamics of the top ring as it travels in the dry region. The development of this upward groove tilt strategy assumed that the top ring would conform fairly well to the lower groove flank and that as a result, the position of the minimum point on the top ring would be lower on the profile when the groove tilt was increased. However, the top ring does not actually conform very well to the lower groove flank during this part of the engine cycle. This is confirmed by the model predictions, and is illustrated by a plot of the top ring twist as shown below in Figure 5-9 for the case of three upward groove tilts with normalized values of 0.429, 0.857 and 1. It should be noted that the small fluctuations in the ring twist Figure 5-9 are a result of the instability of the ring in this configuration due to the concentrated outer diameter contact on the lower groove flank. As can be seen from this figure, the top ring twist increases between groove tilts of 0.429 and 0.857, but between 0.857 and 1, there is no significant increase. As a result, the minimum point position does not change and there is no reason to expect a reduction in FMEP.

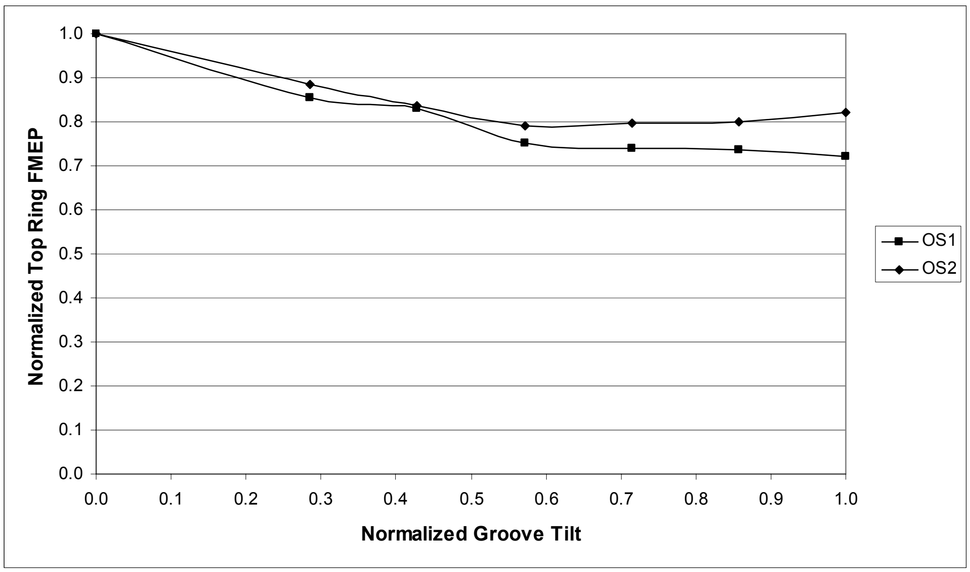

Figure 5-7: Effect of Top Ring Groove Upward Tilt on Top Ring FMEP

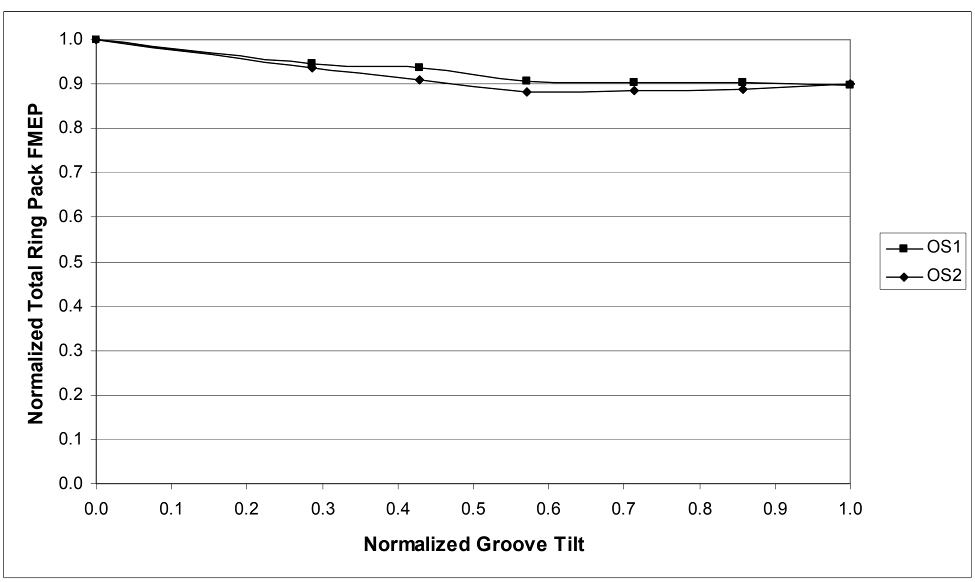

Figure 5-8: Effect of Upward Top Ring Groove Tilt on Top Ring FMEP

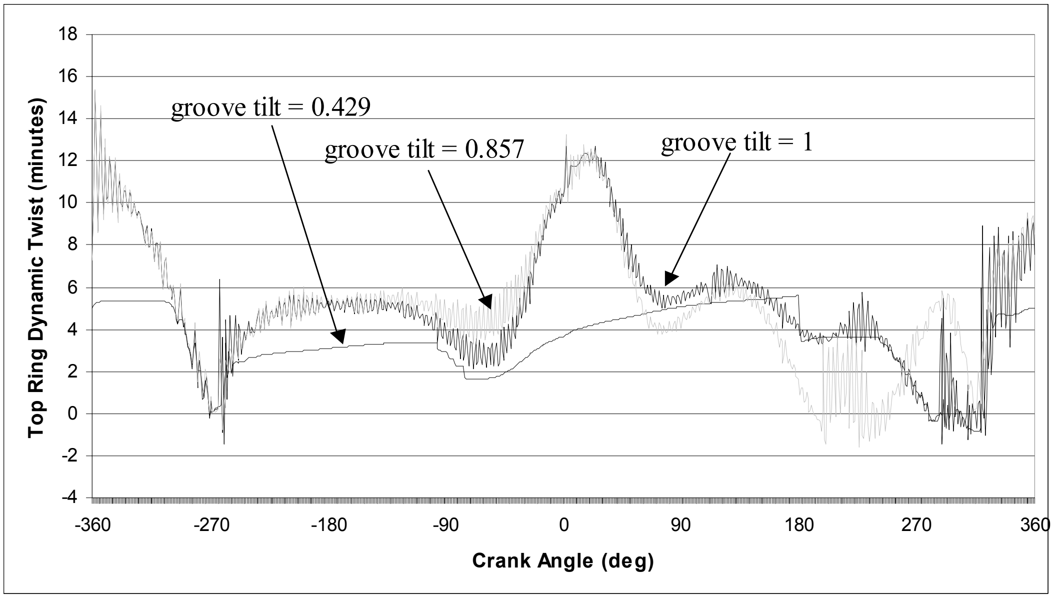

Figure 5-9: Effect of Groove Tilt on Top Ring Dynamic Twist

Before providing insight into this apparent limit in top ring twist that is reached after a certain groove tilt is exceeded, the governing forces and moments acting on the top ring to create the positive twist around TDC of compression must first be described. The positive top ring twist around TDC of compression is a result of the counterclockwise net moment acting on the top ring during this period. In Figure 5-10, the integrated moments acting on the top ring around TDC of compression are plotted, along with the resulting top ring dynamic twist. The convention adopted in this figure is that a positive moment results in a positive or counterclockwise twist. It can be seen from Figure 5-10 that there is a clockwise moment exerted by the high gas pressure acting on the part of the top ring surface that is exposed to the clearance between the groove and the liner. Moments due to gas pressures acting on the rest of the top and bottom ring surfaces are balanced, because of the ability of the high-pressure gas to penetrate to the region below the ring due to the ring-groove configuration, as can be seen in the illustration of the top ring-groove configuration in Figure 5-11. The net moment due to the high gas pressure acting on the ring in the clearance between the groove and the liner is roughly balanced by the counterclockwise moment from asperity contact between the bottom face of the ring and the lower groove flank. The unbalanced positive moment acting on the top ring that results in the positive twist around TDC of compression comes from the force due ring-liner interaction.

To better explain the source of this moment, a simple diagram illustrating the forces and acting on the top ring around TDC of compression is shown in Figure 5-11. For illustrative purposes, without loss of generality, the second land pressure is assumed to be zero. The net force exerted by the ring on the liner due to the radial pressure difference is balanced by a reaction force of equal magnitude from the liner on the ring, which is concentrated around the minimum point. For simplicity, this force is assumed to act through the minimum point. There is thus a net positive moment acting on the ring because the line of action of the resultant of the pressure force acting on the inside surface of the ring is below the line of action of the resultant force acting at the minimum point.

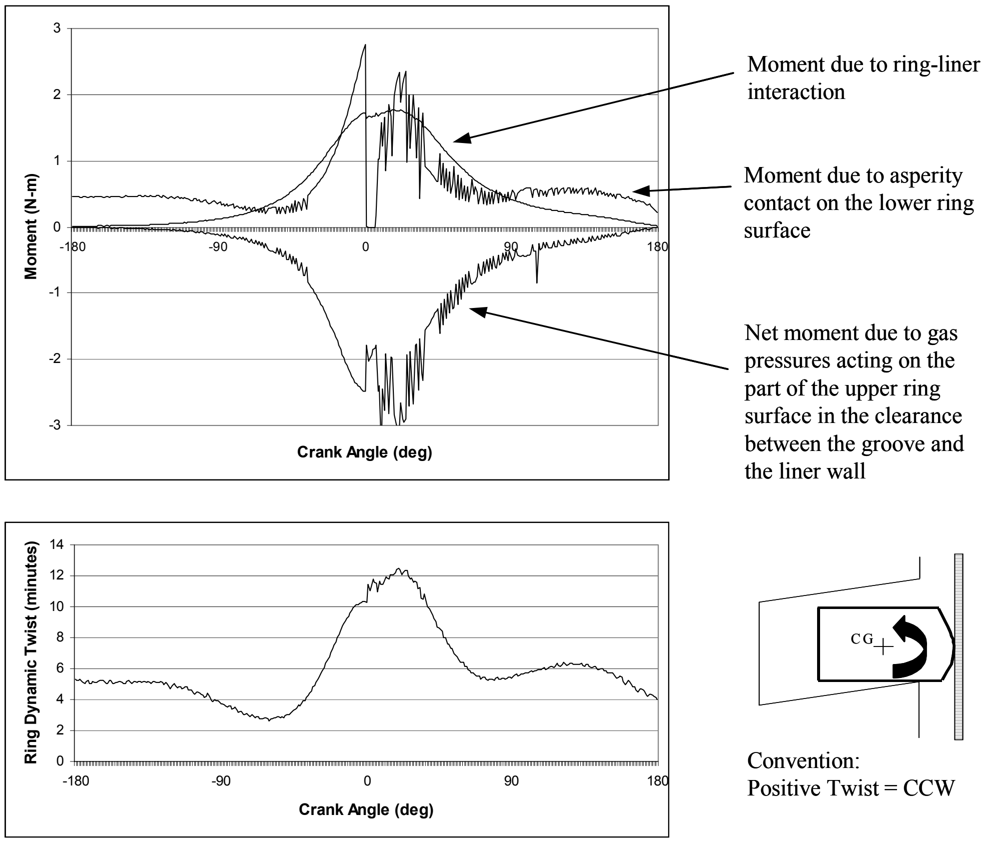

Figure 5-10: Top Ring Moments and Twist

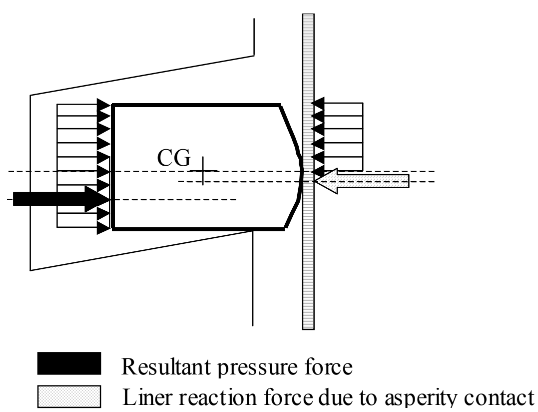

Figure 5-11: Illustration of Moments due to Ring-Liner Interaction

Now that the governing forces that lead to the top ring twist around TDC of compression have been described, insight can be given to explain the effect of increasing groove tilt on top ring twist. The difference in the top ring dynamic twist observed when top ring upward groove tilt is increased is actually a result of the change in the moment acting on the lower face of the top ring due to oil and gas pressure. When the upward groove tilt is small, there is less space between the lower ring surface and the groove and therefore more of the force acting on the lower ring surface comes from oil squeezing from the oil layer between the lower ring flank and the lower groove flank. As groove tilt is increased, more space exists between the ID of the lower surface of the top ring and the lower groove flank, and therefore there is less contact with oil. As a result, less negative moment is generated by oil squeezing and therefore the ring tends to twist more positively. This is shown below in Figure 5-12, which shows the integrated moment due to oil squeezing acting on the lower flank of the top ring for normalized groove tilts of 0.571 and 0.714, respectively. As can be seen in this figure, for a normalized groove tilt of 0.571, the integrated moment due to oil squeezing acts to create a positive twist at first, but then as the ring twists, the direction of this moment reverses due to the increasing contact area with the oil towards the ID of the top ring and the net oil squeezing moment becomes negative. For the case of a normalized groove tilt of 0.714, the oil squeezing moment is always positive because the larger groove tilt creates more space between the top ring and the lower groove flank towards the ID corner of the ring and therefore there is no contact with the oil to create a negative moment.

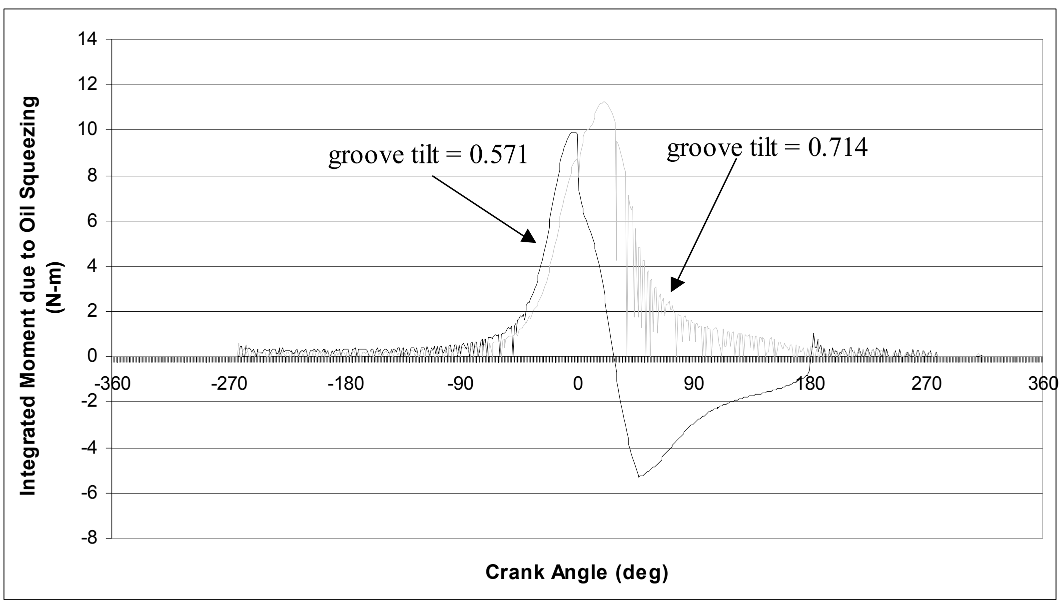

Figure 5-12: Effect of Groove Tilt on Oil Squeezing

Beyond a certain increase in groove tilt, there is no noticeable difference in the ring twist because no contact is made with the oil film between the lower ring surface and the groove and therefore further increase in groove tilt angle has no effect on top ring dynamics.

In summary, the net positive top ring twist that occurs around TDC of compression comes from the unbalanced moment due to ring-liner interaction. As groove tilt is increased, the contribution of the negative moment from oil squeezing between the lower ring surface and the lower groove flank decreases because less contact is made with the oil film. This occurs until a certain groove tilt is exceeded, at which point no further contact is made with the oil film. Therefore, there is no further increase in top ring positive twist beyond that groove tilt.

(B) EXPERIMENTAL

6. Experimental Validation

6.1 Test Matrix of Ring-Pack Designs

In order to validate the model predictions that were described in the previous sections, several reduced friction ring designs were procured and tested on the engine described in Section 5.1. All of the experimental work in this study was conducted at Colorado State University by students and faculty in the Engines and Energy Conversion Laboratory. The experiments were conducted with the primary goal of assessing the friction reduction achieved by the implementation of the reduced friction designs. Based on the model predictions obtained in the previous sections and the methods developed to minimize the adverse effects of the reduced friction designs, certain combinations of designs were selected for testing in this study. These are presented in the test matrix contained in Table 6-1 below.

Design Name	Top Ring	Second Ring	OCR	Piston
Baseline	Stock	Stock	Stock	Stock
Low-Tension OCR	Stock	Stock	Reduced Tension	Stock
Skewed Barrel Top Ring	Skewed Barrel	Stock	Stock	Stock
Low-Tension OCR, Reduced Oil Consumption	Stock	Negative Static Twist	Reduced Tension	Stock
Upward Top Ring Groove Tilt	High Static Twist	Stock	Stock	Upward Top Ring Groove Tilt
Optimized System	Skewed Barrel	Negative Static Twist	Reduced Tension	Stock

Table 6-1: Test Matrix

It should be noted that the reduced axial height top rings were not procured and tested in the experimental evaluation because the reduction in friction expected from this design is less than the reduction in friction expected from implementation of the other low-friction top ring designs. In addition, the smaller axial height is expected to reduce ring life. Therefore, this design was not investigated in the experimental portion of this study. In addition, although they were originally intended to be included in the experimental portion of this study, time constraints prevented the experimental investigation of the top ring groove upward tilt design and the second ring with negative twist.

6.2 Experimental Test Facility and Instrumentation

The Waukesha VGF-F18GL inline 6 engine described in Section 5.1 was used in the experiments at the Engines and Energy Conversion Laboratory at Colorado State University. The engine is an ARES (Advanced Reciprocating Engine Systems) class engine, which is a high efficiency low emissions engine typically in the 1 MW range used for power generation. The engine was installed and instrumented in a dynamometer test cell with the normal engine performance measurements (rpm, torque, coolant, lubricant, operating temperatures, etc.); see Figure 6-1. Specific measurements required included in-cylinder pressure from all cylinders from which the indicated effective pressure could be calculated. Brake torque measurement was required to determine the engine mechanical efficiency. Inter-ring pressure transducers were required in the engine to record inter-ring pressures for determination and validation of piston ring behavior. Blow-by and oil consumption measurements were recorded to check against model calculations and to monitor effects of friction variations on blow-by and oil consumption due to component changes.

Figure 6-1: Waukesha VGF-F18GL Installed at the Large Bore Engine Test Bed at Colorado State University

Instrumentation

A Midwest Dynamometer model 322 eddy-current dynamometer was used to control load on the engine, as shown in Figure 6-2. Rosemount 3051 pressure transmitters were employed for most of the system pressure measurement. Temperatures were measured using type Omega J type thermocouples. Control and monitoring of the system was accomplished using National Instruments Field Point DAQ and control in conjunction with LabView software. For in cylinder pressure measurement Kistler 6067C water cooled pressure transducers generously donated by Kistler Corporation were used due to the high level of accuracy needed in computing mean effective pressures.

6.3 Measurements

6.3.1 Friction and Mean Effective Pressures

The key measurement of friction levels within and engine is friction mean effective pressure (FMEP). FMEP is calculated using two parameters derived from measurement: net (indicated) mean effective pressure (NMEP) and brake mean effective pressure (BMEP)

$$FMEP = NMEP - BMEP$$

Equation 1

BMEP is the shaft output power measured as torque by the dynamometer.

Figure 6-2: Eddy Current Dynamometer

In order to calculate FMEP, BMEP and NMEP must be calculated. BMEP is calculated from torque using the equation:

$$BMEP = \frac{4 * \pi * \tau}{V_d}$$

Equation 2

Where τ is engine torque and V_d is the engine displacement. Engine torque is measured using an eddy current dynamometer. The dynamometer is accurate to .5% of scale. For this test series full scale was 1525 ft*lbs.

NMEP is the power created within the cylinder minus the pumping losses. NMEP was calculated from recordings of cylinder pressure traces using:

$$NMEP = \frac{\frac{2\pi}{360} \int_{-360}^{360} (P \frac{dV}{d\theta}) d\theta}{V_d}$$

Equation 3

NMEP was calculated for each cycle and averaged over 1000 cycles. The data acquisition system used was a Hi-Techniques Win600 high speed DAQ model. Calculations were made using REVelation software provided with the high speed DAQ.

Friction reduction was quantified by measuring the change in FMEP from the baseline design for each of the reduced friction designs. More details of the method used for this calculation are described in Appendix B. It was not possible to measure the specific FMEP contribution from the piston ring pack in this study, because this would require knowing the exact contribution of the ring pack to overall friction in the engine. Although this information was available from motoring friction data obtained from a teardown test, motoring friction data does not reflect the effect of high pressures in the cylinder, which has a very important effect on friction [1]. Therefore, the only way in which the designs could be evaluated was by measuring the change in FMEP for each of the designs compared to the baseline case. With this method, it is not necessary to know the specific contribution of the ring pack friction to overall FMEP, as the change in FMEP should reflect only the effect of changing the piston rings, provided everything else is held relatively constant.

6.3.2 Oil Consumption Measurements

A highly accurate oil consumption meter, AVL model 403S, shown in Figure 6-3, was used to measure oil consumption. This device uses a sensor to measure the change in oil level in the sump. The sensor is a cylindrical container of oil filled to the same level as the sump, mounted at the same height above the ground. To measure oil consumption, a refill method is used in which a predetermined mass of oil to be used to refill the system is set as an input into the control unit. This oil consumption meter has a refill accuracy of ±1gram and a refill level accuracy of ±2 μm allowing for relatively short test points (~3 hours). The method used for testing was a constant level method. At the beginning of a test point the oil consumption meter records the initial level of the oil in the crankcase. It then meters in a precise amount of oil. This creates a rise in the oil level within the crankcase. The meter then measures the time it takes for the oil level to return to its original level at which time the oil is considered consumed. The process is repeated, for ~3 hours and an average is taken over all of the fills. Obtaining accurate results with this method requires that no changes in speed and load of the engine be made during the measurement time. In addition, the engine must be at a thermally stable at the desired operating condition when the test begins.

6.3.3 Blow-by Flow Measurements

For blow-by flow, a J-Tec Associates VF563B in-line flow meter specifically designed for blow-by flow measurement was used, as shown in Figure 6-4. Its accuracy is ± 2% of full scale, which is 16 ACFM for this meter. This meter uses the principle of vortex shedding to measure the flow rate of the blowby gases. A small strut inside the flow tube creates Karman vortices, and the frequency of the vortices is measured by an ultrasonic beam. Since the Strouhal number, $St = fL/v$, is constant over a wide range of Reynolds numbers, the flow velocity is directly proportional to the vortex shedding frequency. The volumetric flow rate is determined from the flow velocity.

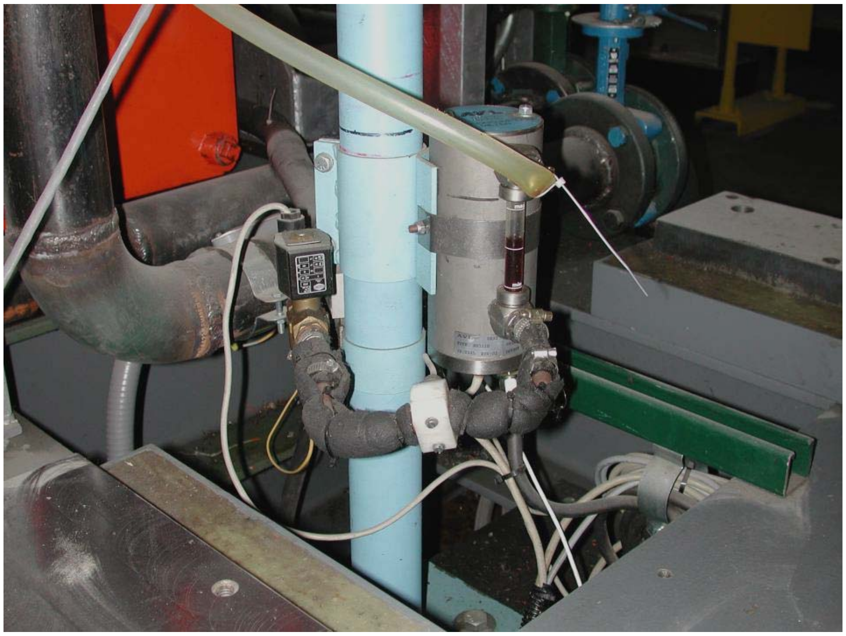

Figure 6-3: AVL 403S Oil Consumption Meter

Figure 6-4: J-Tech Associates VF563B In-Line Blow-by Meter

6.3.4 Inter-Ring Pressures

The inter-ring pressure transducers were located at three specific positions along the liner in cylinder #5, Figure 6-5. For this application, the Kistler 6052A pressure transducer was chosen due to its compact size and sleeve mounting capability. Installation of these sensors required precision machining to be done both on the engine and on the cylinder liner. These sensors were required to mount through the crankcase, through a jacket water cavity and were attached to the cylinder liner. Transducer 1 was located in between the TDC position of the top ring and the TDC position of the second ring. Transducer 2 was located between the TDC position of the second ring and the TDC position of the oil control ring. Transducer 3 was located between the BDC position of the top ring and the BDC position of the second ring. These locations were chosen so as to provide pressure data in the most interesting parts of the engine cycle for this study. As mentioned previously, the accuracy of pressure measurements obtained from pressure transducers makes this an effective method by which to check the consistency between the model and the experiment.

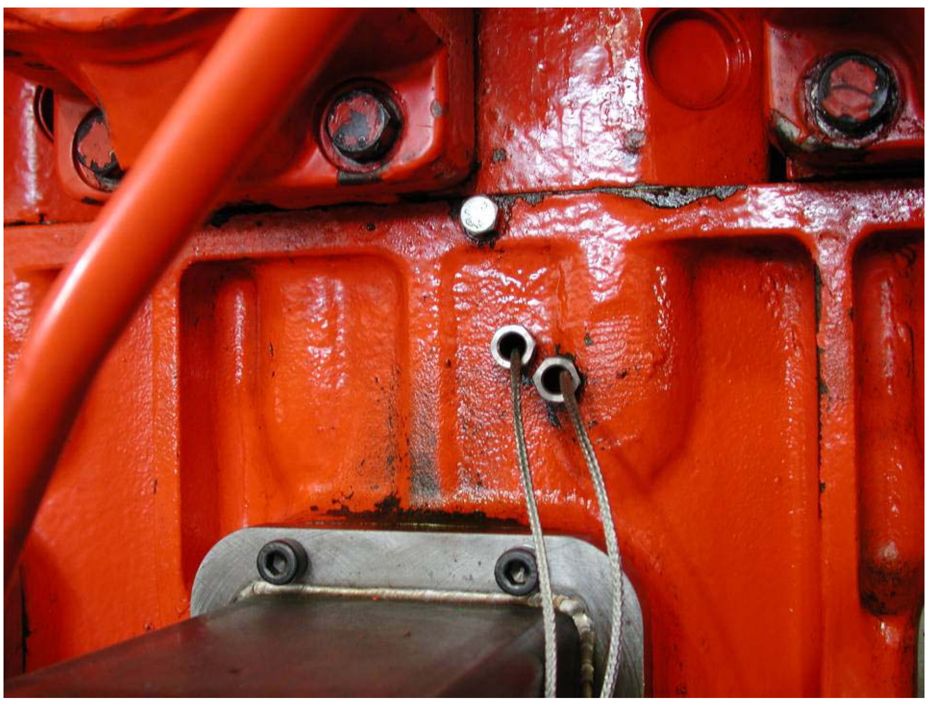

Figure 5-5: Inter-ring Pressure Transducers Installed on Engine

6.4 Experimental Procedure

6.4.1 Engine Operating Condition and Data Acquisition

For this study, the five engine operating points were tested, shown in Table 6-2. The fifth point in the matrix (point 5) equates to the engine operating at 200 psi BMEP. Complete emissions, DAQ and combustion data points were taken at each test point. The DAQ data was averaged over five minute test points, and the combustion data was averaged over 1000 cycles. Oil consumption data was only taken at test point five due to the time necessary to ensure accurate oil consumption data. During this ~3 hour data point, three emissions, DAQ, and combustion data points were taken: one at the beginning of the oil consumption test, one approximately half way through the point and one at the end. This repetition was used to ensure that engine operation was remaining stable during the oil consumption point. For each of the ring packs discussed in this report, other than the baseline case which had already been broken in, initial break-in was done at Waukesha Engine Dresser Inc.

Test Point	Speed		Load	
	RPM	% of Rated	ft*lbs	% of Rated
1	1800	100	875	60
2	1800	100	1021	70
3	1800	100	1167	80
4	1800	100	1313	90
5	1800	100	1459	100

Table 6-2: Friction Reduction Engine Operating-Condition Test Points

6.4.2 Test and Measurement Steps

The following procedure was used to obtain the required data from the experiment for each set of piston rings as described in the test matrix in Table 6-1.

For each test that was conducted, the engine was run for 30-45 minutes to allow it to reach thermal stability. Thermal stability was achieved when the cooling water reached 180°C and the oil temperature reached 175°C. After these temperatures were reached, they were held at that level by a closed-loop control system. Once thermal stability was achieved, 1000 cycles of cylinder pressure data were recorded over all 6 cylinders. In addition, 1000 cycles of inter-ring pressure data were recorded in cylinder #5.

The torque and blowby flow rate, along with other slow-speed measurement data such as temperatures and pressures taken in various parts of the engine were then taken using a 5 minute running average with a 1 Hz sampling frequency during that time. It should be noted that the load cell used to measure torque was calibrated to an accuracy of +/-10 Nm.

Oil consumption data was averaged over three hours and measurements were taken on an hourly basis following the 30-45 minute warm-up period to thermally stabilize the engine, and the 5 minute running average tests. Oil consumption was measured for each of the different designs, but could not be compared to any specific model prediction, as the model is not currently capable of predicting overall oil consumption quantitatively.

Before any of the reduced friction designs were investigated, test results were first obtained from running the engine with the stock piston ring pack. This was done for several purposes:

- To investigate and evaluate the variability and repeatability of the pressure measurements obtained by CSU
- To compare the land pressure measurements with the model predictions in order to assess the level of agreement between the model predictions and experimental results

- To obtain baseline values for FMEP, blowby and oil consumption to assess both the level of agreement between the model and the experiment, and the change in these measured values resulting from implementation of the reduced friction designs

Results from the baseline test in terms of each of the above criteria are presented in the sections that follow.

6.5 Data Analysis

6.5.1 Variability and Repeatability of Measured Data

One of the most major concerns in this study in the comparison between the model predictions and experimental results was the potential variation in the ambient conditions and engine operation that might lead to appreciable variations in the IMEP data obtained and lack of repeatability in the measurements. If the variability in the IMEP data were on the order of the expected friction reduction, the experimental component of this study would be inconclusive. This was less likely to be the case with a larger data set, and therefore three test runs were conducted at the rated operating condition being tested. An average was taken over the three tests in order to try to minimize the potential errors introduced by these factors.

In order to evaluate the variability and repeatability of the pressure measurements, IMEP data was calculated from the cylinder pressure data for each of the 1000 cycles over all six cylinders, and is plotted in a histogram in Figure 6-6. For ease of comparison, a normal distribution is plotted above the IMEP data. It should also be noted that the data in Figure 6-6 was only taken over one test run. In the tests that were conducted for the purposes of evaluating friction reduction in this study, the data was taken over three test runs and averaged, which should reduce the standard deviation and make the actual distribution even closer to normal.

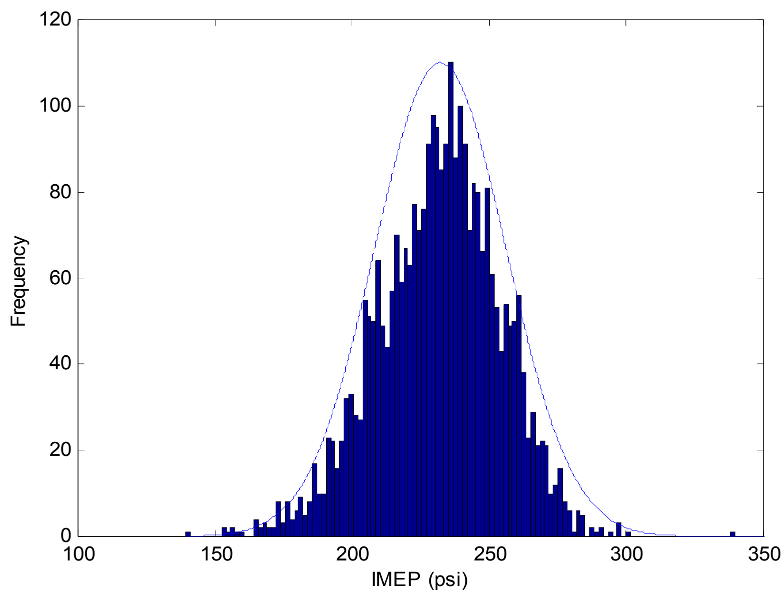

Figure 6-6: Distribution of IMEP Measurements

Since the data follows a normal distribution, if a reduction in friction is observed on average between the different designs that are to be investigated in this study, it is much more credible than if the data were scattered in a more random pattern. Since the reduction in friction is expected to be small compared to the values being measured, the credibility of any conclusions that are drawn depends on the spread of the data obtained. A normal distribution indicates that a sufficient number of data points have been taken to ensure that a credible average value is obtained, and this lends belief to conclusions that were drawn in this study.

To further reinforce the quality of the conclusions drawn from this study, a statistical analysis was conducted on all of the data obtained from each of the tests in order to determine whether or not a change has occurred between designs. Hypothesis testing was conducted on the difference in the mean values using a confidence interval of 95%. The details of this calculation are described in Appendix B.

6.5.2 Comparison of Inter-Ring Pressure Data

To assess the level of agreement between the model and the experiment, the interring pressure data obtained from the transducers in cylinder #5 was compared to the land pressures predicted by the model. In order to carry out this comparison, a representative cycle was taken out of the 1000 cycles of pressure data recorded. A representative cycle was used rather than averaged data so that no physically significant fluctuations in the pressure were damped out by the averaging process. The experimentally obtained pressure data is shown in Figure 6-7 below, along with a diagram illustrating the locations of the pressure transducers along the liner in cylinder #5.

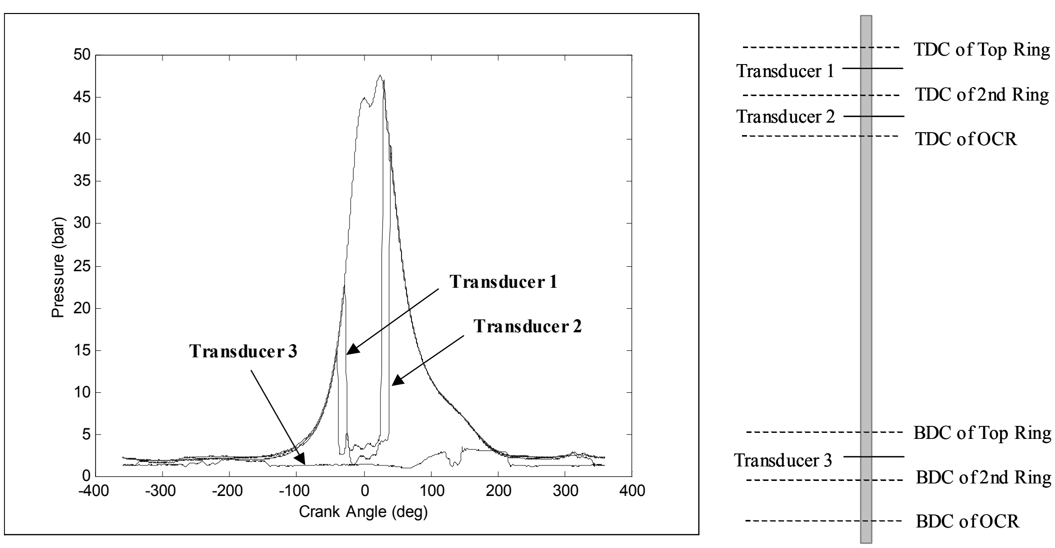

Figure 6-7: Experimental Pressure Data

The cylinder pressure data from the representative cycle mentioned above was used as input into the model and inter-ring pressure predictions were obtained. In order to more carefully consider the qualitative agreement between the experiment and the model, certain parts of the engine cycle were compared more closely. It should be noted that data for the entire engine cycle could not be compared because the pressure transducers only measure interring pressures in certain parts of the cycle, whereas the model predicts land pressure data throughout the cycle. The region of most significance for comparison is the region around TDC of compression, as this is where two of the transducers are located. For clarity, the pressure predictions obtained experimentally are magnified below in Figure 6-8 to show the region of interest.

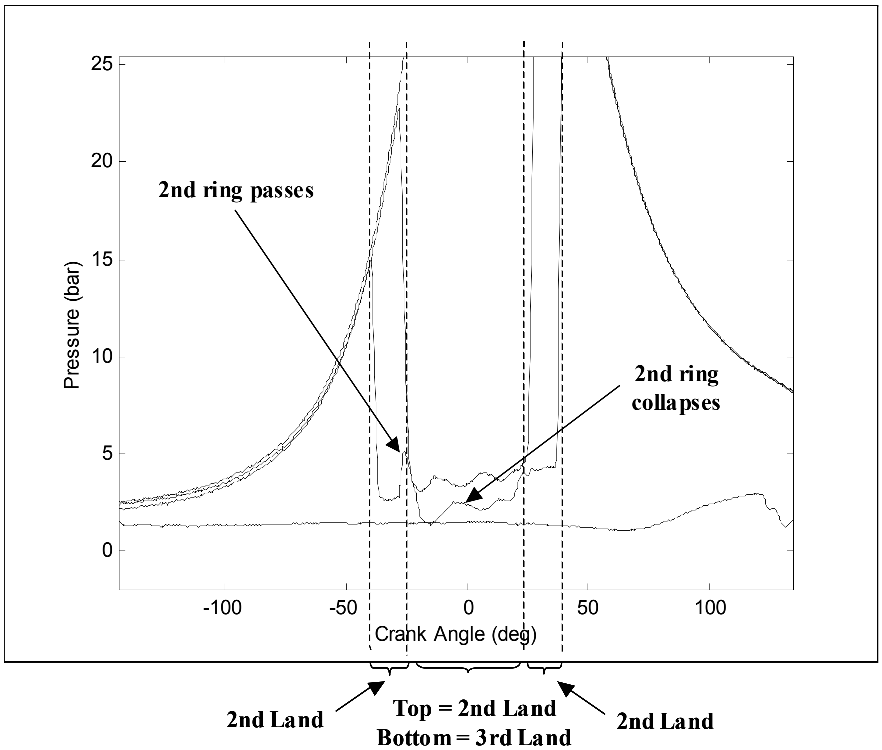

Figure 6-8: Magnified View of Pressure Data around TDC of Compression

The fluctuations that can be seen in the land pressure data are likely to be a result of a phenomenon called second ring collapse, which was briefly mentioned in Section 4.4.2. The physics of second ring collapse is discussed in detail in [21]. Ring collapse occurs when the upper ID corner of the ring is sealed against the top of the groove, and therefore the pressure acting downward on the ring face is able to push the ring inward before it can push it downward, as was depicted in Figure 4-7. This results in a large flow rate of gases from the cylinder passing through the ring-liner interface until the tension of the ring pushes it back against the liner and the process repeats again. This phenomenon happens more readily to the second ring as a result of its tendency to seal the upper OD corner of the groove and block the path for gas flow into the second ring groove. The spike that is present in the data from Transducer 2 in Figure 6-8 occurs when the second ring passes the transducer. When this happens, the volume of the region exposed to the transducer hole is significantly reduced and therefore the pressure increases, resulting in the spike. It is interesting to note that the same spike is not observed when the second ring passes at the beginning of the expansion stroke. If the second ring were collapsing during that period, there would be a significantly larger separation between the ring and the liner and this would explain the missing pressure spike.

To evaluate the agreement between the model and experiment, both model predictions and experimental pressure data are plotted in the region of interest around TDC of compression in Figure 6-9 below. In this figure, the dot-dashed lines indicate the pressure transducer data that was shown in Figure 6-8, and the solid lines represent data obtained by the model as indicated in the figure.

Overall, there is very good qualitative and quantitative agreement between the experimental and the model. In accordance with experimental findings, the model predicts second ring collapse in the region around TDC of compression as shown by the pressure fluctuations in the second and third land that are similar in magnitude to the experimental predictions. Good agreement is obtained in terms of the magnitude of the pressure data over most of the region under consideration.

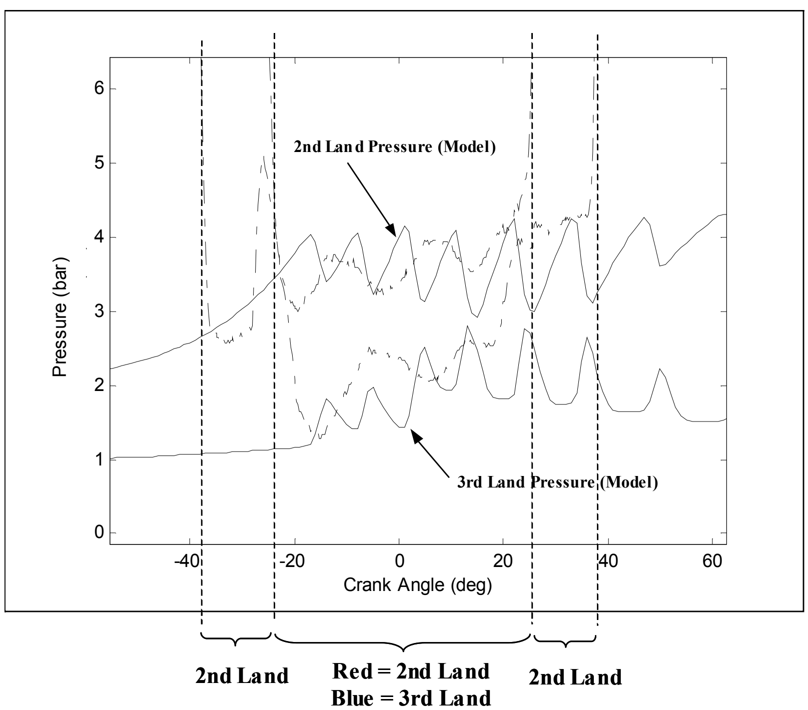

Figure 6-9: Comparison of Pressure Data between Model and Experiment

This comparison between the pressure data was carried out for each of the ring designs that were investigated in this study. For brevity, data is not shown for each case, as there was generally good agreement observed.

Having established good agreement in the pressure data between the model and the experiment, the designs were then evaluated and compared to assess friction reduction, as well as any potential changes in oil consumption or blowby. These results are included in the sections that follow, beginning with the baseline test results, which were used as a basis for comparison for each of the reduced friction designs.

6.6 Results for Baseline Ring-Pack Configuration

After commissioning of the engine, baseline measurements were taken. The data showed an FMEP of between 137.9 and 144.8 kPa (20 and 21 psi) at rated speed and load, blow-by of approximately 69.4 l/min (2.5 SCFM) and oil consumption of 48.4 (g/hr). Three DAQ and combustion points were taken over the course of the oil consumption point. These are the three points represented in Figures 6-10 and 6-11 for the 100% load point.

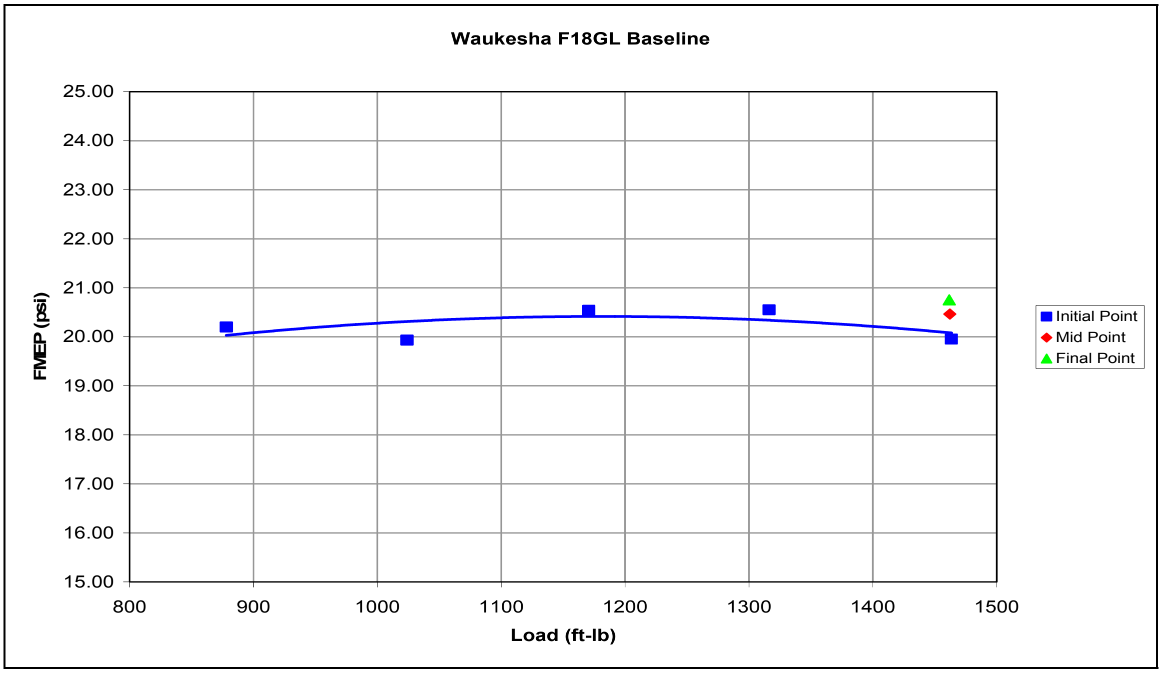

Figure 6-10: Baseline FMEP Measurements

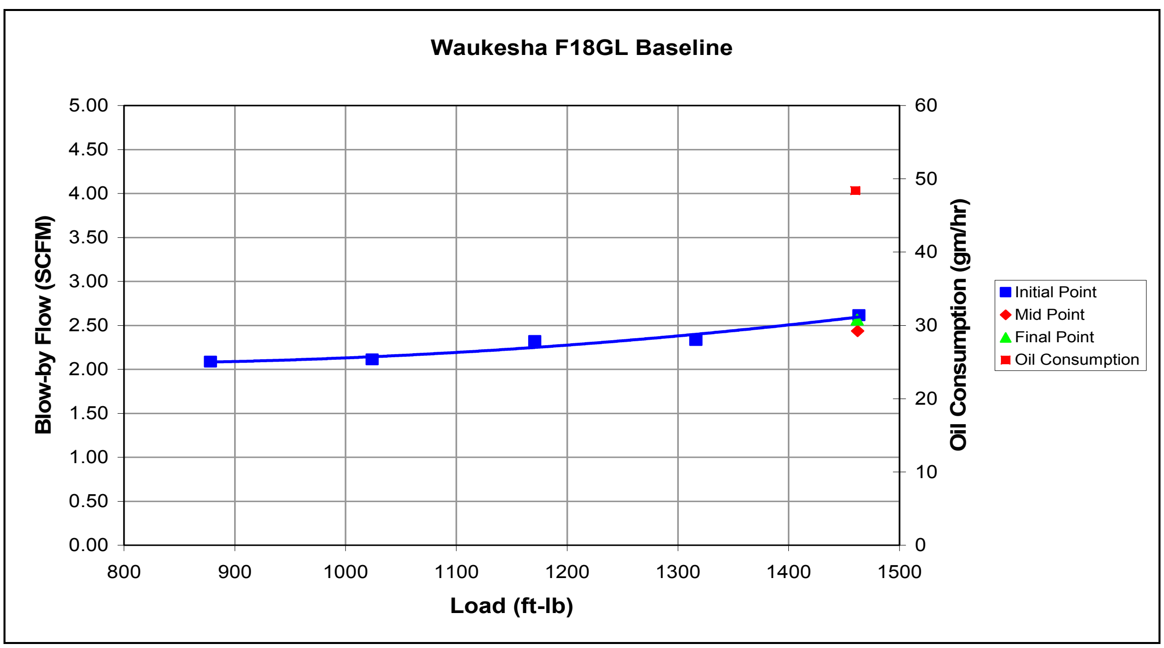

Figure 6-11: Baseline Blow-by Flow and Oil Consumption Measurements

The baseline test results for ring-pack friction per cylinder are summarized in Table 6-3 below. As discussed previously, the FMEP value obtained experimentally represents friction power losses in the entire engine, whereas the model predicted value represents the FMEP contribution from the piston ring pack alone. As a result, the FMEP contribution from the piston rings based on the experimental data that is given in the table is estimated assuming that the rings account for 20% of the total engine friction losses. This is the best estimate that can be made using the available data.

	Model Prediction		**Experimental Data**
	OS1	OS2	
FMEP (kPa)	18.97	33.29	28.25
Blowby (l/min)	69.4	69.4	72.35 ± 2.39
Oil Consumption (g/hr)	N/A	N/A	48.30 ± 0.34

Table 6-3: Results for the Baseline Case

It can be seen from the table that the estimated FMEP obtained experimentally lies in between the values corresponding to the minimum and maximum oil supply conditions obtained using the model. The fact that it is closer to the value obtained from the model for the minimum oil supply condition indicates that there may in fact be very little oil supply to the dry region. However, this cannot be established conclusively here, as this value was obtained based on an estimate for the contribution of the piston rings to overall engine friction. Blowby data also shows good agreement between the model and the experiment. A specific value for oil consumption could not be predicted by the model, and therefore a comparison could not be made with the experimentally obtained value.

6.7 Results for Reduced-Tension Oil-Control Ring

The first modified piston rings installed were low tension oil control rings. The stock oil control ring was modified to reduce tension by 50% for this test. This was accomplished by cutting the spring in half, as the length of the spring is directly proportional to the ring tension. The springs were cut by the ring manufacturer, and the tension of each of the rings was subsequently measured to ensure that no significant variation existed between the rings to be used in the different cylinders. These rings were tested and showed reduced friction, lowering FMEP from the baseline of between 20 and 21 (psi) to under 19 (psi). However, the reduced tension on the oil control ring also resulted in oil consumption increasing from 48.4 (g/hr) to 100.2 (g/hr) more than doubling the oil consumption. Since the oil control ring has little effect on blow-by, those numbers remained relatively similar to the baseline. The trends of this data are contained in Figure 6-12 and Figure 6-13.

The model predictions for the low-tension oil control ring design were obtained using the average ring tension between all of the rings as input. The results for this test are shown below in Table 6-4. It should be noted that FMEP reduction is the first category in this table,

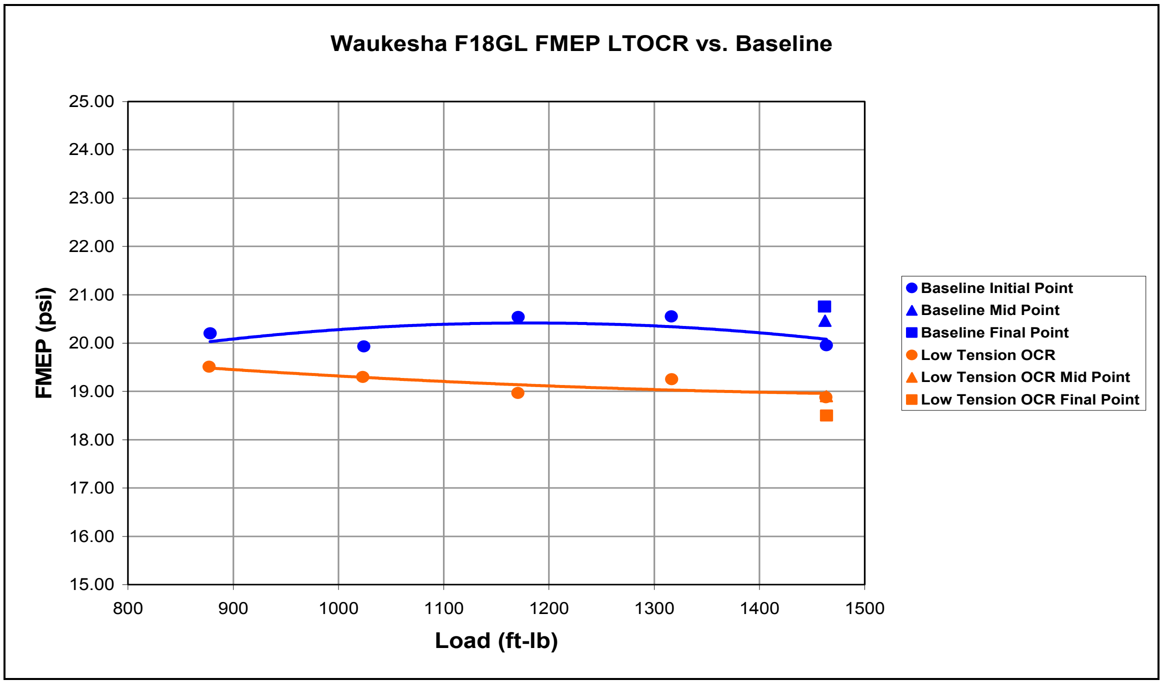

Figure 6-12: Low Tension Oil Control Rings vs. Baseline FMEP

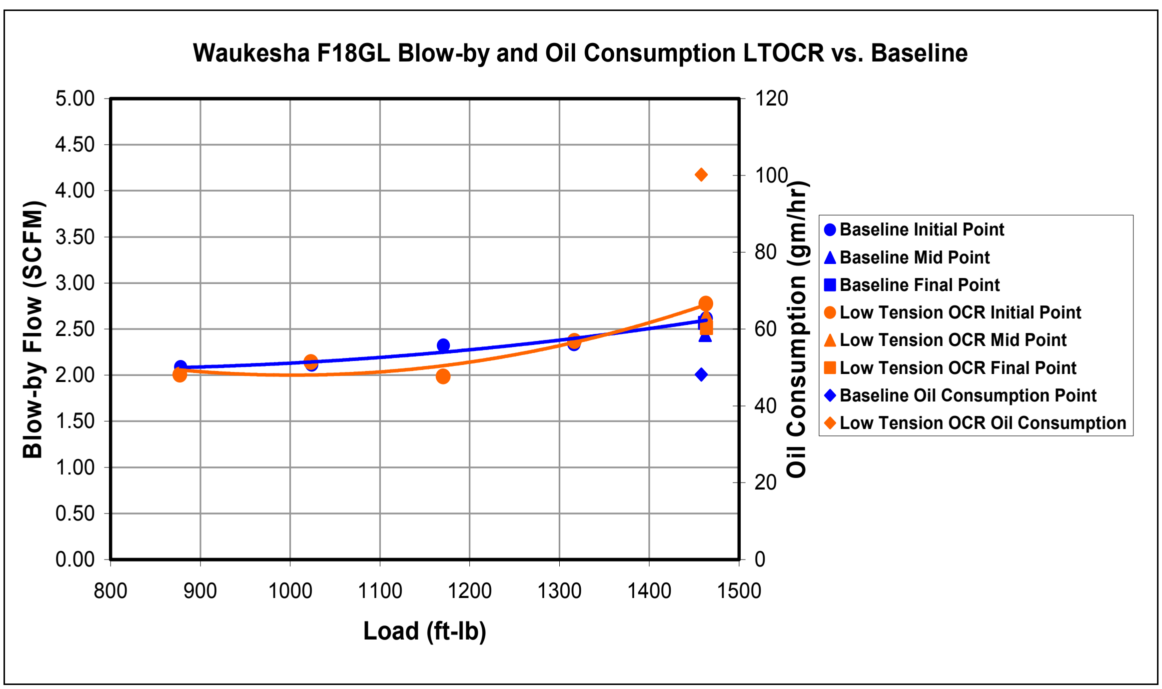

Figure 6-13: Low Tension Oil Control Rings vs. Baseline Blow-by Flow and Oil Consumption

as opposed to the table in the previous section, which listed the actual FMEP. This is the metric that is used to compare the model and the experiment in this study, and since the contribution of the piston rings to the overall friction is not known exactly, this is the most effective way to quantify the results.

	Model Prediction		**Experimental Data**
	OS1	OS2	
FMEP Reduction from Baseline (kPa)	4.71	9.15	11.17 ± 1.54
Blowby (l/min)	83.9	83.9	75.43 ± 3.40
Oil Consumption (g/hr)	N/A	N/A	105.73 ± 1.50

Table 6-4: Results for Reduced Tension Oil Control Ring

FMEP was reduced by between 5 and 10 kPa using this design according to the model predictions for both OS1 and OS2, and by 11.17 kPa according to the experimental data within a 95% confidence interval. Oil consumption increased by a factor of roughly 2 as a result of this change, as was expected because of the reduced ability of the oil control ring to conform to the liner due to its reduced tension. The predicted ring-pack friction percentage reductions were 24.8% and 27.4% for the low and high oil supply cases, and the measured percentage FMEP reduction for the entire engine was 39.5%, for the values shown in Table 6-3 and Table 6-4.

6.8 Results for Skewed-Barrel Top Ring

The stock top ring was modified by introducing a skewed barrel profile as described in Section 4.1.1. The extent of the skewness was such that the location of the minimum point was 15% of the total axial height from the bottom surface of the ring in the untwisted state.

A skewed barrel top ring design actually has a similar effect on groove wear as the upward tilted groove design discussed in Section 4.3.2. As the top ring is pushed down to conform to the lower groove flank around TDC of compression/expansion, there is an unbalanced pressure force acting on the upper ring face in the clearance between the groove and the liner which causes the top ring to rotate around the lower OD corner of the groove. There is therefore more concentrated contact at the OD corner of the groove, which tends to wear down the groove and may result in the minimum point moving up along the profile if the ring stays conformed to the groove, which would result in higher friction.

As a result, a slight positive static twist was introduced in the top ring in order to prevent this concentrated OD contact. The exact dimensions of the groove required to achieve a certain static twist were determined using a set of models developed by L. Liu with a detailed ring-design model [23].

The results for the top ring with a skewed barrel profile are shown below in Table 6-5. It was mentioned previously that it is difficult to manufacture a skewed barrel profile to the exact desired dimensions. As a result, there was some variation in the exact location of the minimum point on the profile between the different rings. To facilitate the modeling process, the ring manufacturer measured the final dimensions of each of the rings at different circumferential locations. To account for this in the model predictions, a minimum and maximum case was obtained for each oil supply condition for the range of values that were measured on the different rings after the machining process. Extreme cases represented the mean value for all of the rings plus or minus one standard deviation.

	Model Prediction		**Experimental Data**
	OS1	OS2	
FMEP Reduction from Baseline (kPa)	1.19-1.47	5.59-6.14	TBD
Blowby (L/min)	84.9	83.8	66.07 ± 1.03
Oil Consumption (g/hr)	N/A	N/A	38.58 ± 0.39

Table 6-5: Results for Skewed Barrel Profile Top Ring

Since the skewed barrel tests were run close to the end of this reporting period, experimental data for FMEP reduction still await further analysis. This additional data analysis is particularly important because the combustion conditions varied significantly between this test and the baseline test. This is probably a result of the seasonal variation in the composition of the natural gas that was obtained from the pipeline at the different times of year at which the tests were conducted. The low-tension oil control ring test was conducted only several weeks after the baseline test, and therefore the fuel composition did not vary significantly over this period of time. However, much more time elapsed between the low-tension oil control ring test and the skewed barrel top ring test. The amount of variation in the fuel composition was so significant that the air-fuel ratio had to be varied in an attempt to achieve similar stability in the combustion conditions. Unfortunately, this introduced significant variation in the experimental data and as a result, no conclusive friction data can be reported in time for this case. The model shows promising results, with values for friction reduction from the baseline case between 1 and 6 kPa, depending on the oil supply condition assumed.

Oil consumption data is exactly what was expected for this case. Oil consumption for the skewed barrel top ring reduced by 20% compared to the baseline case, which is due to the reduced force from radial pressure acting on the top ring near TDC of compression/expansion. Because of the reduced net radial load on the top ring in this part of the engine cycle, the ring does not conform as well to the liner, and this allows more downward gas flow to escape through the ring-liner interface, which can carry oil towards the combustion chamber.

Blowby actually reduced for this case, but this may have been affected by the variation in the engine operating conditions. Blowby typically scales roughly with peak cylinder pressure, which is greatly affected by the combustion conditions. Since the combustion conditions varied significantly in this test compared to the baseline test, the blowby data obtained for this case may not include similar variability. The blowby predicted by the model is almost identical for the case of the skewed barrel top ring compared to the baseline case.

6.9 Results for Combined System

The original intention of this study was to test an optimized system that combines all of the individual benefits of each of the designs discussed in the previous sections. Such a system would consist of the best low-friction top ring design, the second ring design with negative twist, and the reduced tension oil control ring. Model predictions indicated that the top ring design that resulted in the largest friction reduction was the skewed barrel top ring. This design also contributes to a reduction in oil consumption, which was shown experimentally. Therefore, according to the model predictions, the optimized system should consist of a skewed barrel top ring, a negative twist second ring, and a reduced tension oil control ring.

The model predictions for this optimized system are presented in Table 6-6 below. Due to the sensitivity of these predictions to the exact shape of the skewed barrel top ring, the approach used and described in Section 6.8 was used to account for the tolerances involved in the top ring profile. As a result, a range of values was obtained for friction reduction for each oil supply condition according to the model predictions.

	Model Prediction		**Experimental Data**
	OS1	OS2	
FMEP Reduction from Baseline (kPa)	13.44-13.71	15.32-20.96	TBD
Blowby (L/min)	91.8	91.8	TBD
Oil Consumption (g/hr)	N/A	N/A	TBD

Table 6-6: Results for Combined System

As can be seen from this table of results, FMEP can be reduced by as much as 21 kPa according to the model predictions. In addition, there was no significantly adverse effect on blowby introduced by these design changes. Tests are to be done in the summer of 2004 and results will be further examined. Oil consumption however is expected to be close to the baseline value, because the increase in oil consumption due to the reduced oil control ring tension is expected to be offset by the reduction in oil consumption due to the second ring negative twist and the skewed barrel top ring.

Overall, according to the model predictions, a reduction in ring-pack friction of 35% is possible by implementing the skewed barrel top ring, the second ring with negative twist, and the low-tension oil control ring. This optimized system thus has the potential to improve efficiency and reduce emissions in high load, low speed engines.

III. SUMMARY AND CONCLUSIONS

The piston ring pack is the largest single contributor to friction power losses in modern internal combustion engines. In this study, reduced friction piston ring designs were developed with the help of modeling tools and tested on a full-scale engine. Additional designs were also developed to eliminate adverse effects such as increased oil consumption, blowby or wear that might accompany changes in ring designs to reduce friction.

The impact of engine design and operating conditions on the main contributors to piston ring friction were identified, and the focus of this study was placed on gas-fired reciprocating engines operating in high load, low speed conditions.

For these operating conditions, the primary sources of friction in the piston ring pack were identified as the top compression ring around TDC of compression/expansion and the oil control ring throughout the engine cycle. The top ring's high contribution to friction near TDC of compression/expansion was a result of the lack of oil supply to this region, in combination with the high gas pressure acting on the back of the ring during this part of the engine cycle. The oil control ring's high contribution was a result of the high tension force acting on the small lands of the ring rails, which resulted in low oil film thickness and therefore a larger part of the engine cycle spent in mixed or boundary lubrication conditions.

Friction reduction strategies were developed in order to reduce the contribution of these primary sources of piston ring friction. For the top ring, the designs that were investigated included a skewed barrel profile, a reduced axial height and an upward tilted top ring groove in the piston. For the oil control ring, the use of rings with lower tension was recommended to achieve a reduction in friction.

Adverse effects that could occur as a result of the implementation of these designs were subsequently identified. The extent of the skewness of the barrel profile on the top ring was limited by manufacturing considerations as well as the potential onset of boundary lubrication conditions throughout the engine cycle. The reduced axial height compromised the structural strength of the top ring, resulting in earlier failure according to previous studies. The upward tilted piston groove was shown to be worn significantly by the top ring, resulting in the elimination of the upward tilt and therefore a shorter-lasting design. The reduced tension oil control ring design caused oil consumption to increase significantly.

Several additional design modifications were proposed to eliminate these adverse effects. The top ring to be used with the upward tilted piston groove was designed to have a positive static twist in order to prevent increased groove wear. A second ring with negative static twist was implemented with the reduced tension oil control ring in order to reduce oil consumption. The skewed barrel top ring was predicted to reduce oil consumption.

To investigate the practical potential of these design strategies, prototypes for the reduced friction ring designs were procured and tested on a full-scale Waukesha natural gas power generation engine. First, model predictions were obtained to assess the friction reduction potential of each of the designs. These results were then compared with experimental results obtained from running the full-scale engine with the reduced friction ring designs. The experimental results were obtained by Colorado State University.

The model indicated that the implementation of the combination of all of the low-friction ring designs could reduce ring-pack friction in the Waukesha engine by 35%. Due to time constraints and difficulties in achieving consistent combustion conditions in this study, the only experimental data that was obtained for this reporting period was for the low-tension oil control ring test. Generally good agreement was found between the model predictions and the experimental results for this case.

Several other potential friction reduction opportunities were also identified in this study and left open as potential areas for further investigation. Reduced liner roughness and smaller piston land heights on friction were found to have potential to reduce friction, but were limited by practical considerations such as manufacturability and structural considerations. Another potential area for future investigation was identified as top ring friction at midstroke, which can become significant in high speed, low load operating conditions.

The computer models indicated that the combination of the skewed barrel top ring, the second ring with negative twist, and the low-tension oil control ring would result in an optimized system with which engine friction was reduced by 35%, without any adverse effects on oil consumption, blowby or wear. In addition, it should be emphasized that no additional cost would result from the implementation of such designs, and no complex modifications would be needed on existing engine components.

The design strategies developed in this study thus have promising potential for application in all modern internal combustion engines as they represent simple, low-cost methods to extract significant fuel savings and to reduce harmful environmental damage, without compromising engine performance.

IV. CONTINUING PLANS

First, the remaining recommended piston ring designs would be tested and data analyzed. Team discussions will be held to ensure that the potential for ring-pack improvements will have been fully and practically explored. Key elements of the continuing work include optimizing the design of the engine piston itself, application of surface and material developments in conjunction with improved lubricant properties, system modeling and analysis, and continued technology demonstration in an actual full-sized reciprocating natural-gas engine.

We will expand the analysis of piston friction, including the effects of piston skirt material rigidity (material compliance or stiffness matrix), piston skirt axial profile, ovality, material coatings, and surface characteristics on piston friction, and test low friction pistons in an existing ARES engine. Then, mechanical design, lubricant selection, and material effects will be studied as an integrated system. Specific designs of components, lubricant, and material/surface characteristics for a full-scale ARES engine will be recommended, tested and demonstrated. The aggregate improvements will be quantified.

V. ACKNOWLEDGEMENT

This project is sponsored by the United States Department of Energy, as part of the Advanced University Reciprocating Engines Program (AUREP) under DOE Cooperative Agreement Number DE-FC26-02NT41339. We appreciate the support of Colorado State University, Dr. Bryan Willson, Ted Bestor, Nathan Lorenz and others, in performing the experiments and validation of the results. They are our important university partner in this project. The authors would also like to thank our industrial partner, Waukesha Engine Dresser, Inc for their support and insight in this study. The authors would like to specifically acknowledge the technical contributions of Ed Reinbold and Rick Donahue of Waukesha, who have worked closely with the MIT team and provided useful input and suggestions throughout the duration of the project. We thank the DOE ARES project monitors, Tom George, Rob Martinez, and in particular our technical project monitor Raj Sekar, and especially the DOE manager and sponsor, Ronald Fiskum for the encouragement and support. Feedback from other industry participants such as Caterpillar and Cummins was very helpful. Prior work and the methodology used in the analyses were supported by related research in the MIT Industrial Consortium on Lubrication in I.C. Engines.

VI. REFERENCES

1. Richardson, D.E., “Review of Power Cylinder Friction for Diesel Engines”, Internal Report, Cummins Engine Company
2. Nakada, M., “Piston and Piston Ring Tribology and Fuel Economy”, Proceedings of International Tribology Conference, Yokohama, 1995
3. Ting, L.L., “A Review of Present Information on Piston Ring Tribology”, SAE Paper 852355, 1985
4. Hill, S.B. and Newman, B.A., “Piston Ring Designs for Reduced Friction”, SAE Paper 841222, 1984
5. McGeehan, J.A., “A Literature Review of the Effects of Piston and Ring Friction and Lubricating Oil Viscosity on Fuel Economy”, SAE Paper 780673, 1978
6. Cullen, Joao A. and Frodsham, Gary M., “Reduced Cross Section Compression Rings for Diesel Engines”, SAE Paper 971146, 1997
7. Economou, P.N., Dowson, D. and Baker, A.J.S., “Piston Ring Lubrication – Part I. The Historical Development of Piston Ring Technology”, Energy Conservation Through Fluid Film Lubrication Technology: Frontiers in Research and Design, winter annual meeting of the ASME, New York, Dec. 2-7, 1979, Pg. 1-22
8. Rohde, S.M., Whitaker, K.W. and McAllister, G.T., “A Study of the Effects of Piston Ring and Engine Design Variables on Piston Ring Friction”, Energy Conservation through Fluid Film Lubrication Technology: Frontiers in Research and Design, winter annual meeting of the ASME, New York, Dec. 2-7, 1979, Pg. 117-134
9. Jeng, Y., “Friction and Lubrication Analysis of a Piston Ring Pack”, SAE Paper 920492, 1992
10. Tomanik, E., Nigro, E., Zabeu, C.B. and Peixoto, V.J.M., “Reduced Friction Power Cell Components”, SAE Paper 2000-01-3321, 2000
11. Tian, T., “Modeling the Performance of the Piston Ring Pack in Internal Combustion Engines”, PhD Thesis, Department of Mechanical Engineering, Massachusetts Institute of Technology, June 1997

12. Hu, Y., Cheng, S., Takayuki, A., Kobayashi, Y., Aoyama, S., “Numerical Simulation of Piston Ring in Mixed Lubrication - A Nonaxisymmetrical Analysis”, Transactions of the ASME, Journal of Tribology, Vol. 116, July 1994, Pg. 470-478
13. Greenwood, J.A., Tripp, J.H., “The Contact of Two Nominally Flat Rough Surfaces”, Proc. Inst. Mech. Engrs., Vol. 185, Pg. 625-633
14. Patir, N., Cheng, H.S., “Application of Average Flow Model to Lubrication Between Rough Sliding Surfaces”, Transaction of the ASME, Journal of Lubrication Technology, Vol. 101, April 1979, Pg. 220-229
15. Tian, T., Wong, V.W. and Heywood, J.B., “A Piston Ring Pack Film Thickness and Friction Model for Multigrade Oils and Rough Surfaces”, SAE Paper 962032, 1996; Also in SAE Trans., J. Fuels Lubricants, 1996, 105(4), Pg. 1783-1795
16. Tian, T., Noordzij, L.B., Wong, V.W. and Heywood, J.B., “Modeling Piston-Ring Dynamics, Blowby, and Ring-Twist Effects”, ICE - Vol. 27-2, 1996 ASME Fall Technical Conference, Vol. 2, pp. 67-80, Fairborn, Ohio, Oct. 1996
17. Vokac, A., “An Experimental Study of the Oil Evolution in Critical Piston Ring Pack Regions and the Effect of Piston and Ring Designs in an Internal Combustion Engine Utilizing Two-Dimensional Laser Induced Fluorescence and the Impact on Maritime Economics”, MS Thesis, Department of Mechanical Engineering, Massachusetts Institute of Technology, June 2004
18. Thirouard, B., “Characterization and Modeling of the Fundamental Aspects of Oil Transport in the Piston Ring Pack of Internal Combustion Engines”, PhD Thesis, Department of Mechanical Engineering, Massachusetts Institute of Technology, June 2001
19. Tian, T., “Dynamic Behaviors of Piston Rings and their Practical Impact. Part 2: Oil Transport, Friction and Wear of Ring/Liner Interface and the Effects of Piston and Ring Dynamics”, ImechE 2002, Pg. 229-247
20. Heywood, J.B., “Internal Combustion Engine Fundamentals”, McGraw-Hill Inc., © 1988
21. Tian, T., “Dynamic Behaviors of Piston Rings and their Practical Impact. Part 1: Ring Flutter and Ring Collapse and their Effects on Gas Flow and Oil Transport”, ImechE 2002, Pg. 209-227
22. Yilmaz, E., Thirouard, B., Tian, T., Wong, V., Heywood, J.B. and Lee, N., “Analysis of Oil Consumption Behavior During Ramp Transients in a Production SI Engine”, SAE Paper 2001-01-3544, presented at the 2001 SAE Fall Fuel and Lubricant Meeting and Exposition, San Antonio, TX, Sept. 2001
23. Liu, L., Tian, T. and Rabute, R., “Development and Applications of an Analytical Tool for Ring Design”, SAE Paper 2003-01-3112, 2003
24. Montgomery, Douglas C., Runger, George C., Hubele, Norma F., “Engineering Statistics”, Second Edition, John Wiley & Sons, Inc., © 2001
25. Energy Information Administration, “US Total Natural Gas Prices”, 5/6/2004, http://tonto.eia.doe.gov/dnav/ng/ng_pri_sum_nus_m_d.htm
26. Pinkus, Oscar and Sternlicht, Beno, “Theory of Hydrodynamic Lubrication”, McGraw-Hill, 1961
27. Frene, J., Nicolas, D., Degueurce, B., Berthe, D., Godet, M., Hydrodynamic Lubrication: Tribology Series (Vol. 33), Elsevier, 1997
28. Class Notes from Measurement Lab, Department of Mechanical Engineering, McGill University, Montreal, 1998 Edition

APPENDIX A

DERIVATION OF FUNDAMENTAL EQUATIONS

A.1. Shear Stress Between the Ring and the Liner and Volumetric Flow Rate of Oil

The shear stress generated between the ring and the liner and the volumetric flow rate of oil can be determined by applying conservation of mass and momentum to a fluid element under the ring surface as follows.

Conservation of Mass [26,27]:

$$\frac{d\rho}{dt}+\frac{\partial}{\partial x}(\rho u)+\frac{\partial}{\partial y}(\rho v)+\frac{\partial}{\partial z}(\rho w)=0 \tag{A.1}$$

Conservation of Momentum (Navier-Stokes Equations) [26,27]:

x-direction:

$$\rho\left(\frac{\partial u}{\partial t}+u\frac{\partial u}{\partial x}+v\frac{\partial u}{\partial y}+w\frac{\partial u}{\partial z}\right)=-\frac{\partial p}{\partial x}+\mu\left(\frac{\partial^2 u}{\partial x^2}+\frac{\partial^2 u}{\partial y^2}+\frac{\partial^2 u}{\partial z^2}\right)+\rho X$$

y-direction:

$$\rho\left(\frac{\partial v}{\partial t}+u\frac{\partial v}{\partial x}+v\frac{\partial v}{\partial y}+w\frac{\partial v}{\partial z}\right)=-\frac{\partial p}{\partial y}+\mu\left(\frac{\partial^2 v}{\partial x^2}+\frac{\partial^2 v}{\partial y^2}+\frac{\partial^2 v}{\partial z^2}\right)+\rho Y \tag{A.2}$$

z-direction:

$$\rho\left(\frac{\partial w}{\partial t}+u\frac{\partial w}{\partial x}+v\frac{\partial w}{\partial y}+w\frac{\partial w}{\partial z}\right)=-\frac{\partial p}{\partial z}+\mu\left(\frac{\partial^2 w}{\partial x^2}+\frac{\partial^2 w}{\partial y^2}+\frac{\partial^2 w}{\partial z^2}\right)+\rho Z$$

For this particular case and in most bearing lubrication applications, the following assumptions are valid [26,27]:

1. Height of fluid film y << x, z (film curvature can be ignored)
2. Negligible pressure variation across fluid film $\Rightarrow \frac{\partial p}{\partial y}=0$
3. Laminar flow
4. No external forces act on fluid film $\Rightarrow X=Y=Z=0$
5. Fluid inertia is small compared to viscous shear $\Rightarrow$ LHS terms in Eq. (A.2) neglected
6. All velocity gradients are negligible compared to $\frac{\partial u}{\partial y}, \frac{\partial w}{\partial y}$.

With the above assumptions, Eq. (A.2) reduces to:

$$\frac{1}{\mu}\frac{\partial p}{\partial x}=\frac{\partial^2 u}{\partial y^2} \tag{A.3}$$

$$\frac{1}{\mu}\frac{\partial p}{\partial z} = \frac{\partial^2 w}{\partial y^2}$$

An expression for shear stress can be obtained as follows. The following boundary conditions are needed:

$$u(y = 0) = 0$$

$$u(y = h) = U$$

Integrating the x-direction component of Eq. (A.3) with respect to y and applying the above boundary conditions, an expression for u(y) can be obtained:

$$u(y) = \frac{1}{2\mu}\frac{dp}{dx}(y^2 - hy) + \frac{Uy}{h} \qquad \text{(A.4)}$$

It should be noted that performing the integration in this way assumes that the viscosity is not a function of the distance from the liner in the cross-flow direction. However, for a shear-thinning fluid, the viscosity is a function of the local shear rate, which is given by the rate of change of the velocity in the cross-flow direction. Although many oils are shear-thinning fluids, it has been shown in [11] that accurate results can be obtained for these oils by approximating the viscosity as the piston speed divided by the average distance between the nominal lines defining the ring and liner surfaces. Therefore, the above integration is still valid even in these cases.

Shear stress is given by:

$$\tau(x) = \mu \left.\frac{\partial u}{\partial y}\right|_{y=0}$$

Using Eq. (A.4):

$$\tau(x) = \frac{\mu U}{h} - \frac{h}{2}\frac{dp}{dx} \qquad \text{(A.5)}$$

The volumetric flow rate can also be derived using the above results:

$$Q(x) = \int_0^h u(y)dy$$

Using Eq. (A.4):

$$Q(x) = -\frac{h^3}{12\mu}\frac{dp}{dx} + \frac{Uh}{2} \qquad \text{(A.6)}$$

A.2. Derivation of the Reynolds Equation

A relationship between the film height and width and the pressure distribution under the ring surface can be derived by applying conservation of mass and conservation of momentum to a fluid element under the ring surface.

Starting again with Eq. (A.3), the following boundary conditions can be applied, which assume that the motion of the ring surface occurs only in the x-direction:

$$u(y=0)=0$$
$$u(y=h)=U$$
$$w(y=0)=0$$
$$w(y=h)=0$$

Integration of Eq. (A.3) and application of the above boundary conditions yields the following result:

$$\begin{aligned} u &= \frac{1}{2\mu}\frac{\partial p}{\partial x}y(y-h)+\frac{h-y}{h}U \\ w &= \frac{1}{2\mu}\frac{\partial p}{\partial z}y(y-h) \end{aligned} \tag{A.7}$$

Substitution of Eq. (A.7) into the expression for conservation of mass given by Eq. (A.1) yields:

$$\frac{\partial}{\partial y}(\rho v)=-\frac{\partial}{\partial x}(\rho u)-\frac{\partial}{\partial z}(\rho w) \tag{A.8}$$

The following boundary conditions will be applied [26,27]:

$$v(y=0)=\frac{\partial h}{\partial t}$$
$$v(y=h)=0$$

Now, integrating Eq. (A.8) with respect to y and applying the boundary conditions, assuming an incompressible lubricant, yields [26,27]:

$$\frac{\partial}{\partial x}\left(\frac{h^3}{\mu}\frac{\partial p}{\partial x}\right)+\frac{\partial}{\partial z}\left(\frac{h^3}{\mu}\frac{\partial p}{\partial z}\right)=6U\frac{\partial h}{\partial x}+12\frac{\partial h}{\partial t} \tag{A.9}$$

This is the two-dimensional Reynolds Equation for incompressible lubricants. This equation relates the pressure distribution in the oil film with the film height and width between the ring and the liner.

APPENDIX B

METRICS FOR EVALUATING FRICTION REDUCTION

B.1. Determination of FMEP in the Friction Model

FMEP is a measure of the work done by friction normalized by the engine's displaced volume. It is thus a useful metric with which to compare the performance of different engines in a way that removes the effect of engine or component size. In this study, it is useful in that it provides a simple metric to use in order to evaluate and compare the performance of different piston ring designs.

The determination of the friction force was derived in Section 2 for pure hydrodynamic, mixed and pure boundary lubrication conditions. Friction power losses can be obtained from friction force by the following relationship:

$$P_f = UF_f \tag{B.1}$$

In other words, the friction power loss at a given crank angle in the engine cycle can be determined by the product of the friction force and the piston velocity. FMEP is defined as follows:

$$FMEP = \frac{W_f}{V_d} \tag{B.2}$$

To obtain the work done by friction from friction power losses, the following relationship is needed:

$$P_f = \frac{dW_f}{dt} \tag{B.3}$$

This can be rearranged to yield:

$$W_f = \int P_f dt \tag{B.4}$$

Substituting into Eq. (B.2) yields:

$$FMEP = \frac{\int P_f dt}{V_d} \tag{B.5}$$

The friction model discussed in Section 2.4 provides the friction power loss of the different piston rings at each crank angle throughout the engine cycle as output. To convert from time to crank angle, the following relation is needed:

$$\omega = \frac{d\theta}{dt} \tag{B.6}$$

where θ is the crank angle, and ω is the angular velocity of the crankshaft in radians per second. Rearranging and substituting this relationship into Eq. (B.5) yields:

$$FMEP = \frac{\int_{cycle} P_f d\theta}{\omega V_d} \tag{B.7}$$

This integration is carried out numerically in the friction model described in Section 2.4, since friction power loss can be determined at every crank angle from Eq. (B.1).

B.2. Determination of FMEP from the Experimental Results

Before the determination of the FMEP for a given ring design can be described, some introductory comments are required. In particular, the exact definitions of gross IMEP, net IMEP and their relationship to BMEP and FMEP must be clarified.

IMEP defines the work that is delivered to the piston by the cylinder gases. In this study, IMEP was determined from the cylinder pressure data as follows:

$$IMEP = \frac{\int p dV}{V_d} \tag{B.8}$$

The distance between the crank axis and the piston axis at any crank angle is given in [20]:

$$s = a\cos\theta + (l^2 - a^2\sin^2\theta)^{1/2} \tag{B.9}$$

where a is the crank radius and l is the connecting rod length. The volume change at any crank angle can be expressed as:

$$dV = -\frac{\pi B^2}{4}\frac{ds}{d\theta}d\theta$$

where B is the bore diameter of the engine, and the negative sign is added to reflect the positive volume change induced by a reduction of the distance between the crank axis and the piston axis. Differentiating Eq. (B.9) and substituting it into the above expression yields:

$$dV = \frac{\pi B^2}{4}\left\{a\sin\theta\left[1 + \frac{\cos\theta}{\left[l^2 - a^2\sin^2\theta\right]^{1/2}}\right]\right\}d\theta \tag{B.10}$$

The displaced volume can be expressed as:

$$V_d = \frac{\pi B^2}{4}L \tag{B.11}$$

where L is the stroke length of the engine. Substituting Eq. (B.10) and Eq. (B.11) into Eq. (B.8) yields the desired expression for IMEP:

$$IMEP = \frac{1}{L}\int p(\theta)\left\{a\sin\theta\left[1 + \frac{\cos\theta}{\left[l^2 - a^2\sin^2\theta\right]^{1/2}}\right]\right\}d\theta \tag{B.12}$$

The bounds of integration in Eq. (B.12) depend on whether or not the work done to flush out exhaust gases and bring in fresh charge, also called pumping work or PMEP, is to be included in the IMEP. If Eq. (B.12) is integrated over the compression and expansion strokes only, the result is referred to as gross IMEP, or $IMEP_g$. If Eq. (B.12) is integrated over the intake and exhaust strokes only, and the result is subtracted from the gross IMEP, this yields the net IMEP. In other words, gross and net IMEP are related as follows [20]:

$$IMEP_n = IMEP_g - PMEP \tag{B.13}$$

BMEP defines the work that is available at the engine's crankshaft. Therefore, the relationship between gross IMEP, net IMEP, BMEP and FMEP can be summarized as follows [20]:

$$\begin{aligned} IMEP_g &= BMEP + FMEP + PMEP \\ IMEP_n &= BMEP + FMEP \end{aligned} \tag{B.14}$$

In principle, if the BMEP could be held exactly constant, the difference in FMEP between two designs could be determined by comparing the net IMEP of each of the designs. In reality,

there is some variation in the BMEP as the load cannot be perfectly controlled by the dynamometer.
As a result, the following process was used to determine the FMEP of a given design. First, the gross IMEP was determined by integrating the expression in Eq. (B.12) using cylinder pressure data taken over 1000 engine cycles from each of the cylinders over three test runs. The integration was carried out over the compression and expansion strokes for each of the 1000 cycles, six cylinders and three test runs, and the mean value from this data set is the desired gross IMEP. This process was repeated over the entire cycle to determine the net IMEP. The average BMEP was obtained from a set of torque values that were measured from the dynamometer at a rate of 1 Hz for a 5 minute sampling period (or 1 measurement per second). BMEP was determined from torque by dividing by the engine's displaced volume. FMEP was then determined as the difference between the net IMEP and the BMEP. The change in FMEP between designs was evaluated by finding the difference between the FMEP for each of the individual designs. There was therefore a significant amount of error introduced while finding this value, since it is the result of two subtractions and two averaging processes. This error is discussed in detail and quantified in the section that follows.

B.3. Error Analysis of the Experimental Results

For each of the rings that were tested, a statistical analysis was conducted to determined whether or not a reduction in the mean FMEP was achieved. This section begins with a detailed description of this calculation, followed by a short description of the determination of the error in the experimentally measured oil consumption and blowby values.

BMEP data was first obtained for each of the three test runs. Since the data was taken at a rate of 1 sample per second, and this test was conducted over a period of 5 minutes, 300 values were obtained in total for each test. The mean and standard deviation of this data set was taken for each ring design that was tested.

Gross IMEP data was then obtained from the cylinder pressure data as described in the previous section. 1000 cycles of data were taken in each of the six cylinders for the three test runs, yielding a sample size of 18,000 of gross IMEP values. The mean and standard deviation for this data set was determined. A similar approach was also to determine the mean and standard deviation for the PMEP.

The procedure described in the previous section was then used to determine the change in FMEP between two designs once gross IMEP, PMEP and BMEP were determined. As mentioned previously, since each of these values has an average and a standard deviation, a significant amount of error was introduced in manipulating these values.

The following general equation was used to determine the error as a result of a calculation. For a function of two variables, $f(x_1,x_2)$, if the errors in the independent variables were Δx_1 and Δx_2, the error as a result of an operation is determined by [28]:

$$\Delta f(x_1,x_2) = \sqrt{\left(\frac{\partial f}{\partial x_1}\Delta x_1\right)^2 + \left(\frac{\partial f}{\partial x_2}\Delta x_2\right)^2} \qquad \text{(B.15)}$$

For example, since net IMEP is determined by the difference between the gross IMEP and PMEP, the associated error was determined as:

$$\Delta IMEP_n = \sqrt{(\Delta IMEP_g)^2 + (\Delta PMEP)^2}$$

This error propagation was carried out for each of the subtractions involved in the determination of the difference in the FMEP between two designs. However, using this method, the error in the result always ended up being larger than the value itself. As a result, a statistical approach was required to assess whether or not there was a difference in the mean FMEP values between different designs.

For this purpose, a hypothesis test was conducted [24]. In this approach, a hypothesis is made about a quantity of interest, in this case, the difference in the FMEP values between two different ring designs. The initial hypothesis is that the difference between the FMEP values between two designs is actually zero. The idea is to use statistical evidence to reject this hypothesis within a certain level of confidence.
Specifically, the hypothesis that the difference in the mean FMEP values between two tests is zero can be rejected provided that:

$$z_0 = \frac{\overline{x_1} - \overline{x_2} - \Delta_0}{\sqrt{\frac{\sigma_1^{\,2}}{n_1} + \frac{\sigma_2^{\,2}}{n_2}}} > z_\alpha \qquad \text{(B.16)}$$

where $\overline{x_1}$ and $\overline{x_2}$ are the mean FMEP values for the ring designs being compared, Δ_0 is the hypothesized value of the difference in the mean values (zero in this case), σ_1 and σ_2 are the standard deviations associated with the mean FMEP values, and n_1 and n_2 are the associated sample sizes. z_α is a value obtained from the standard normal distribution for a given α, which is a measure of the confidence with which the conclusion can be reached. In this study, a 95% confidence interval was used, which corresponds to α=0.05.

An example is used to illustrate this approach as well as the process used to conduct the error analysis in this study. For this purpose, the low-tension oil control ring results will be used. The mean values and associated standard deviations from data obtained from the baseline test and the low-tension OCR test are summarized in Table B-1 below.

	Baseline	**Low-Tension OCR**
BMEP (psi)	200.848 ± 0.152	200.998 ± 0.141
$IMEP_n$ (psi)	221.610 ± 13.094	220.118 ± 8.251
FMEP (psi)	20.762 ± 13.095	19.120 ± 8.252

Table B-1: Data Summary

To determine the associated error in the FMEP, the statistical analysis described above was used with the following values:

$\overline{x_1}$ = 20.762
$\overline{x_2}$ = 19.120
$n_1 = n_2$ = 18,000

$\sigma_1 = 13.095$
$\sigma_2 = 8.252$
$\alpha=0.05$

With these values, the hypothesis that the mean FMEP was the same for the low-tension OCR design as for the baseline design could be rejected because the criteria defined in Eq. (B.16) was met. Specifically, by substituting the above values into Eq. (B.16), the following result is obtained: 14.237>1.645.

The error on the difference in FMEP within 95% confidence can be determined as follows:

$$Error = z_{\alpha/2}\sqrt{\frac{\sigma_1^{\;2}}{n_1}+\frac{\sigma_2^{\;2}}{n_2}} \qquad \text{(B.17)}$$

With $z_{\alpha/2}$ = 1.96, the error on the FMEP within 95% confidence is 0.226 psi. In kPa, the mean value and error associated with the difference in FMEP for the case of the low-tension oil control ring is 11.17 ± 1.54. This is the result that appears in Table 6-4.

The error in the blowby data was determined by calculating the standard deviation based on the sample of 300 data points obtained from the blowby flow meter over the five minute averaging period for the three test runs that were considered. To determine the error in oil consumption measured experimentally, it was assumed to be possible to read the refill meter within an accuracy of 1%. Since this value was measured several times and averaged, the overall error was determined by applying the method in Eq. (B.15).

Oil consumption was not determined using the model and therefore no comparison could be made between the model and the experiment. Blowby was measured experimentally and was determined by the model, and a comparison could be therefore be made directly. The change in FMEP between designs was also compared directly. Some explanation should be given to justify this comparison. This is provided in the following section.

B.4. Comparison of FMEP between Model and Experiment

The model and the experiment use slightly different approaches to determine FMEP. In the model, the same cylinder pressure (and therefore IMEP) is used as input and the ring design parameters are varied. The FMEP contribution from the ring pack is provided as output from the model. In the experiment, the FMEP is determined by fixing the BMEP, and by measuring the change in cylinder pressure (and therefore IMEP) resulting from a change in the ring design. These two methods are entirely equivalent. The model's approach assumes that the changes in the ring design affect BMEP, whereas the experimental approach allows the changes in the ring design to affect IMEP. To ensure a consistent comparison between the experimental data and the results from the model, the experimentally measured cylinder pressure data from the baseline case was used as input into the model for all of the different cases considered. This is equivalent to fixing the IMEP. In the experimental approach, BMEP is fixed and the variation in net IMEP between the cases considered reflects the change in the FMEP of the ring pack.